Global Analysis of the Proton Elastic Form Factors in the Space-like Region

by

Craig M^{c}Rae

A thesis submitted to The Faculty of Graduate Studies of
The University of Manitoba
in partial fulfilment of the requirements of the degree of

Master of Science

Department of Physics and Astronomy
University of Manitoba

"These problems are solved, not by giving new information, but by arranging what we have long since known."

— Ludwig Wittgenstein, Philosophical Investigations

Abstract

The response of the proton to elastic scattering events has long been known to be described via two functions of the squared momentum transfer Q^2: the Sachs electric and magnetic form factors $G_E\left(Q^2\right)$ and $G_M\left(Q^2\right)$, respectively. To understand the elastic structure of the proton there are two main observables which constrain the form factors: unpolarized cross section data from elastic electron-proton scattering events, and polarization transfer measurements, which generate 'polarization ratio' data. After taking into account tree-level radiative corrections, separate fits of the form factors to these data lead to fits which disagree significantly with one another. Higher loop corrections, especially two-photon-exchange corrections, have been assumed to play a larger role than previously thought in order to explain this discrepancy. We present our global reanalysis which takes special care to treat normalization uncertainties in a most statistically rigorous manner, with additional work done to understand how to extend certain statistical methods only defined for linear models, to non-linear models. We find only minor differences to fits when normalization uncertainty is correctly accounted for. We also present a simultaneous global fit to the two-photon-exchange corrected cross section data and polarization ratio data. In addition to the above, an independent recalculation of the resonance contribution to the $F_3^{\gamma Z}$ structure function is computed using quark model helicity amplitudes.

Acknowledgements

First and foremost, I would like to thank my advisor Dr. Peter Blunden for his assistance and input during this masters degree. Academically I am also indebted to several other fantastic mentors at the University of Manitoba (comprising most of our department of Physics and Astronomy), though in particular I would like to thank Dr. Roy Roshko, Dr. Adam Rogers, Dr. Eric Schippers, Dr. Kyle Shiells, Dr. Rhonda Martens, and Dr. Avery Miller, for their guidance and support throughout all my years here.

Thank you to the excellent, friendly, and incredibly helpful staff of our department of Physics and Astronomy, especially Susan Beshta, Robyn Beaulieu, and Maiko Langelaar for swiftly solving any and all of my bureaucratic, administrative, and technical issues as they arose.

As well, I thank my many friends for their support during my graduate career thus far, including but certainly not limited to, Waweru Kariuki for our many discussions, during which I learned a great deal about statistical analysis, August Mendelsohn, Cole Coughlin, and Garrett Leverick for the dozens of hours of their lives I filled with my ramblings about my latest physics fixation, and Lucas Johnston and Brandon Sitch for their incessant pestering regarding the progress of my thesis work — I am not sure it ever helped.

Lastly I would like to thank Ashley Schers, for her unyielding love and support, and without whom I would surely have gone fully mad by now.

Contents

List of Figures

List of Tables

Physical Constants

Name	Symbol		Value[1]
Fine Structure Constant	$\alpha_\gamma\left(Q^2=0\right)$	$=$	$1/137.035999084(21)$
Proton Mass	M_p	$=$	$0.93827208816(29)$ GeV
Neutron Mass	M_n	$=$	$0.93956542052(54)$ GeV
Proton Magnetic Moment	μ_p	$=$	$+2.79284734463(82)\ \mu_N$
Neutron Magnetic Moment	μ_n	$=$	$-1.91304273(45)\ \mu_N$
Up Quark Electric Charge	e_u	$=$	$+\frac{2}{3}$
Down Quark Electric Charge	e_d	$=$	$-\frac{1}{3}$
Up Quark Axial Charge	T_u^3	$=$	$+\frac{1}{2}$
Down Quark Axial Charge	T_d^3	$=$	$-\frac{1}{2}$

[1] Taken from 2018 NIST-CODATA online database [2].

Dedicated to the substitute teacher who threw a meter stick across the room at just the right time.

Chapter 1

Definitions and Preliminaries

1.1 Cross sections and form factors

In subatomic scattering experiments, the primary observable available to physicists is the differential cross section, which is directly dependent on the square of what is called the invariant amplitude:

$$\frac{d\sigma}{d\Omega} \sim |\mathcal{M}|^2 \,. \tag{1.1}$$

In the 'one photon exchange' approximation of the scattering event, the invariant amplitude may be read off the Feynman diagram in Fig. (1.1) via the usual Feynman

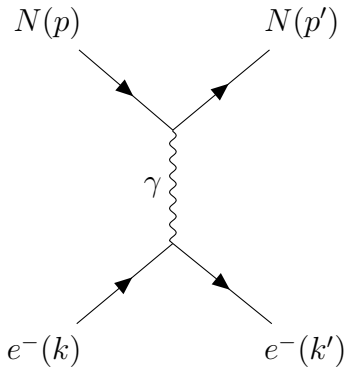

FIGURE 1.1: A 'One Photon Exchange' diagram of electron proton scattering. Particle momenta are indicated in parentheses.

rules:

$$\mathcal{M} = \left(ie\bar{u}_N(p')\,\Gamma^\mu u_N(p)\right)\frac{g_{\mu\nu}}{(k'-k)^2}\left(-ie\bar{u}_e(k')\,\gamma^\mu u_e(k)\right). \tag{1.2}$$

Throughout this thesis we will use units where $\hbar = c = 1$. Thus energy, momentum, and mass will all be expressed in units of GeV. The the metric convention is

$$(g_{\mu\nu}) = \mathrm{diag}\{1,-1,-1,-1\}. \tag{1.3}$$

It is useful to define the Mandelstam invariants:

$$s = (p+k)^2, \tag{1.4a}$$
$$t = (k'-k)^2 = q^2, \tag{1.4b}$$
$$u = (k'-p)^2, \tag{1.4c}$$

with

$$s + t + u = 2M^2 + 2m_e^2, \tag{1.5}$$

where $M[m_e]$ is the nucleon[electron] mass. The variable t here is the momentum transfer squared, often denoted q^2. This value is negative when the difference in the momenta is a 'space-like' vector:[1]

$$q_0^2 < \sum_i q_i^2. \tag{1.6}$$

The whole region of negative momentum transfer squared is called the space-like region. It is useful in the space-like region to define the positive quantity which is the negative of the momentum transfer squared:

$$Q^2 = -q^2 > 0, \tag{1.7}$$

[1] When $q^2 = 0$ the vector is null or light-like, and when $q^2 > 0$ the vector is time-like.

as well as this quantity scaled appropriately by the proton mass, in order to have a dimensionless Lorentz invariant:

$$\tau = \frac{Q^2}{4M^2}. \tag{1.8}$$

With these variables in place we may simplify the invariant amplitude Eq. (1.2) by identifying the spinor inner products over their respective Lorentz (gamma) structures as the currents of the electron and nucleon respectively

$$j_{\gamma\mu} = \bar{u}_e(k')\,\gamma_\mu u_e(k), \tag{1.9a}$$

$$J^\mu_\gamma = \bar{u}_N(p')\,\Gamma^\mu_\gamma(q) u_N(p). \tag{1.9b}$$

Here u_e and u_N are the spinors (satisfying the Dirac equation) for the electron and nucleon respectively, given their respective momenta defined in the Feynman diagram. For the nucleon, the vertex interaction is not point-like, as such the more complicated structure of its current is parameterized by the baryon current operator:

$$\Gamma^\mu_\gamma(q) = \gamma^\mu F_1\left(Q^2\right) + \frac{i\sigma^{\mu v} q_v}{2M} F_2\left(Q^2\right). \tag{1.10}$$

With $\sigma^{\mu\nu} = [\gamma^\mu, \gamma^\nu]$. These general functions $F_{1,2}(Q^2)$ are known as the Dirac and Pauli form factors respectively. With these defined we may rewrite the invariant amplitude as the inner product of the currents

$$\mathcal{M} = \frac{-e^2}{q^2} J^\mu j_\mu. \tag{1.11}$$

Finally, if E is the energy of the incoming electron, we can define the scattering angle of the electron in the lab frame θ, and the energy of the outgoing electron E':

$$E' = E - 2M\tau, \tag{1.12a}$$

$$\sin^2\frac{\theta}{2} = \frac{Q^2}{4EE'}. \tag{1.12b}$$

With our kinematics defined we may write down the differential cross section concretely

$$\frac{d\sigma}{d\Omega} = \left(\frac{\alpha}{4MQ^2}\frac{E'}{E}\right)^2 |\mathcal{M}|^2 . \tag{1.13}$$

The expansion and simplification of this cross section in the laboratory frame for $e-p$ scattering may be found in several textbooks, though Halzen and Martin [3] give a rather simple derivation via a modification to the electron-muon cross section. Starting from their derivation, and using the derived invariant amplitude (the inner product of currents), the lab frame differential cross section can be written as:

$$\left.\frac{d\sigma}{d\Omega}\right|_{\text{lab}} = \frac{\alpha_\gamma^2}{4E^2\sin^4\frac{\theta}{2}}\frac{E'}{E}\left[\left(F_1^2+\tau F_2^2\right)\cos^2\frac{\theta}{2}+\tau\left(F_1+F_2\right)^2\sin^2\frac{\theta}{2}\right]. \tag{1.14}$$

By introducing the Sachs electric and magnetic form factors $G_{E,M}\left(Q^2\right)$, related to the former form factors via:

$$G_E\left(Q^2\right) = F_1\left(Q^2\right) - \tau F_2\left(Q^2\right), \tag{1.15a}$$

$$G_M\left(Q^2\right) = F_1\left(Q^2\right) + F_2\left(Q^2\right), \tag{1.15b}$$

we may rewrite the cross section as follows:

$$\begin{aligned}\left.\frac{d\sigma}{d\Omega}\right|_{\text{lab}} &= \frac{\alpha_\gamma^2}{4E^2\sin^4\frac{\theta}{2}}\frac{E'}{E}\left[\frac{G_E^2+\tau G_M^2}{1+\tau}\cos^2\frac{\theta}{2}+2\tau G_M^2\sin^2\frac{\theta}{2}\right] \\ &= \frac{\alpha_\gamma^2 E'\cos^2\frac{\theta}{2}}{4E^3\sin^4\frac{\theta}{2}}\left[\frac{G_E^2+\tau G_M^2}{1+\tau}+2\tau G_M^2\tan^2\frac{\theta}{2}\right].\end{aligned} \tag{1.16}$$

The new form factors are normalized such that $G_E^{p[n]}(0) = 1[0]$ and $G_M^{p[n]}(0) = \mu_{p[n]}$ $= 2.793[-1.913]$ is the proton[neutron] magnetic moment in units of nuclear magentons. In fact, in the non-relativistic limit (see Ref. [4]), the Sachs form factors are the Fourier transforms of the charge and magnetization densities of the nucleon, e.g.:

$$G_E(q^2) = \int \rho(\vec{r})\exp\left(-i\vec{r}\cdot\vec{q}\right)\mathrm{d}^3 r. \tag{1.17}$$

These form factors are more convenient because there are no cross terms involving

products of the form factors. We may simplify further by introducing two quantities. Firstly the Mott cross section, the cross section for scattering from a point particle:

$$\sigma_{\text{Mott}} = \frac{\alpha_\gamma^2 E' \cos^2 \frac{\theta}{2}}{4E^3 \sin^4 \frac{\theta}{2}}. \tag{1.18}$$

Secondly the variable ε, which may be interpreted as the 'relative flux of longitudinal virtual photons'

$$\varepsilon = \left(1 + 2(1+\tau)\tan^2\frac{\theta}{2}\right)^{-1}, \quad 0 \leq \varepsilon \leq 1. \tag{1.19}$$

With these the above becomes

$$\begin{aligned}
\left.\frac{d\sigma}{d\Omega}\right|_{\text{lab}} &= \frac{\sigma_{\text{Mott}}}{1+\tau}\left[G_E^2 + \tau G_M^2 + 2(1+\tau)\tau G_M^2 \tan^2\frac{\theta}{2}\right] \\
&= \frac{\sigma_{\text{Mott}}}{1+\tau}\left[G_E^2 + \tau G_M^2\left(1 + 2(1+\tau)\tan^2\frac{\theta}{2}\right)\right] \\
&= \frac{\sigma_{\text{Mott}}}{\varepsilon(1+\tau)}\left[\varepsilon G_E^2 + \tau G_M^2\right] \\
&= \frac{\sigma_{\text{Mott}}}{\varepsilon(1+\tau)}\sigma_R.
\end{aligned} \tag{1.20}$$

In practise, computing the Mott cross section for an experiment is not an issue – the 'reduced' cross section is the place where the interesting physics happens

$$\sigma_R = \varepsilon G_E^2\left(Q^2\right) + \tau G_M^2\left(Q^2\right). \tag{1.21}$$

Experimental (measured) differential cross sections should in theory have contributions from all higher order diagrams, while the expression above for the reduced cross section assumes one-photon exchange (OPE) diagrams only. Because higher order diagrams contribute to the invariant amplitude ($\mathcal{M}$) terms of order α_γ^n with $n \geq 2$, they are expected contribute less than 1% to the total amplitude, and so the OPE approximation is a good approximation. For extreme precision measurements however, we may wish to correct the data for the contributions from higher order diagrams, such as the two-photon-exchange diagrams. In principle this is simple: compute the higher order corrections to the cross section, and divide them out of the

measured cross section data, so that our models for the form factors are really fitting the data strictly representing OPE reduced cross section as specified in Eq. (1.21). Generally this looks something like:

$$\sigma_R^{\text{Measured}} \approx \sigma_R \exp\left(\delta_{\text{virt}} + \delta_{\text{brem}} + \ldots\right), \tag{1.22}$$

where δ_{virt} and δ_{brem} represent higher order corrections from virtual and real (bremsstrahlung) photons relative to one photon exchange. Once the data has been corrected to the desired degree, a common technique to extract the values of the form factors is to use the Rosenbluth extraction technique: at constant values of momentum transfer Q^2, the reduced cross section depends linearly on ε. Thus if one measures the cross section at many ε's and some constant Q_c^2, a linear fit to the data will give a slope and an intercept which, within uncertainties, should equal $G_E^2(Q_c^2)$ and $\tau_c G_M^2(Q_c^2)$ respectively. With enough extracted data points we may construct reasonable functions for the form factors and use these for our calculations involving form factors.

While Rosenbluth extractions work for extracting values of the squared form factors, there is another experimental method which can be used in order to extract the ratio of the form factors, known as the polarization transfer ratio, colloquially referred to as 'polarization ratio data' or 'PT'. Arrington *et al.* review these two methods of form factor extraction in Ref. [5], and show the following forms for the two polarization transfer cross sections. Firstly the elastic cross section (in the OPE approximation) for scattering a longitudinally polarized electron[2] with a recoil proton polarized longitudinally is given by

$$\frac{d\sigma^{(L)}}{d\Omega} = \sigma_{\text{Mott}} \frac{E + E'}{M} \sqrt{\frac{\tau}{1+\tau}} \tan^2\frac{\theta}{2} G_M^2. \tag{1.23}$$

Conversely, the elastic cross section (in the OPE approximation) for scattering a longitudinally polarized electron with a recoil proton polarized transversely is given by

[2]The polarization direction of the electron is defined with respect to the electrons momentum.

$$\frac{d\sigma^{(T)}}{d\Omega} = 2\sigma_{\text{Mott}}\sqrt{\frac{\tau}{1+\tau}}\tan\frac{\theta}{2}G_E G_M. \tag{1.24}$$

Thus we may access the (normalized) ratio R of the form factors via:

$$R = \mu_p\frac{G_E}{G_M} = \mu_p\tan\frac{\theta}{2}\frac{E+E'}{2M}\left(\frac{d\sigma^{(T)}}{d\Omega}\right)/\left(\frac{d\sigma^{(L)}}{d\Omega}\right). \tag{1.25}$$

We now have three distinct experimental observables (the two polarized cross sections, and the one unpolarized cross section) which give us two independent methods for extracting the value of the nucleon form factor ratio at some particular Q^2: the ratio of the polarized cross sections R (PT data), and the ratio of the slope and intercept from the linear fits of the Rosenbluth extractions (LT data). Alarmingly, these independent methods for extracting the form factor ratios (see Ref. [5]) show a significant difference in the value extracted from the polarization transfer (PT) data, and by the longitudinal-transverse data (LT). The most common explanation of this discrepancy is that for LT data, higher order corrections, particularly two-photon-exchange (TPE) corrections, are required in order to close the gap. As for PT data, by its nature as a ratio of measurements, it is far less sensitive to higher order corrections, as well as certain kinds of systematic errors (the normalization uncertainties of the next section, in particular), and so are generally agreed to be the more accurate results.[3]

1.1.1 The state of form factor extraction

Recently, a low Q^2 global analysis by Bernauer [7] demonstrates that performing Rosenbluth extractions of the LT data and fitting form factors to the extractions themselves, does not typically lead to better or more reasonable fits for the form factors, when compared to simply fitting to the cross section data itself against a model of the cross section. Additionally, we will see in Sec. (2.2) that when the aforementioned multiplicative uncertainty is correctly taken into account, single Rosenbluth extractions of data taken from more than one experiment are largely

[3] Another point in favour of this is that polarization transfer data also falls off as predicted by QCD arguments (see Ref. [6]), while the LT fits and extractions do not.

meaningless. Given this, the challenge is to find appropriate models for the Sach's form factors, and fit them to the cross section and polarization data.

The current state of the art regarding analysis of LT data is the GMp12 reanalysis [8]. The GMp12 collaboration takes data from several prior electron proton LT scattering experiments, along with their own newer data, and after applying updated radiative corrections, perform a global fit to the cross section data using what is known as the penalty trick (explained in the Sec. (1.2)). The GMp12 group does not include two-photon-exchange effects in their corrections, and as such still find significant disagreement between separate fits of the LT and PT data. The analysis in this thesis differs significantly from the GMp12 analysis in two ways. Firstly, a great deal of effort is put into developing an alternative to the penalty trick, in order to avoid several issues of the fitting procedure (outlined in Ref. [9] as well as the following section). Secondly, with access to model-dependent two-photon-exchange corrections of Ahmed *et al.* [10], we can perform a truly global analysis of the LT and PT data simultaneously, in order to explore the quality of two-photon-exchange corrections, and in the case of good agreement, have access to the most up-to-date form factors. In order to do all this of course, we must understand the fitting procedure.

1.2 Statistics review

1.2.1 Beware the χ^2

How does one go about analysing the goodness of a fit? Most physics students will be told a χ^2 is the way to go. Though rarely done, it is not hard to explain where this comes from, and doing so is useful since it also shows that χ^2 has its limits, especially the reduced χ^2 statistic.

What is a measurement?

Firstly we must acknowledge that most modern error analysis assumes that a measurement is best represented by a distribution, not a strict interval. That is to say,

a measurement resulting in $x \pm \Delta x$ is not a statement that the true value of x is strictly in the interval $[x - \Delta x, x + \Delta x]$, but that the true value of x has a probability of being distributed according to a distribution characterized by a mean of x and a variance of $(\Delta x)^2$. But how do we know which probability distribution to use? This is a tricky and often unexplored question, and the real answer is that we don't know, but we can use some of the mathematical tools at our disposal to reasonably accommodate this ignorance.

The maximum entropy distribution

The probability density which assumes the least information about our data is known as a maximum entropy distribution,[4] and when we know only the mean and variance (central value and symmetric experimental uncertainty), it is not hard to show the maximum entropy distribution over the whole real line is a normal distribution. Thus the density function due to performing N independent uncorrelated measurements $y_i \pm \Delta y_i$ is given by:

$$P\left(y_1, y_2, \ldots, y_N | M_i\right) = \prod_{i=1}^{N} \frac{1}{\sqrt{2\pi}\Delta y_i} e^{-\frac{1}{2}(y_i - M_i)^2/(\Delta y_i)^2}. \tag{1.26}$$

M_i here is some theoretical value, or hypothetical true value of the measured value. If we had complete faith in our theoretical value of M_i, this distribution would simply serve to provide the probabilities of receiving our measurements y_i, useful for say, calibrating a newly constructed experiment. However we can read this in reverse (essentially applying Bayes theorem): if we really trust our experiment and data, then how likely is it that our model is correct? More concretely, if we have some flexibility in our model, we would like the model which maximizes the likelihood $P(M_i|y_i)$. If we stick with a particular functional form, we are in essence finding the model which, if it were correct, would be the most likely to generate the data we have.

[4] This is found by maximizing the functional $\int_\Omega -p\left(x\right) \ln\left(p\left(x\right)\right) dx$, where Ω is the support of your distribution. Additionally you must require the density integrate to one, along with any higher moments that are specified.

From now on we will assume when we see M_i, we really mean some function of the form $M(\vec{x};\boldsymbol{\alpha})$. Here M depends on a set of independent variables $x^1, x^2, ...$ (superscripts, not exponents) at specific values $x_i^1, x_i^2, ...$ and a set of free parameters $\boldsymbol{\alpha}$. The independent variables come from the experiment along with the observed data y_i, and thus we wish to vary the parameters $\boldsymbol{\alpha}$ in order to maximize the likelihood of finding our data given said model. The probability density, Eq. (1.26), is a generally a long product, which will be a pain to take the derivative of. In this case we may take the log of the distribution, and find what is known as the 'log-likelihood'. Since the log is monotonic, the parameters which maximize the log-likelihood will be the same parameters which maximize the original likelihood. With the properties of logarithms the product is simplified immensely. We may also ignore any constant terms since the derivative in the optimization will get rid of them. The object we wish to maximize is now merely a sum over the terms in the exponents of the initial Gaussian distribution:

$$\sum_{i=1}^{N} -\frac{\left(y_i - M(\vec{x}_i;\boldsymbol{\alpha})\right)^2}{2\Delta y_i^2}, \tag{1.27}$$

much better than the unwieldy Gaussian product. We can remove the minus sign and minimize instead, and we can remove any constant factors, such as the $\frac{1}{2}$ in every term, since it will have no effect on the location of any minima. Finally we have reduced our maximum likelihood problem, to a minimization of what is colloquially called a chi-square.

$$\chi^2(\boldsymbol{\alpha}) = \sum_{i=1}^{N} \frac{\left(y_i - M_i\right)^2}{\Delta y_i^2}. \tag{1.28}$$

This was not simply an exercise in derivation, keeping in mind all the requirements needed to derive this all too common minimization technique will keep us from making naive mistakes during our analysis. Some things which easily slip under the radar:

1) The principle of maximum entropy tells us our likelihood for a single measurement is Gaussian, both in the data and in the model. Any modifications to the χ^2 which cause this to be false, mean minimizing the chi-square is no longer equivalent to maximizing the likelihood function (the penalty trick we will see is an

example of this). Of course, if one assumes a different underlying distribution for measurements (such as log-normal), the whole analysis would need to be redone, and the optimization problem would look different.

2) We've assumed our measured data can, in principle, take values on the whole real line. This is often not the case, and the maximum entropy distribution in that case will be a truncated Gaussian. In practise this difference is very minor for any experiment with uncertainty an order of magnitude smaller than the mean, and is probably not worth the bother. Nonetheless it cannot hurt to keep in mind that because say, cross sections cannot be negative, the interpretation of the error must also account for this fact.

So far we're convinced we've justified everything correctly, and so we can minimize the χ^2 and divide it by the degrees of freedom, and this should give us a reasonable way to compare models and fits, right? Unfortunately this is jumping the gun. The degrees of freedom for a fit are not always well defined, and even when they are defined, they are not always constant during the fitting procedure, this is shown explicitly in Ref. [11]. It is easy to convince yourself that $f(x; A, B, C) = A \sin(Bx + C)$ having only 3 free parameters, given a large enough amplitude and frequency, can perfectly over-fit any data.[5] We are only guaranteed that the degrees of freedom are well defined when the model is linear in the fitting parameters. That is not to say non-linearity implies that degrees of freedom are ill-defined, just that if we intend to compare non-linear models, we must take the reduced χ^2 with a grain of salt, because the degrees of freedom may not always be what we would naively believe them to be.

1.2.2 Monte Carlo methods: making up data the right way

Given that the fitted data has uncertainty, it is not enough to find the best fit parameters of a model; in order for the model to be meaningful the uncertainty in the parameters and of the model itself must be found as well. For a model that is linear in

[5] 1 dimensional, non-overlapping data.

its parameters, this corresponds exactly to finding the Hessian of the χ^2 with respect to the model parameters, and inverting it to acquire a co-variance matrix for the fitted parameters.[6] This is because the Hessian gives you information about the curvature of the Gaussian and curvature is inversely proportional to the (co)variance of the Gaussian (see Ref. [12]). When a model is non-linear in its parameters, the Hessian method will often give multiple solutions, and will only be an approximation of the actual parameter co-variance matrix, because while the likelihood is Gaussian in the model, it is no longer Gaussian in the model's parameters. Monte Carlo simulations are an independent way around these issues. The idea is to generate so-called 'replica' data, which has an expected value of the original data, and same variance as the original data, and after fitting all the replica data, we will have a distribution of fitted parameters, and thus a distribution of the Model. There are several ways to perform this replication.

The method which assumes the least about our data, is known as *bootstrapping*. It works by constructing replicas which are simple random samples of the original data.[7] The bootstrap is appealing because it does not assume any underlying distribution for the data, something we should have a healthy scepticism about given that we simply used the maximum entropy distribution to build our maximum likelihood estimator. In reality the distribution for a measurement might be something different,[8] and using the bootstrap avoids 'doubling down' as it were. In other words, bootstrapping would fit many 'shufflings' of the data set. This works great when we have many data points for a single physical quantity we wish to model, however when it comes to the cross section data, each value of Q^2 is its own physically meaningful quantity, so unless every Q^2 has at least a dozen or so points to work with, the bootstrap is not the best method for fitting a whole function.

[6] Be careful not to confuse the co-variance matrix of a fit with the co-variance matrix of the experimental data.

[7] Like constructing a new deck of cards by pulling a card from 52 full and shuffled decks. No new data is ever introduced, and each bootstrapped sample will be approximately representative of the original data (though the sample will almost certainty contain copies of some data points while missing others).

[8] In principle we could find the distribution by measuring the same quantity many times, but this is expensive, and would end up with largely redundant data sets.

A more appropriate and familiar method is a distribution based Monte Carlo replication. If we are happy to double down on our Gaussian assumption, for each data point we can draw samples from the distribution $N(y_i, \Delta y_i)$. Drawing from this distribution ensures the replicas will have a mean of the measured data, with a variance of the squared uncertainty of that measurement. This is the appeal of the distribution based replication, it takes not only the data but also the uncertainty into account when constructing replicas, at the rather low cost of assuming our maximum entropy distribution is the correct underlying distribution of the measurement data.

If we were only interested in (or had sufficient data for) specific Q^2 values, we could combine these methods to maximize our usage of our statistical knowledge of the data. However this isn't feasible given how many Q^2 values have only single digit counts in our data sets, though it may be worth looking into for future Rosenbluth separation analyses. For the remainder of the thesis Monte Carlo replication will be performed to generate the replica data. We shall also see this choice is immensely convenient for performing the normalization error combination analysis of Ball *et al.* [9] which appears in the next section.

1.2.3 Multiplicative normalization uncertainty and you

Several of our data sets have an overall 'normalization' error Δn_i, which (with the standard Gaussian interpretation of error), means that for some experiment, labelled i, with an array of measurement data y_i, these data may actually be different from true value of the observable, by a multiplicative factor n_i, where n_i is distributed according to $N(1, \Delta n_i)$. This is typically written as:

$$y_i \cdot (1 \pm \Delta n_i). \tag{1.29}$$

Synonyms for this type of error are 'multiplicative uncertainty' or 'scale uncertainty', differentiated from the familiar 'additive' or 'offset' uncertainty. These kinds of errors arise when the entire data set is subject to the same errors during the process of extracting the data. One place these appear is in radiative corrections, since these are

in most cases model dependent, and as such the radiative corrections will themselves have an associated uncertainty. For example, for some correction c with uncertainty c_{err}, the application of the correction looks like,

$$y_i \cdot (c \pm \Delta c_{\text{err}}) = c\, y_i \cdot \left(1 \pm \frac{\Delta c_{\text{err}}}{c}\right). \tag{1.30}$$

The latter form is always used for presenting the scale uncertainties.[9] Thus after the correction is applied the corrected data will still have the uncertainty of the radiative correction to contend with. Why do we not simply multiply the quantity through, and add the uncertainties in quadrature as usual? The short answer is that we don't do this because the absolute scale uncertainties depend on the data, and it is best to have the errors reported be as context-free as possible for clarity of the statistics and physics involved (we should be wary about uncertainties depending directly on the data, because this ruins the Gaussian structure of our likelihoods).

1.2.3.1 The penalty trick

The question then becomes how one should go about combining these two kinds of uncertainty. It seems reasonable at first to attempt to 'find' these overall multiplicative factors along with the fit to the data, for which one common method is the 'Penalty Trick', found for example in Ref. [13]:

$$\chi^2_p = \sum_{i=1}^{\mathcal{N}} \left[\frac{(n_i - 1)^2}{(\Delta n_i)^2} + \sum_{j=1}^{N_i} \frac{(n_i \cdot y_{ij} - \mathrm{M}_{ij})^2}{(\Delta y_{ij})^2} \right]. \tag{1.31}$$

or alternatively, an updated penalty trick which scales the errors as well:

$$\begin{aligned} \chi^2_p &= \sum_{i=1}^{\mathcal{N}} \left[\frac{(n_i - 1)^2}{(\Delta n_i)^2} + \sum_{j=1}^{N_i} \frac{(n_i \cdot y_{ij} - \mathrm{M}_{ij})^2}{(n_i \Delta y_{ij})^2} \right] \\ &= \sum_{i=1}^{\mathcal{N}} \left[\frac{(n_i - 1)^2}{(\Delta n_i)^2} + \sum_{j=1}^{N_i} \frac{(y_{ij} - \mathrm{M}_{ij}/n_i)^2}{(\Delta y_{ij})^2} \right]. \end{aligned} \tag{1.32}$$

[9] This should also make clear why normalization uncertainties can be combined in quadrature, since this is simply the result of multiplication of the scale uncertainties.

Here i indexes the $\mathcal{N}$ experiments, and j indexes the N_i data points of each experiment. This indeed scales the data, while constraining the normalization factors to be close to 1. However notice immediately we have written down a contradiction of our assumptions of the maximum likelihood parameter estimate: this likelihood, $P_p = N_p \exp(-\frac{1}{2}\chi_p^2)$, is no longer Gaussian in the normalization factor n_i. In fact, the overall probability distribution function's normalization N_p will now depend directly upon the data, not only on the data co-variance matrix, which implies P_p is no longer Gaussian in the measurement data either. This means minimizing this χ^2 is no longer the same as maximizing the likelihood of our model generating the given data, which is the whole point of fitting in the first place! Ball *et al.* [9] do go on to show that in the case of a single experiment, Eq. (1.32) does give the correct best fit parameters while correctly accounting for normalization uncertainty. However this fails to be true when combining data from more than one experiment. It is easy to see why this may be true: for a single normalization uncertainty the second form of the penalty trick Eq. (1.32) gives a single model fit to all the data. But for $\mathcal{N}$ experiments, while often presented as scaling the data, what is actually happening is that there are $\mathcal{N}$ different models being fit to the data sets. When thinking of the set of objects $\mathrm{M}_i\,/n_i$ as the rather grossly correlated family of models that they are, instead of imagining the n_i's as some 'true' value of a fit, the fact that the penalty trick does not treat normalization uncertainties correctly becomes rather unsurprising.

At the risk of feeding a fed horse: another point of contention is the interpretation of the fitted 'normalizations' n_i. When fitting a free parameter, we are attempting to produce a central value, and constrain it within some standard error. This cannot be what is happening for the normalizations here, because they all already have a central value of 1, along with an uncertainty, just like any other data point. What is actually happening when we allow the tuning of these normalizations n_i, is exactly analogous to the act of tuning one's measurement data to different central values $\hat{y}_{ij}$ within their respective uncertainty bands, in order to obtain a better fit.

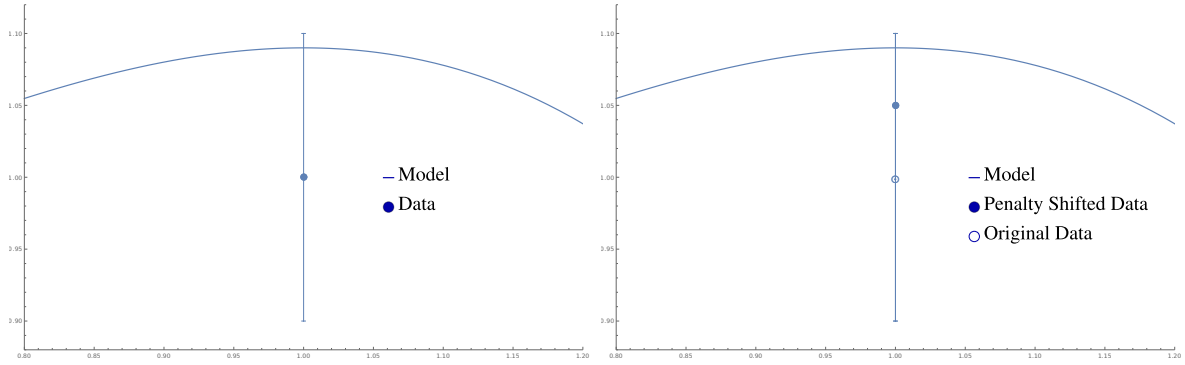

FIGURE 1.2: This figure shows a simple example of a model (solid blue curve) passing by a data point, and how the distance between the model and the data point shrinks when a normalization parameter of $n = 1.05$ is applied, meanwhile the model does not actually fit the data any better. Normally a chi-square may only be shrunk by constructing a better model, however the penalty trick makes possible shrinking the numerator of a chi-square by pushing central values of the data towards the model.

Figure (1.2) shows how the the penalty trick's normalization factors allows a chi-square to shrink without fitting the raw data better. Analogously we may imagine someone modeling a fit for the optimal 'true' central values $\hat{y}_{ij}$ via adding something like the following terms:

$$\chi^2 \sim \frac{(\hat{y}_{ij} - \mathrm{M}_{ij})^2}{(\Delta y_{ij})^2} + \frac{(\hat{y}_{ij} - y_{ij})^2}{(\Delta y_{ij})^2}. \tag{1.33}$$

This person would be (rightly) accused of hacking the data to minimize their *apparent* goodness of fit, instead of improving the actual quality of the fit to the data; and yet, this is precisely what the penalty trick does. Of course these new central values are perfectly plausible measurements, but this tuning not only flies in the face of the purpose of error analysis[10] but it depends upon the particular model chosen, and possibly upon all other data points and their uncertainties. Even if one were committed to this method of fitting, the new central values reported would not be of any significance outside of the specific fit. The resulting model does not actually fit the data as well as it reports, it fits different data, with modified central values. The resultant model is burdened by the context of its fit, a covert and gross over-fitting.

[10]Properly taking uncertainty into account should already imply the true value might be any value within the error bands.

The issue with combining multiple experiments with different normalization uncertainties, is that most naive approaches do not behave statistically reasonably, even when they do not suffer from all the peculiarities of the penalty trick. For example, if one experiment has an very large normalization uncertainty, its data ought to decouple and have little effect on the fit. Simultaneously, any one data point having a large uncertainty should decouple that single data point from the fit. As well, if all the uncertainties are equal, then the analysis should produce the typical maximum likelihood estimates for the Gaussian distribution: in that case the model should simply produce the mean of the measurements. It is surprisingly hard to come up with a method which keeps all of these properties in tact, while ensuring our chi-square is still representative of a Gaussian.

1.2.3.2 The t_0 method of Ball *et al.*

Luckily, the hard work has been done for us in a wonderful paper by Ball *et al.* [9]. Not only do they rigorously show the biases in the usual approaches for combining multiple experimental data sets with multiplicative normalization uncertainties, but they also construct a Monte Carlo method which takes the normalization uncertainty into account without compromising the integrity of the fit. Through the power of expectation values, we are freed of thinking about finding any specific n_i for each data set. As long as we correctly take the uncertainty into consideration during the fit, we are done. Their paper takes a rather roundabout way of presenting the method, but it is not hard to see how they arrive at their solution. Firstly, perform the usual error propagation for multiplying data with uncertainty:

$$(y_{ij} \pm \Delta y_{ij}) \cdot (n_i \pm \Delta n_i) = n_i \cdot y_{ij} \pm \sqrt{(n_i \Delta y_{ij})^2 + (y_{ij} \Delta n_i)^2}. \tag{1.34}$$

Then build a chi-square for some model M to this data:

$$\chi^2 = \sum_{i=1}^{\mathcal{N}} \left[\sum_{j=1}^{N_i} \frac{(n_i \cdot y_{ij} - \mathrm{M}_{ij})^2}{(n_i \Delta y_{ij})^2 + (y_{ij} \Delta n_i)^2} \right]. \tag{1.35}$$

We may simplify things by substituting the natural value[11] of 1 for the scale values n_i. This results in the chi-square becoming:

$$\sum_{i=1}^{\mathcal{N}} \left[\sum_{j=1}^{N_i} \frac{(y_{ij} - \mathrm{M}_{ij})^2}{(\Delta y_{ij})^2 + (y_{ij} \Delta n_i)^2} \right]. \tag{1.36}$$

We cannot stop here, since the likelihood is no longer Gaussian in the data, as the data points now appear alongside the uncertainties in the denominator. The clever trick here is to realize that if our model is a good fit for the data (which we intend to make true), we can use our model as a stand-in for the data in the denominator:

$$\chi^2 = \sum_{i=1}^{\mathcal{N}} \left[\sum_{j=1}^{N_i} \frac{(y_{ij} - \mathrm{M}_{ij})^2}{(\Delta y_{ij})^2 + (\mathrm{M}_{ij} \, \Delta n_i)^2} \right]. \tag{1.37}$$

This leaves things Gaussian in the data, but not in the model, so the correct optimization procedure gains a correction term from the likelihood's normalization factor $\ln N_p(M)$.[12] The next leap of ingenuity is to replace the model in the denominator with a best guess: $\hat{\mathrm{M}}(\vec{x}, \hat{\boldsymbol{\alpha}})$.

$$\chi^2 = \sum_{i=1}^{\mathcal{N}} \left[\sum_{j=1}^{N_i} \frac{(y_{ij} - \mathrm{M}_{ij})^2}{(\Delta y_{ij})^2 + \left(\hat{\mathrm{M}}_{ij} \Delta n_i\right)^2} \right]. \tag{1.38}$$

This χ^2 has all the nice statistical properties we expect, and remains Gaussian in the model and the data, for the small price of asking for omniscience. If our best guess coincides with the model given from the optimization, we are done. Else, we can use the optimized model as our ensuing guess, and perform an iterative process until (hopefully) the model converges.

For ease of derivation, all the chi-square's presented above have implicitly assumed that each experiment has had only one data point. In full generality, the

[11] 1 is the natural value for normalization scale because when building the total normalization uncertainty for an experiment, the multiplicative uncertainties are always presented as a relative error, just as discussed around Eq. (1.30).

[12] In principle one could solve this for the parameters of M, but it is unlikely to be fruitful due to the non-linearity in M.

chi-square must take into account the full covariance matrix of the data:

$$\chi^2 = \sum_{i=1}^{\mathcal{N}} (y_i - \mathrm{M}_i)^T (\mathrm{Cov}_i)^{-1} (y_i - \mathrm{M}_i) . \tag{1.39}$$

Here the data minus model terms are treated as vectors of length N_i, and the covariance matrix is of dimension $N_i \times N_i$, where N_i is the number of data points in the i^{th} experiment. With uncorrelated errors, this matrix is diagonal and so looks just as the traditional chi-square in Eq. (1.28). However when we include the correlated normalization errors, the extra term in the denominator is added to every entry in the matrix. Below is an example for some i^{th} experiment, with two data points having no correlated additive errors:

$$\begin{aligned}
(\mathrm{Cov}_{t_0})_i &= \mathrm{Cov}_i + \left(\hat{\mathrm{M}}_{ij}\Delta n_i\right)^2 \\
&= \begin{pmatrix} (\Delta y_{i1})^2 & 0 \\ 0 & (\Delta y_{i2})^2 \end{pmatrix} + \left(\hat{\mathrm{M}}_{ij}\Delta n_i\right)^2 \\
&= \begin{pmatrix} (\Delta y_{i1})^2 + \left(\hat{\mathrm{M}}_{i1}\Delta n_i\right)^2 & \left(\hat{\mathrm{M}}_{i?}\Delta n_i\right)^2 \\ \left(\hat{\mathrm{M}}_{i?}\Delta n_i\right)^2 & (\Delta y_{i2})^2 + \left(\hat{\mathrm{M}}_{i2}\Delta n_i\right)^2 \end{pmatrix}
\end{aligned} \tag{1.40}$$

The question mark subscripts are intentional here, as this is the first time we run into an ambiguity with extending the t_0 method: what values do we use for the off diagonal elements which contain factors of the model $\hat{\mathrm{M}}_i$? Were this an experiment with a single data point, it would be clear that we should evaluate the model evaluated at those same kinematics x_{ij} for which we found the experimental result y_{ij}. What are we to do in this more complicated situation, where the data points with different kinematics, and hence different model values, come from the same experiment and hence share these correlated normalization uncertainties? In the original work this is not a problem, as Ball *et al.* [9] are looking at multiple experiments for extracting a single physical value, namely the strong coupling constant $\alpha_s(Q^2)$, either at $Q^2 = 0$ or $Q^2 = M_Z^2$. Because of this, their model is always simply a single parameter (called t_0, hence the name), and the terms appended to their covariance matrices are always uniformly the normalization uncertainty scaled by this parameter.

We also cannot simply treat each data point as its own experiment, even though one may interpret the form factors at distinct Q^2 values as unique physical constants to be extracted, because this would not be an accurate representation of correlated statistics of the measurement data. As these errors are multiplicative in nature and not additive, and as these errors at the off diagonal elements generally correlate measurements at different kinematics, the choice was made to extend the t_0 method by having the (square of the) geometric mean of the models. That is to say, the additive covariance matrix is appended by the matrix defined by

$$M_{ij}M_{ik}(\Delta n_i)^2, \tag{1.41}$$

where again i indexes the experiment and j, k both stand in for the kinematics of the experiments j^{th} or k^{th} data point. This gives a final covariance matrix for the extended t_0 method (in our 2×2 example) of

$$\left(\text{Cov}_{t_0}\right)_i = \begin{pmatrix} (\Delta y_{i1})^2 + \left(\hat{\text{M}}_{i1}\Delta n_i\right)^2 & \hat{\text{M}}_{i1}\hat{\text{M}}_{i2}\left(\Delta n_i\right)^2 \\ \hat{\text{M}}_{i1}\hat{\text{M}}_{i2}\left(\Delta n_i\right)^2 & (\Delta y_{i2})^2 + \left(\hat{\text{M}}_{i2}\Delta n_i\right)^2 \end{pmatrix}. \tag{1.42}$$

This is a natural choice for many reasons. Firstly, it reproduces the diagonal entries we expect. Secondly, it assures the covariance matrix remains symmetric, which all covariance matrices must be. Lastly, if our model really is a good stand in for the data, then this ensures the data is correlated just as we expect it should be: all data is simultaneously multiplicatively correlated to one another (weighted by the other data's central values and the normalization uncertainty). Generally then, the t_0 covariance matrix looks like:

$$\text{Cov}_{t_0} = \text{Cov}_i + \left(\Delta n_i\right)^2 \hat{\text{M}}_{ij}\hat{\text{M}}_{ik}, \qquad \forall j, k, \tag{1.43}$$

where Cov_i is the original data covariance matrix from the i^{th} experiment, and j and k span the number of data points of the i^{th} experiment. Each experiment will have a covariance matrix like this, and the total chi-square will be the sum of these matrix inner products for each experiment

$$\chi^2_{t_0} = \sum_{i=1}^{\mathcal{N}} \left(y_i - \mathrm{M}_i\right)^T \left(\mathrm{Cov}_{t_0}\right)_i^{-1} \left(y_i - \mathrm{M}_i\right). \tag{1.44}$$

With this clarified, in order to properly ensure the uncertainties are all correctly taken into account, the final step of the original t_0 method is performed. First we build Monte Carlo replica data Y^R which for each data point is pulled from the normal distribution $N(y_i, \Delta y_i)$. We also generate Monte Carlo normalization factors pulled from Gaussian distribution $N_R \in N(1, \Delta n_i)$, and then fit each of the following replica chi-squares:

$$\chi^2_{t_0,R} = \sum_{i=1}^{\mathcal{N}} \left(N_i^R Y_i^R - \mathrm{M}_i\right)^T \left(\mathrm{Cov}_{t_0}\right)_i^{-1} \left(N_i^R Y_i^R - \mathrm{M}_i\right). \tag{1.45}$$

Modifying the χ^2 in the way described above, and then finally averaging the model over all the replica fits, gives a model-fit with uncertainty (that uncertainty being the standard deviation of the distribution of fitted replica models), which correctly accounts for the normalization uncertainty, which behaves correctly in all limiting cases, and is manifestly unbiased. Even if not explicitly stated, all future fits using a minimization of the t_0 chi-square, should be understood to be averages of many minimization's of Monte Carlo replicated t_0 chi-squares.

1.2.4 Why care about unbiased fitting?

The penalty trick, despite its flaws, seems to consistently provide reasonable fits, which agree with other experiments. So why put in all this extra effort for presumably, a small gain? D'Agostini in Ref. [14] outlines how during the fitting of hadronizing electron-positron annihilation events from the CELLO collaboration in Ref. [15], the naive treatment of normalization uncertainties via the penalty trick, Eq. (1.31), leads to a 'repulsion' of the fit from the data, while the chi-square per degrees of freedom remained approximately constant. At the time, this was remedied by updating the penalty trick to scale the uncertainties as well, which is equivalent to scaling the model by one over the fitted normalization, as seen in Eq. (1.32). However as mentioned previously Ball *et al.* [9] show this version still fails to be free of bias when combining multiple experimental data sets. This means in theory, there is nothing stopping

analogous misbehaviour of fits with the updated penalty trick, thus we ought to look for ways to fit the data which are manifestly unbiased, so we know for certain the aforementioned misbehaviour is not happening, in any capacity. We also know that the penalty trick does not necessarily give the parameters most likely to reproduce the data, while the t_0 method does. If we are interested in having models used as stand ins for data, or approaching the true value of some parameter, using the penalty trick will never allow us to be certain our results or analysis are sound. Another benefit of the new fitting procedure is that the number of parameters stays constant as more data is introduced, whereas the penalty trick becomes, for lack of a better word, trickier to deal with as more data sets are introduced, due to the presence of more parameters and multiple solutions.

1.2.5 Building an intuition for the t_0 chi-square

Having built this modified chi-square, and convincing ourselves of its correctness, uses, and limitations, it is worth seeing what the new chi-square can tell us about our data. Usually the wisdom of the reduced chi-square statistic is passed down from professor to student as follows: "A reduced chi-square of 1 is a good fit. Less than one, and you're over-fitting, greater than one and you're under-fitting." It's not hard to see where this comes from. Let's take a look at the traditional chi-square:

$$\chi^2 = \sum_{i=1}^{N} \frac{(\mathrm{M}_i - y_i)^2}{(\Delta y_i)^2}. \tag{1.46}$$

To say the reduced chi-square should be close to 1, is to say this sum should be close to N. The easiest way for that to happen would be if each of the N terms was 1, and indeed this is where the intuition comes from: a model M which is a distance of exactly one uncertainty band Δy away from each data point y, would have a reduced chi-square of 1 since the numerator would equal the denominator at each point. On the other hand, a model which passes exactly through each central point of the data would have a chi-square of 0, which becomes guaranteed the more you over-fit. The 1 benchmark of course allows wiggle room: having one point fit exactly while another is

modeled 2 standard deviations away from the data, is more or less the same quality of fit. Furthermore the p parameters of the fit, in theory should allow the model to exactly fit p data points, so the actual expected value of the chi-square will be the degrees of freedom $N - p$.

How can we translate this wisdom to the new chi-square? It seems reasonable to ask for the same qualitative outcome: that the model in the best case is osculating the uncertainty bands of each data point. If that is what we consider the ideal fit, it is clear that the chi-square we've generated will not be 1. For the case where all of our data comes from distinct experiments, this statistic is easy to build. Reminding ourselves what the t_0 chi-square looks like in that case:[13]

$$\chi^2 = \sum_{i=1}^{N} \frac{(\mathrm{M}_i - y_i)^2}{(\Delta y_i)^2 + (y_i \Delta n)^2}. \tag{1.47}$$

For a good fit to mean the same thing regardless of the chi-square we're employing, is to say that numerator would be the same as before in the ideal case: the distance between model and data, should be around 1 standard deviation of the data's uncertainty (it would be equal to that first term in the denominator, not the whole denominator here). In that ideal case each term would look like:

$$\sim \frac{(\Delta y_i)^2}{(\Delta y_i)^2 + (y_i \Delta n)^2} = \frac{1}{1 + (\Delta n \frac{y_i}{\Delta y_i})^2}. \tag{1.48}$$

To figure out what the ideal minimized chi-square should look like, we simply sum up these terms for each data point in the fit:

$$\chi^2_{t_0-\text{ideal}} = \sum_{i}^{N} \frac{1}{1 + (\Delta n \frac{y_i}{\Delta y_i})^2}. \tag{1.49}$$

Notice that if we are in a situation where there is no normalization uncertainty ($\Delta n = 0$) the above ideal statistic collapses to the familiar one, the sum collapses to N, as expected. The consideration of parameters is markedly more complicated in this

[13] In the denominator we have re-replaced the model with the data again, to ensure our best fit statistic is not model dependent.

case, because each data point contributes a different amount to the ideal chi-square value, we cannot simply subtract this value by p to build the t_0 chi-square equivalent to the degrees of freedom. One alternative could be to imagine for each data set, excluding every possible combination of p data points (those p data points the model is hypothetically fitting exactly) calculating this subset ideal chi-square, and averaging over all of the subset chi-squares. However, depending on the size of the data sets this task can range from computationally intense to intractable. As such for the remainder of the thesis we will simply use this easy to compute ideal as the statistic of interest, and understand that it is expected that a good fit will be a bit lesser than this, so long as the number of parameters stays considerably lower in number than the number of data points in the fit.

The situation is remarkably less clear when each experiment has multiple data points and a full covariance matrix, since the covariance may make it essentially impossible for certain points to be simultaneously fit to the same degree. Due to this, in the thesis we regularly report the chi-square without reducing it by any factors. At the very least, we can be certain now that our analysis is sound, and use this fitting procedure on cross section data to compare how this correct and unbiased fitting compares to usual fits with the penalty trick.

Chapter 2

Linear Models of G_E^2 and G_M^2

2.1 The penalty trick vs. the t_0 method

In this section, we compare the newly extended t_0 method against the fitting procedure used in Gramolin and Nikolenko [13], to understand how the ubiquitous penalty trick differs from the more statistically rigorous method. In the following fits we will be using 3 groupings of the cross section data set: (A) The global cross section data set, which does not include model-dependent two-photon-exchange effects, (B) The subset of the global data set for which model-dependent TPE corrections can be applied, but have not yet been applied ('uncorrected' data), (C) The fully TPE-corrected data. (B) and (C) are of course subsets of, or derived from subsets of, the global cross section data set with Q^2 values between 1 GeV^2 and 6.275 GeV^2. The upper bound was chosen so that Blunden TPE corrections are reliable on the cross section data, and the lower to have a well defined consistent data range for convenient comparison in future works. Tables containing all the data used in this thesis can be found in Appendix (C).

In their paper Gramolin and Nikolenko [13] use a simple fit to the square of the form factors in order to ensure the fitting procedure becomes a linear algebra problem in the parameters:

$$\begin{aligned} G_E^2(\tau) &= \left(1 - a_1\tau - a_2\tau^2 - a_3\tau^3\right) G_D^2(\tau), \\ G_M^2(\tau) &= \left(1 - b_1\tau - b_2\tau^2 - b_3\tau^3\right) \mu_p^2 G_D^2(\tau). \end{aligned} \tag{2.1}$$

The downside to using such a simple model is manyfold. The square form factors have nothing preventing them from becoming negative, the form factors do not fall off as predicted by QCD scaling laws (see Ref. [6]), and if one wishes to include say, polarization data, the fitting procedure becomes non-linear losing any of its initial appeal. Nonetheless it makes for a rather convenient point of comparison.

2.1.1 Analysis on 'uncorrected' data set (B)

2.1.1.1 Fit via the penalty trick

Gramolin and Nikolenko intentionally build a linear model to use the first penalty trick (see Eq. (1.31)), so that all the parameters enter the chi-square equally. For our case with 9 data sets, this chi-square is quadratic in the nine parameters a_i, b_i and n_j ($1 \leq i \leq 3$, $1 \leq j \leq 9$), and thus the minimization procedure of solving

$$\frac{\partial \chi^2}{\partial \alpha_i} = 0, \tag{2.2}$$

(for each parameter α_i) gives fifteen linear equations – solving the system of equations becomes a linear algebra problem. Furthermore, this linearity is doubly convenient as the (constant) Hessian matrix of this chi-square is not only independent of the parameters, but its inverse serves as the covariance matrix for the minimized parameter values.[1] Solving this system in Eq. (2.2) without applying model-dependent TPE-corrections to the data, we receive the following parameters in Tab. (2.1):

[1] It's also convenient that the Hessian is the inverse of a covariance matrix, so it must be positive definite, thus we are guaranteed before performing a second derivative test that the extremum point we find is in fact a minimum.

Penalty fit	$i=1$	$i=2$	$i=3$
a_i	0.4153 ± 0.04	-0.2912 ± 0.2	0.1582 ± 0.06
b_i	-0.3989 ± 0.002	0.4038 ± 0.003	-0.1027 ± 0.0006

TABLE 2.1: Fitted parameters of the linear model (Eq. (2.1)) on the 'uncorrected' data using the penalty trick. The covariance matrix for the fit is the inverse of its chi-squares Hessian, the fitted normalizations are found at Tab. (B.1).

	$i=1$	$i=2$	$i=3$	$i=4$	$i=5$
n_i	1.006 ± 0.008	1.003 ± 0.008	0.9596 ± 0.01	0.9788 ± 0.009	0.9989 ± 0.01
	$i=6$	$i=7$	$i=8$	$i=9$	
n_i	1.016 ± 0.01	1.064 ± 0.01	1.005 ± 0.02	0.9948 ± 0.008	

TABLE 2.2: Fitted normalizations for the OPE data fit via the linear model of Gramolin and Nikolenko (via the penalty trick)

2.1.1.2 Fit via the extended t_0 method

For the extended t_0 method, of course using the same data and same model as with the penalty trick fit, we construct $\mathcal{R}$ replica data sets and then build the t_0 chi-square for each replica, constructing a distribution of parameters by minimizing each of the replica chi-squares:

$$\chi^2_{(k),R} = \sum_{i=1}^{\mathcal{N}} \left(n_i^R \sigma_i^R - \mathrm{M}_i\right)^T \left(\mathrm{Cov}_{(k),t_0}\right)_i^{-1} \left(n_i^R \sigma_i^R - \mathrm{M}_i\right). \tag{2.3}$$

There is a lot going on here, so let's break it down. Firstly R is an index standing in to remind us that each n_i^{R} is a randomly sampled scale factor from the normal distribution given by $N(1, \Delta n_i)$ and each σ_{ij}^{R} are similarly built replica data pulled from the normal distribution given by $N(\sigma_{ij}, \Delta\sigma_{ij})$. This is nothing unusual if we are using the Gaussian interpretation of error, since to perform this replication is merely to be honest that the true value of the data in all likelihood is somewhere around the reported value. Secondly with the model of the observable

$$\mathrm{M}(\boldsymbol{\alpha}) = \varepsilon\, G_E^2(\tau;\boldsymbol{\alpha}) + \tau\, G_M^2(\tau;\boldsymbol{\alpha}), \tag{2.4}$$

we identify the model evaluated at the relevant independent variables for the j^{th} data point of the i^{th} experiment with the name

$$\mathrm{M}_{ij} = \mathrm{M}\left(\varepsilon_{ij}, \tau_{ij}; \boldsymbol{\alpha}\right) = \varepsilon_{ij}\, G_E^2(\tau_{ij}; \boldsymbol{\alpha}) + \tau_{ij}\, G_M^2(\tau_{ij}; \boldsymbol{\alpha}). \tag{2.5}$$

When we evaluate this model given the parameters from the k^{th} iteration of the fitting procedure, we call it

$$\mathrm{M}_{ij}^{(k)} = \mathrm{M}\left(\varepsilon_{ij}, \tau_{ij}; \boldsymbol{\alpha}^{(k)}\right). \tag{2.6}$$

When the j index is suppressed, M_i is the vector of model values for the i^{th} experiment. Lastly $\mathrm{Cov}_{(k),t_0,i}$ is the t_0 covariance matrix, built from the k^{th} iteration's parameters as specified in Eq. (1.43). Thus we can see Eq. (2.3) is the chi-square of the R^{th} replica data set, in the fitting procedures' k^{th} iteration.

Building and minimizing the chi-square of each replica data set with the initial guess $\boldsymbol{\alpha}_{(0)}$ gives us a distribution of $\mathcal{R}$ sets of best fit parameters $\boldsymbol{\alpha}_{(1)}^{\mathrm{R}}$, one for each replica. In turn this gives a distribution of $\mathcal{R}$ models, one for each fit to replica data. The model to use in the next iteration, $\mathrm{M}^{(1)}$, will be the average of all the replica model fits:

$$\mathrm{M}^{(1)} = \frac{1}{\mathcal{R}} \sum_{\mathrm{R}}^{\mathcal{R}} \mathrm{M}_{\mathrm{R}}^{(1)} = \frac{1}{\mathcal{R}} \sum_{\mathrm{R}}^{\mathcal{R}} \mathrm{M}(\varepsilon, \tau; \boldsymbol{\alpha}_{\mathrm{R}}^{(1)}) = \mathrm{M}\left(\varepsilon, \tau; \sum_{\mathrm{R}}^{\mathcal{R}} \frac{\boldsymbol{\alpha}_{\mathrm{R}}^{(1)}}{\mathcal{R}}\right) = \mathrm{M}(\varepsilon, \tau; \boldsymbol{\alpha}^{(1)}). \tag{2.7}$$

In the second last equality we have identified that for such a convenient (linear) model,[2] this average model will be the same as the model of the average fit parameters:

$$\boldsymbol{\alpha}^{(1)} = \frac{1}{\mathcal{R}} \sum_{\mathrm{R}}^{\mathcal{R}} \boldsymbol{\alpha}_R^{(1)}. \tag{2.8}$$

It should now be clear how the iterative process works. Plug the current guess for the parameters into the instance of the model in the covariance matrix, generate and minimize each replica chi-square, average over the replica best-fit parameters, and use

[2] In fact, the iterative procedure defined by Ball *et al.* in Ref. [9] is only meaningful on models which are linear in their parameters, otherwise the average model does not have the same functional form as the starting model.

that average as the next guess of the parameters. Continue iterating until the condition

$$\boldsymbol{\alpha}^{(k+1)} = \boldsymbol{\alpha}^{(k)}. \tag{2.9}$$

is met.[3] Ball *et al.* do not provide a proof of convergence for this process, but so long as it *does* converge, then the results of the analysis are sound. After we perform this fitting process, the uncertainties in the final best fit parameters are simply the standard deviations of the final replica distribution for each parameter (in fact the co-variance of any two parameters can be readily found from the co-variance matrix of the total distribution of parameters). This averaging at each iteration also ought to quell any worries about not necessarily fitting the actual data, because the constructed data in combination with the averaging guarantees we are fitting data which has an expected value of the actual original data.

Actually performing this fit now, we begin with a model $M^{(0)}$ where all 6 parameters (remember, the t_0 method has no fitted normalizations) are 0 (this sets the model to the standard dipole), and then 10 iterations were performed of the fitting procedure with $\mathcal{R} = 100$ replica data sets fit each iteration, updating the subsequent guess to be the means of the 100 fitted parameters respectively. 10 iterations was enough to ensure the resultant parameters and the input parameters were essentially the same. The parameters in Tab. (2.3) are the mean and standard deviation of that final six dimensional distribution.

t_0 fit	$i = 1$	$i = 2$	$i = 3$
a_i	0.350 ± 0.20	-0.140 ± 0.44	0.0799 ± 0.23
b_i	-0.404 ± 0.037	0.402 ± 0.054	-0.100 ± 0.023

TABLE 2.3: Fitted parameters of the linear model (Eq. (2.1)) on the 'uncorrected' data using the extended t_0 method. The covariance matrix for the fit is found at Eq. (B.2).

We have found consistent best fit parameters, which correctly take into account the multiplicative normalization uncertainty, without any of the usual biases

[3] In reality we would demand the subsequent guess is sufficiently close to the previous guess, for some definition of sufficiently close.

introduced from breaking our Gaussian likelihood, and all while keeping the fit completely context-free with regards to the fitting procedure used, avoiding the need to carry around the nearly meaningless 'fitted normalizations'. Let us now see how the fits compare.

2.1.1.3 Penalty trick fit vs. extended t_0 method fit

In Fig. (2.1) we can see plots of the various form factor fits.

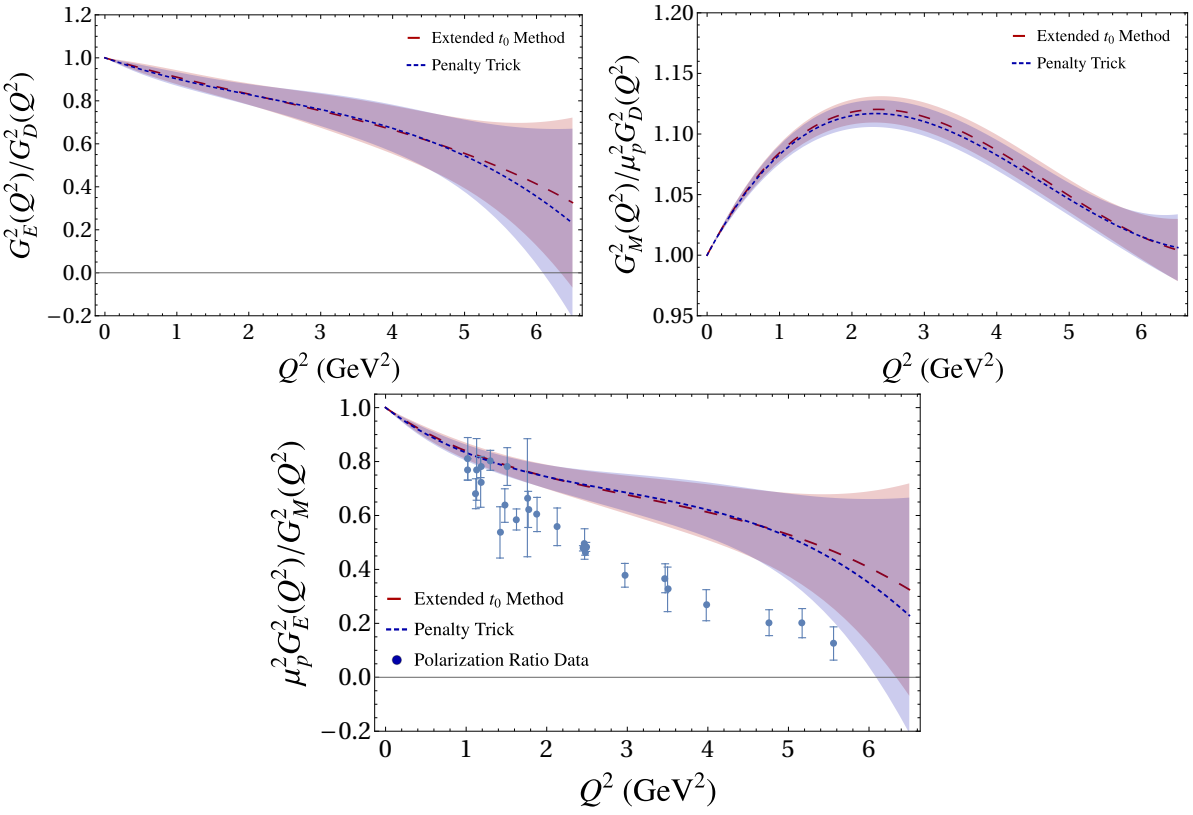

FIGURE 2.1: Fitted square form factors for both the t_0 method and the penalty trick, plotted against one another, and in the case of the form factor ratio, plotted with polarization data with $Q^2 > 1$ (see Tab. (C.2) for these data in a table).

A few things are immediately obvious. Firstly, this is a rather striking endorsement of the quality of the penalty trick as an approximation of the true best fit. The greatest difference appears to be at higher Q^2. Looking at their respective chi-squares:

It is not clear that we can directly compare these χ^2 values, since the chi-square in each case is built rather differently. However given the similarity of the plots, it is

	t_0	penalty
χ^2	58.9	60.0
d.o.f.	79	70

TABLE 2.4: The respective chi-squares and degrees of freedom of the two different fitting procedures: the t_0 method and the penalty trick. Degrees of freedom are computed simply as the number of data points minus the number of free parameters in the fit, hence the 9 floating normalizations decrease the d.o.f for the penalty trick. Important to note is neither of these is the traditional chi-square, both are modifications of it.

clear that they are fitting the data about equally well, and so the very similar chi-squares are likely not a coincidence. We can also realize the extended t_0 method reached a fit of the same quality as the penalty trick, all without the help of the fitted normalizations, which shows they are merely a convenient crutch to approximate the fit using the fully correlated covariance matrix, and they are not physically meaningful on their own. If one truly believes the actual cross section data should be say, 4% smaller, it seems much more appropriate to see if additional corrections achieve this, or to enhance the normalization uncertainty accordingly, rather than scale the whole data set to achieve a better fit.

2.1.2 Analysis on TPE-corrected data

Here an identical analysis is performed as above, but first we apply additional two photon exchange corrections to all the relevant uncorrected cross section data, to work with TPE-corrected data. For the penalty fit, we do as before solving Eq. (2.2), and for the t_0 fit we begin with an initial guess equal to the standard dipole, before fitting the 100 replicas through 10 iterations.

Penalty fit	$i = 1$	$i = 2$	$i = 3$
a_i	0.3715 ± 0.20	-0.01845 ± 0.46	0.1906 ± 0.25
b_i	-0.4250 ± 0.040	0.3859 ± 0.058	-0.09918 ± 0.024

TABLE 2.5: Values of the best-fit parameters for the Gramolin model on the TPE-corrected data using the penalty trick. The fit has a $\chi^2 = 60.1$ with 70 degrees of freedom. The covariance matrix for and fitted normalizations for the fit are found at Eq. (B.3).

	$i=1$	$i=2$	$i=3$	$i=4$	$i=5$
n_i	1.005 ± 0.008	1.003 ± 0.008	0.9586 ± 0.01	0.9781 ± 0.009	0.9987 ± 0.01
	$i=6$	$i=7$	$i=8$	$i=9$	
n_i	1.017 ± 0.01	1.065 ± 0.01	1.005 ± 0.02	0.9945 ± 0.008	

TABLE 2.6: Fitted normalizations for the TPE data fit via the linear model of Gramolin and Nikolenko (via the penalty trick)

t_0 fit	$i=1$	$i=2$	$i=3$
a_i	0.296 ± 0.19	0.114 ± 0.44	0.123 ± 0.24
b_i	-0.430 ± 0.037	0.384 ± 0.055	-0.0963 ± 0.023

TABLE 2.7: Values of the best-fit parameters for the Gramolin model on the TPE-corrected data using the extended t_0 method. The fit has a $\chi^2 = 59.0$ with 79 degrees of freedom. The covariance matrix for the fit is Eq. (B.4).

From the plots in Fig. (2.2) we can see a few things are different now. Firstly, the shapes of the curves are more consistent, and in both cases the error bands are tighter:

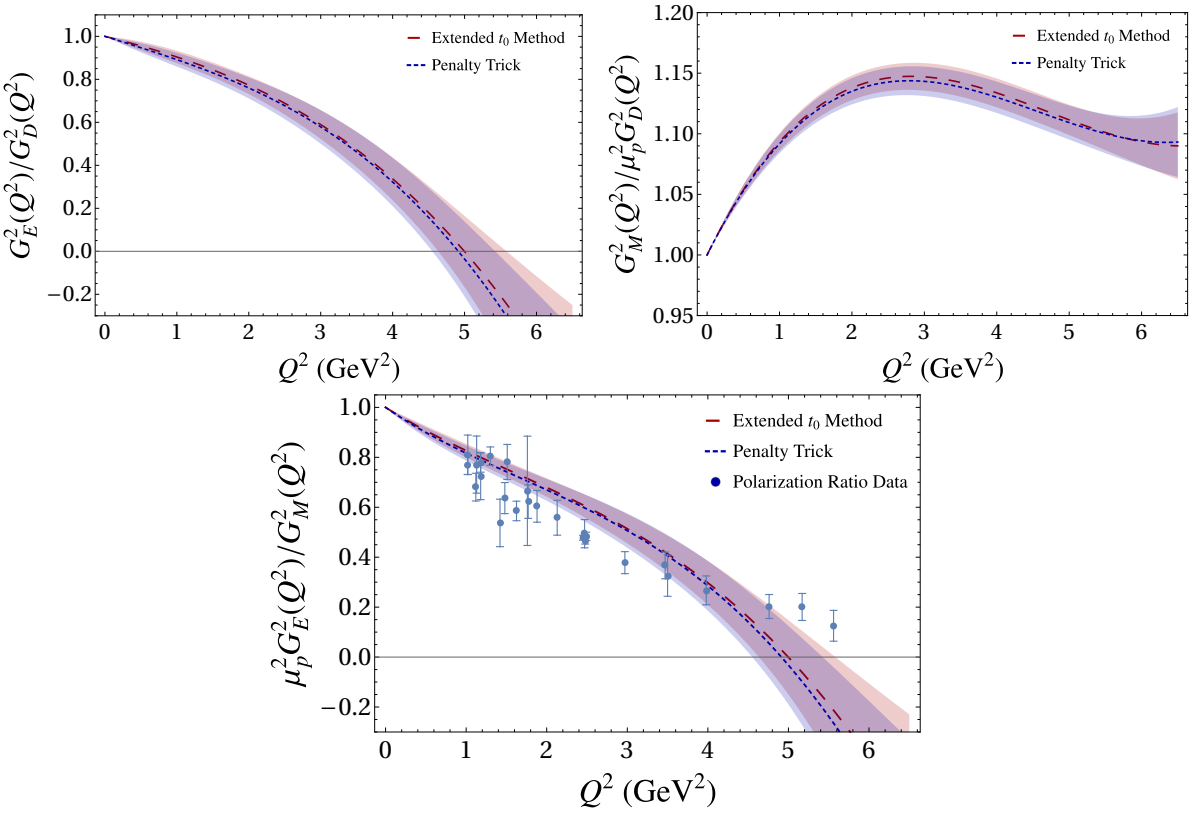

FIGURE 2.2: Fitted square form factors for both the t_0 method and the penalty trick, plotted against one another as well as relevant Rosenbluth extractions, and in the case of the polarization ratio, plotted with polarization data from Tab. (C.2).

the TPE-corrections cause the replica fits to have less variation. Secondly, we can see that the correction has pushed G_E^2 further into the negative for both fits, resulting in unphysical models with negative values for physical quantities which are necessarily non-negative. This has however caused the prediction for the ratio of G_E/G_M to agree far better with the polarization ratio data. The poor quality of the fit at higher Q^2 is directly related to the fact that there is nothing preventing negative squared form factors. What we ought to be doing to remedy this then, is finding more reasonable models of the form factors, so that regardless of the method, the squares of the form factors are non-negative. Unfortunately it is not clear the t_0 method can fit non-linear models, which we now need. The next chapter attempts to address this issue.

2.2 'Unbiased' Rosenbluth extractions of G_E^2 and G_M^2 via LT data

One of the more useful applications of the unbiased fitting, is the ability to stop worrying about the fitted normalizations, and hence what to do if one wishes to fit something *again* to the previously fitted data. For example, in their paper, Ref. [8], the GMp12 group perform Rosenbluth extractions to several binned sets of data with the help of some interpolations – this is all well and good. However, due to the fact it is well known that mistreatment of normalization uncertainties may lead to useless results, and since it is not clear how to continue combining normalization uncertainties via the penalty trick after fitted normalizations have been applied, the collaboration was forced to only have bins consisting of at most one point from any one experiment. This makes the analysis extremely limiting. The extended t_0 method has no such problem. The fits may be carried out in exactly the way prescribed above, only at constant Q^2 and fitted to a linear function of ε. So long as the covariance matrices and chi-square are correctly constructed and minimized, we may combine data in any fashion we desire.

For simplicity's sake, let us fit to only the data from Andivahis [1]. There are 5

Q^2 values for which there are more than 2 data points, which will give 5 Rosenbluth extractions of G_E^2 and G_M^2. At each of these Q^2 values, all but one data point is from the 8 GeV spectrometer data, dubbed 'Andivahis$_1$', and so each chi-square looks like a matrix inner product with the 8 GeV data, plus the single chi-square term for the single 1.6 GeV data. The model of course looks like

$$\mathrm{M} = c\,\varepsilon + d, \tag{2.10a}$$

$$c = G_E^2, \tag{2.10b}$$

$$d = \tau G_M^2. \tag{2.10c}$$

Fitting to each of the 5 subsets of data, by constructing 100 sets of replica data for each of 10 iterations of the extended t_0 method, we find the extractions in Tab. (2.8), shown in next to fits to the Andivahis data in Fig. (2.3). We perform the same analysis via the penalty trick in order to contrast the results with the more common technique.

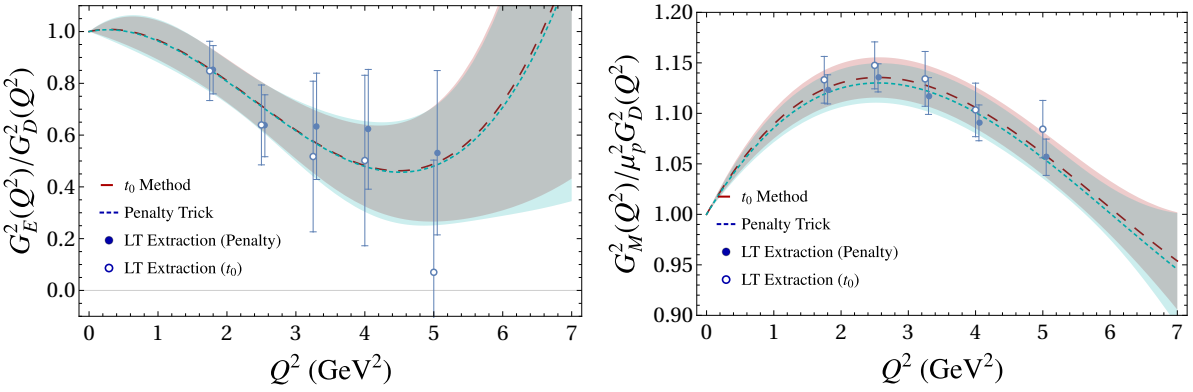

FIGURE 2.3: Rosenbluth extractions of 'Uncorrected'-LT data from Ref. [1] via the two fitting methods, plotted with fits of the linear model used by Gramolin *et al.* to the Andivahis data. The unbiased results are completely blind to any other fits while the penalty trick relies on the fitted normalizations being applied before extraction.

Q^2 GeV^2	1.75	2.50	3.25	4.00	5.00
$G_M^2/\mu_p^2 G_D^2$	1.133 ± 0.023	1.148 ± 0.023	1.134 ± 0.027	1.103 ± 0.026	1.084 ± 0.028
G_E^2/G_D^2	0.85 ± 0.11	0.64 ± 0.15	0.52 ± 0.29	0.50 ± 0.33	0.07 ± 0.43

TABLE 2.8: Rosenbluth extractions via the extended t_0 method.

To get a better view of whats happening in each fit it is useful to plot the linear fits themselves:

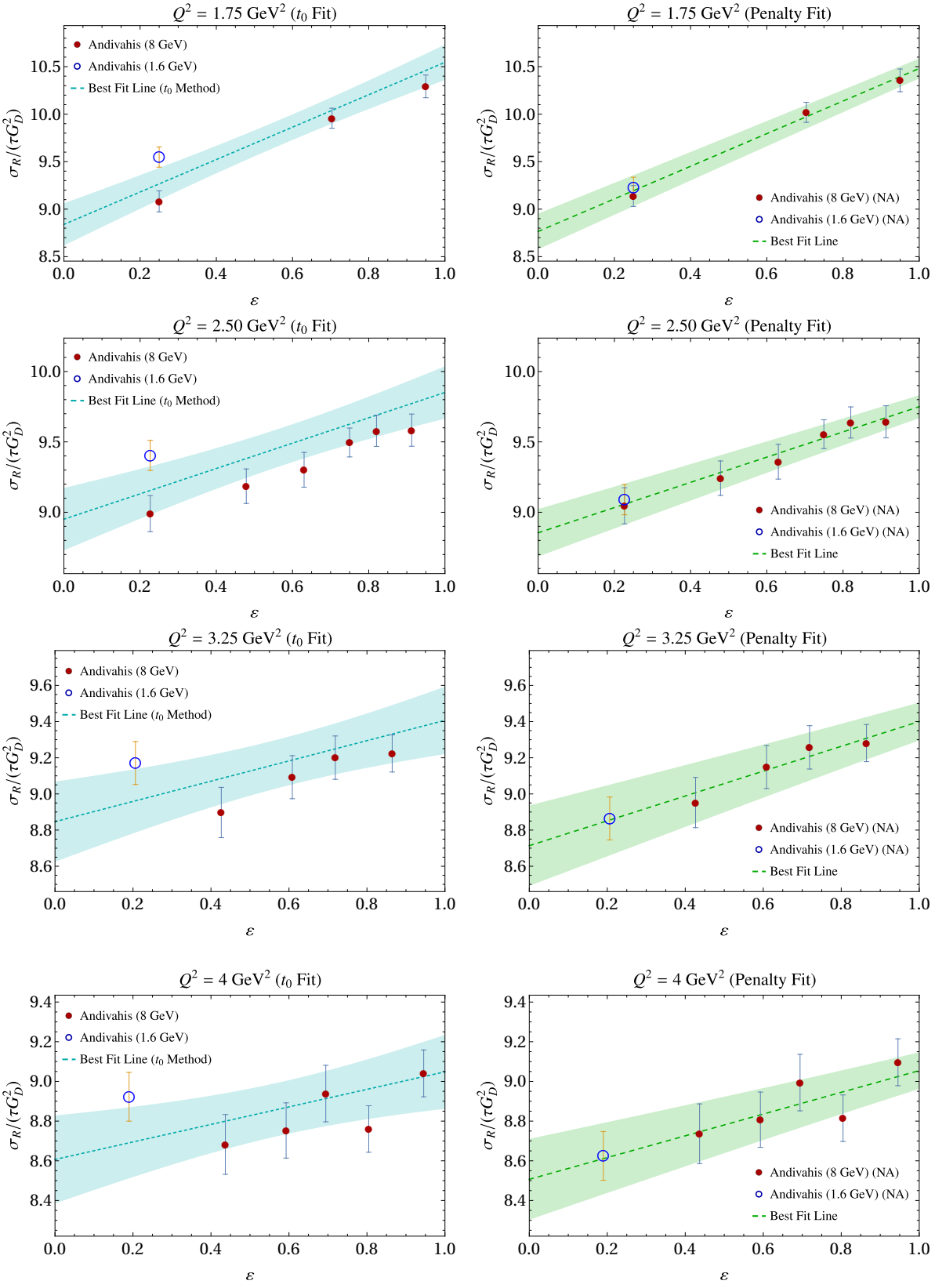
Q^2 = 1.75 GeV^2 (t_0 Fit)
Q^2 = 1.75 GeV^2 (Penalty Fit)
Q^2 = 2.50 GeV^2 (t_0 Fit)
Q^2 = 2.50 GeV^2 (Penalty Fit)
Q^2 = 3.25 GeV^2 (t_0 Fit)
Q^2 = 3.25 GeV^2 (Penalty Fit)
Q^2 = 4 GeV^2 (t_0 Fit)
Q^2 = 4 GeV^2 (Penalty Fit)
Andivahis (8 GeV)
Andivahis (1.6 GeV)
Best Fit Line (t_0 Method)
Andivahis (8 GeV) (NA)
Andivahis (1.6 GeV) (NA)
Best Fit Line
$\sigma_R/(\tau G_D^2)$
ε

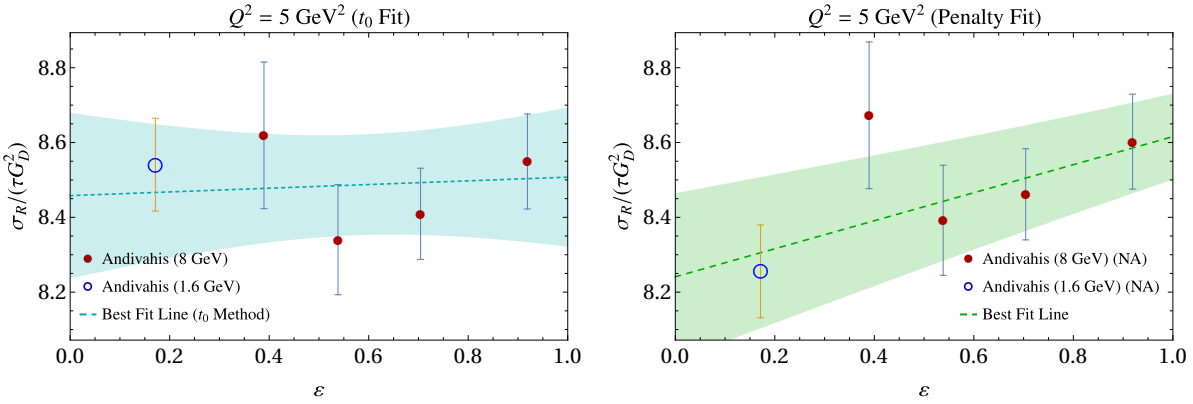

FIGURE 2.4: Rosenbluth extractions for the relevant Q^2 values. The left hand side utilizes the extended t_0 method in order to extract the slope and intercept while taking the normalization uncertainty into account. The right hand side utilizes a traditional linear best fit, after which the fitted normalizations have been applied to the data ('NA' = 'Normalizations Applied'). We can see that the results are largely in agreement except at $Q^2 = 5$ GeV^2.

This is potentially the best example of the 'over-fitting' the penalty trick does. By allowing for the shifts in floating normalization factors, the fact that the data set's strain to be simultaneously fit is shrouded. The mismatch of LT extractions and the overall fit for the t_0 case is not an accident, it is surely caused by an improper treatment of normalization uncertainties. Furthering a point made by Bernauer [7], Rosenbluth extractions are not particularly helpful for fitting in general, since all of these Rosenbluth extractions are correlated by the overall normalization uncertainty of the total data sets, and thus for individual Rosenbluth extractions, it is not clear how to maintain this covariance after or during extraction. That is to say, a global fit is more useful, because the total covariance matrix can be built at each point, whereas a Rosenbluth extraction is forced to focus on a subset of the data, and as such the ability to fit one subset of data, has no bearing on another fit's ability to fit another subset of the data, even though these data are correlated. The reason the 5 GeV^2 slope is so low, is likely due to the fact that the Rosenbluth extraction cannot take the entire covariance matrix into account. This is also why the penalty fit Rosenbluth extractions are not particularly useful either. By virtue of being scaled by the fitted normalizations, they are rather constructed to look like the fitted function, and so no information is gained which is not already contained in the penalty fit.

Chapter 3

Extending the t_0 Method: Directly Modeling G_E and G_M

The main concern which emerges when switching to more direct models of the form factors, is that the t_0 method is only clearly defined for models of observables which are linear in their parameters. Fitting each replica data set Y_i gives us a vector of fit parameters $\boldsymbol{\alpha}_i$, and a replica best fit $f_i = f(x; \boldsymbol{\alpha}_i)$ to the replica data. Then, the best fit to the original data will be the average over all the replica fits:

$$f_{\text{best}} = \bar{f}_i = \frac{1}{N} \sum_i^N f_i. \tag{3.1}$$

where the overline stands for the mean of the value it sits on. If and only if f is linear then

$$f_{\text{best}} = \bar{f}_i = f(x, \bar{\boldsymbol{\alpha}}). \tag{3.2}$$

The first equality is always true for the t_0 method, but the second equality is only true in general when f is linear in $\boldsymbol{\alpha}$. That is to say, only when the model f is linear in the parameters, does the best fit model (the average of the fits) align with the model evaluated at the average parameters. This is a problem for us, because we want to continue to use the same model each time the t_0 method iterates, and in general an

average of non-linear functions will not have the same functional form as each function itself. For example take two quadratic models, f and g, where the former is linear in its parameters and the latter is quadratic in its parameters:

$$\begin{aligned} f(x,\boldsymbol{\alpha}) &= mx^2 + px + b \qquad \boldsymbol{\alpha} = \{m,p,b\}, \\ g(x,\boldsymbol{\beta}) &= (ax+c)^2 \qquad\qquad \boldsymbol{\beta} = \{a,c\}. \end{aligned} \tag{3.3}$$

Suppose we perform two replica fits, resulting in two sets of parameters for the above models: $\boldsymbol{\alpha}_i, \boldsymbol{\beta}_i, i = 1,2$. The statistical best fit in both cases, will be the average of those two fits $\bar{f} = (f_1 + f_2)/2$ and $\bar{g} = (g_1 + g_2)/2$ of course. Expanding these out we can see the issue with the non-linear model:

$$f_{\text{best}}(x,\boldsymbol{\alpha}) = \frac{m_1+m_2}{2}x^2 + \frac{p_1+p_2}{2}x + \frac{b_1+b_2}{2} = \bar{m}x^2 + \bar{p}x + \bar{b} = f(x,\bar{\boldsymbol{\alpha}}), \tag{3.4a}$$

$$g_{\text{best}}(x,\boldsymbol{\beta}) = \frac{a_1^2+a_2^2}{2}x^2 + 2\frac{a_1c_1+a_2c_2}{2}x + \frac{c_1^2+c_2^2}{2} \neq g(x,\bar{\boldsymbol{\beta}}), \tag{3.4b}$$

where

$$\bar{\boldsymbol{\alpha}} = \{\frac{a_1+a_2}{2}\}, \quad \bar{\boldsymbol{\beta}} = \{\frac{b_1+b_2}{2}\}. \tag{3.5}$$

We can see that for the linear model the best fit coincides with the average parameter fit; this is decidedly not the case for the non-linear model. For simple models there is usually a simple way out of the problem. Given the model of the average parameters:

$$g_{\text{avg}} = g(x;\bar{\boldsymbol{\alpha}}) = \frac{a_1^2+a_2^2+2a_1a_2}{4}x^2 + 2\frac{a_1c_1+a_2c_2+a_1c_2+a_2c_1}{4}x + \frac{c_1^2+c_2^2+2c_1c_2}{4}. \tag{3.6}$$

we can rearrange things to find the best fit model in terms of the average model plus something like a 'correction':

$$g_{\text{best}} = \bar{g} = Ng_{\text{avg}} - \frac{2a_1a_2}{N}x^2 - 2\frac{a_1c_2+a_2c_1}{N}x - \frac{2c_1c_2}{N}, \qquad N = 2, \tag{3.7}$$

which lends itself to the general form for averaging many replica fits:

$$g_{\text{best}} = Ng_{\text{avg}} - \frac{1}{N}\left(\sum_{i\neq j}^{N}\left[a_ia_jx^2 + 2a_ic_jx + c_ic_j\right]\right). \tag{3.8}$$

This does not really solve the issue at hand though. While it is nice to have a relationship between the *best* and the *average parameter* fits, this result is of course entirely specific to the function chosen for our example, and even if we can build this relationship for any function, it does not deliver us parameters of the best fit $\{a_{\text{best}}, c_{\text{best}}\}$, which we are in dire need of in order to keep our functional form the same throughout the fitting, and in order to extract uncertainties for the final fits. We may try instead to derive some formula for the best fit parameters; a good guess in this example would seem to be that perhaps:

$$\{a_{\text{best}}, c_{\text{best}}\} \stackrel{?}{=} \{\sqrt{\frac{a_1^2 + a_2^2}{2}}, \sqrt{\frac{c_1^2 + c_2^2}{2}}\}. \tag{3.9}$$

While this assignment of parameters matches the x^2 and constant coefficients of the best fit, the x coefficients must also equal, which unfortunately is not true in general:

$$c_1 a_1 + c_2 a_2 \neq \sqrt{\frac{a_1^2 + a_2^2}{2}} \sqrt{\frac{c_1^2 + c_2^2}{2}}. \tag{3.10}$$

This is a rather sobering no-go point for the quadratic model, and the more one explores non-linear models the more one will find these impossible constraints like Eq. (3.10) popping up everywhere. We are forced to accept that even for a function as reasonable as a quadratic, there is in general no assignment of parameters $\boldsymbol{\alpha}_{\text{best}}$ for which we can build a model $g(x, \boldsymbol{\alpha}_{\text{best}})$ which is equal to the function that is the best-fit to the data (the average of the fits of the replicas $\bar{g}_i$). Another way to say this is that in general, the average of the fits $\bar{g}_i$, simply cannot be massaged into a form that looks like g. It should be clear why this is true for linear functions but not others – it is no surprise that sums of linear functions are linear, but it would be quite the miracle for the sum of 100 randomly distributed squares of linear functions (as g is in Eq. (3.4b)) to be able to be written as the square of a linear function.

What are we to do then? There appear to be two options: the first option is to continue to use the average parameter guess as in the linear case, understanding that convergence of the t_0 method will generally take longer, potentially never converging

at all if the best fit function does not look like the average parameter fit – the second option is to find the parameters $\boldsymbol{\alpha}_{\text{closest}}$ of the model g for which g most closely resembles the behaviour of $\bar{g}_i$. The remainder of this thesis uses the first option, because it is far less computationally expensive, and worked generally well for the relevant models.[1] However, it is worth noting progress towards the end of option two, so it may be explored further in future work.

3.1 The closest model to the best fit

One first has to ask what it means for two functions to be 'close' within some range. For this an intuition seems clear: the measure of closeness may be the absolute vertical distance between the two functions, integrated over the relevant range. This measure will be 0 if the two functions are identical, small if they look similar, and large if they rapidly diverge. Perhaps one could add similar penalty's to the functions derivatives, but as far as a measure to minimize, this seems reasonable as is. With some particular functional form for the model $F(x, \boldsymbol{\alpha})$ and an average of replica fits $f_{\text{best}} = \bar{f}_i$, we can build the following integral to minimize:

$$\int_{x_{\min}}^{x_{\max}} \left|F\left(x, \boldsymbol{\alpha}\right) - \bar{f}_i\right| \mathrm{d}x. \tag{3.11}$$

This integral is also known as the L^1 norm of the function $\left(F\left(x, \boldsymbol{\alpha}\right) - \bar{f}_i\right)$. The goal now would be to minimize the L^1 norm of this difference by solving for optimal fit parameters $\boldsymbol{\alpha}$. This corresponds to the set of differential equations:

$$\begin{aligned} &\frac{\partial}{\partial \boldsymbol{\alpha}} \int_{x_{\min}}^{x_{\max}} \left|F\left(x, \boldsymbol{\alpha}\right) - \bar{f}_i\left(x\right)\right| \mathrm{d}x = \mathbf{0} \\ \overset{?}{\Rightarrow} &\int_{x_{\min}}^{x_{\max}} \frac{F\left(x, \boldsymbol{\alpha}\right) - \bar{f}_i\left(x\right)}{\left|F\left(x, \boldsymbol{\alpha}\right) - \bar{f}_i\left(x\right)\right|} \cdot \frac{\partial F(x; \boldsymbol{\alpha})}{\partial \boldsymbol{\alpha}} \mathrm{d}x = \mathbf{0}. \end{aligned} \tag{3.12}$$

[1] Occasionally fits entered something of a loop, never converging. However this could be remedied by altering the initial parameter guess.

In practice these integrals will often not be solvable analytically, and the existence of unknown parameters cause numerical integration to work poorly or not at all. A way around this would be to use something like a swarm or gradient descent optimization procedure, which guesses some family of initial values for $\boldsymbol{\alpha}$ so that the numerical integration may be carried out, and then hopefully the family of guesses iteratively converges on those values of $\boldsymbol{\alpha}$ which minimize the L^1 norm. The only issue with the latter method is the usual issue with numerical minimization – ending up with a local minimum instead of the global minimum. Usually this can be remedied easily by expanding the search domain. The second line of Eq. (3.12) is left questionable, because while it is enticing to have the ability to change the integrand in the case of running into a function with no anti-derivative, it leaves us in the rather uncomfortable situation where we must start off with the assumption that the model $F \neq \bar{f}_i$ lest we divide by 0. Another problem with the second form is that for good approximations the denominator and numerator will be subject to catastrophic cancellation (see Ref. [16]), leaving their quotient unwieldy as well. One could replace this realizing the quotient is simply the sign(x) function, but this is no help either because the sign of that difference will still be relatively numerically sensitive to floating point rounding errors. We are generally forced to perform the fit in the order prescribed via the first line above if we wish to be able to achieve linear fits, or avoid numerical non-sense on the rare occasion $\bar{f}_i$ can be fit exactly with some F.

All this, in addition to the glaring fact that the integrand is not smooth in general even when $\bar{f}_i$ and F are smooth, may cause us to believe this problem to be intractable and its solution not worth pursuing. But perhaps it is only our choice of measure of closeness that is the problem. A familiar yet still reasonable measure for our idea of closeness, which keeps smooth functions smooth, is the L^2 measure:

$$\sqrt{\int_{x_{\min}}^{x_{\max}} \left(F\left(x, \boldsymbol{\alpha}\right) - \bar{f}_i\right)^2 \, \mathrm{d}x}. \tag{3.13}$$

When it comes to minimization, we may throw away the square-root since we are not interested in the measures actual value, only in minimizing it, and the minimum of a

positive definite function is also the minimum of its square. The minimization problem for the L^2 measure is then:

$$\frac{\partial}{\partial \boldsymbol{\alpha}} \int_{x_{\min}}^{x_{\max}} \left(F\left(x, \boldsymbol{\alpha}\right) - \bar{f}_i\right)^2 \, \mathrm{d}x = 2 \int_{x_{\min}}^{x_{\max}} \left(F\left(x, \boldsymbol{\alpha}\right) - \bar{f}_i\right) \cdot \frac{\partial F(x; \boldsymbol{\alpha})}{\partial \boldsymbol{\alpha}} \, \mathrm{d}x = \mathbf{0}. \quad (3.14)$$

The situation we find ourselves in here is rather preferable to the L^1 case: we have two integrals to play with in the case of a lacking anti-derivative, and a setup that is not so fraught with potential numerical issues. Not only this, but we can also see the integrand is something of a continuous analog to the numerator of a chi-square. Because of this, we should expect L^2 minimized F's to do a better job at replicating minimum chi-square fits than any L^1 minimized F's (L^1 minimized functions would however do a better job at replicating minimum absolute error fits). Have we lost anything in going from L^1 to L^2? The answer to that question is generally, no. The next example attempts to illustrate the difference between the minimization schemes, but the takeaway is that L^1 minimized fits are more forgiving to the existence single large divergences that quickly return to being a close fit, while L^2 fits are more forgiving to fits having many smaller deviations from the best function.

3.1.1 Example of L^1 vs. L^2 sensitivity to outliers

Below in Fig. (3.1) are plots of a function[2] (solid blue) emulating a mean of replica fits $\bar{f}_i$, alongside two 'nearby' functions in large-dashed green (plot begins on Fig. (3.1a) and continues zoomed in on Fig. (3.1b)) and dashed orange (plot begins on Fig. (3.1c) and continues zoomed in on Fig. (3.1d)), which serve as 'F's we intend to compare the closeness of to '$\bar{f}_i$', on the range of $\left[\frac{1}{4}, 65\right]$.

If one computes the L^1 measures of the green 'F' and orange 'F' against the solid blue '$\bar{f}_i$', one finds that the green function is the function which is the closer of the two 'F's:

$$L^1\left[b(x) - g(x)\right] = 10.0, \qquad L^1\left[b(x) - o(x)\right] = 11.1, \quad (3.15)$$

[2] the actual functions are not so important, the lesson they deliver is.

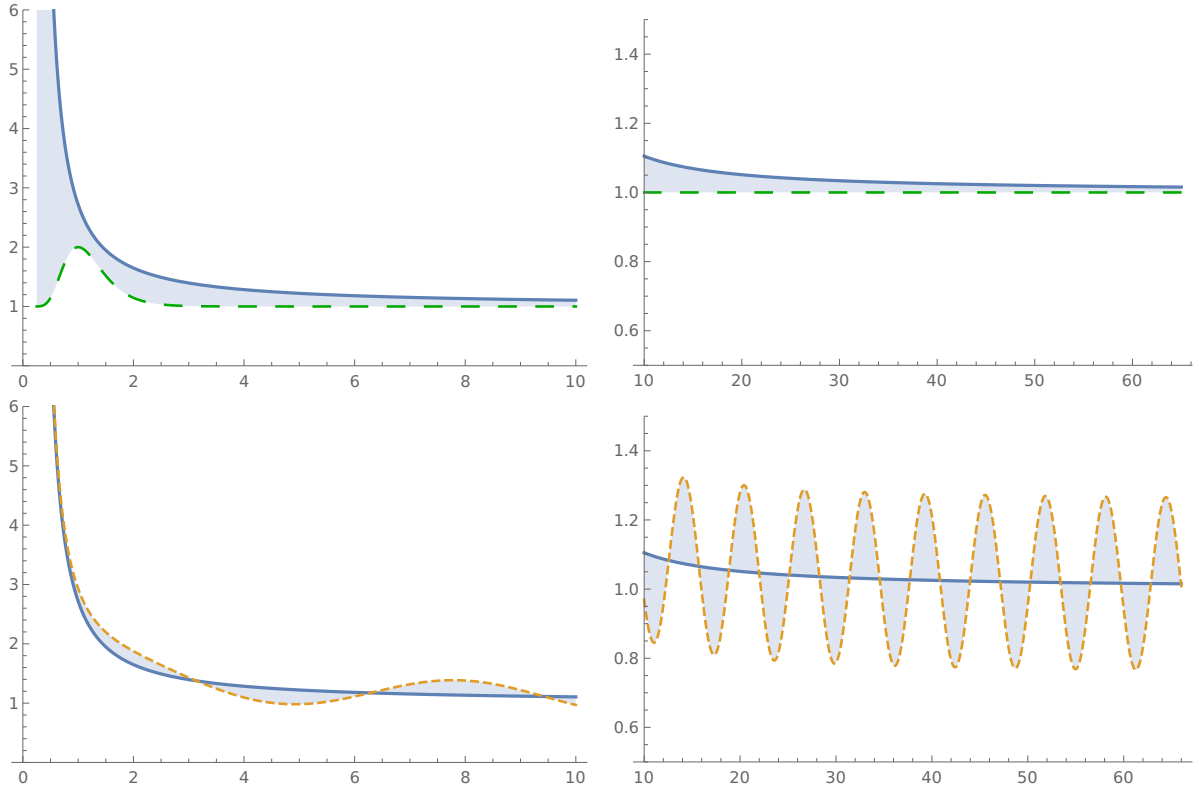

FIGURE 3.1: In both parts of this example we are comparing to the same function $b(x)$ (solid blue) on the range $\left[\frac{1}{4}, 65\right]$. The green large-dashed function $g(x)$ in subfigures (a) and (b) has the same asymptotic behaviour as $b(x)$ in the limit $x \to \infty$, but the functions diverge as $x \to 0$. The orange dashed function $o(x)$ in subfigures (c) and (d) has the same asymptotic behaviour as $b(x)$ in the limit $x \to 0$, but otherwise oscillates around $b(x)$ periodically, keeping the difference between the functions regular but small. This demonstrates the trade-off when choosing between the two measures L^1 and L^2, one must decide if a single divergence should be more or less penalizing than many small deviations: $L^1\left[b(x) - g(x)\right] < L^1\left[b(x) - o(x)\right]$ yet $L^2\left[b(x) - g(x)\right] > L^2\left[b(x) - o(x)\right]$.

which matches our intuition, at least certainly so after $x = 1$. However if one computes the L^2 measures of the two functions, one will discover that

$$L^2\left[b(x) - g(x)\right] = 10.9, \qquad L^2\left[b(x) - o(x)\right] = 1.5. \tag{3.16}$$

Not only has the brief but large difference in the green and blue functions on $x \in \left[\frac{1}{4}, 1\right]$ been amplified, but the small regular differences between the orange and blue functions have been muted. Of course this is rather crafted example, it would be rare for a single form for a model to produce such varied looking 'F's. But the point

remains that generally the measures won't agree about the ordering of closeness of functions: the L^2 measure is far less forgiving about brief outlying ranges of differences in the functions, but it is far more forgiving to functions which may vary quite a bit while generally sticking to an envelope of the underlying function – vice versa for L^1. Physics considered, we are probably okay with the strict penalties the L^2 measure places on rapid divergences, as it is rare for these to be physical, and the asymptotic behaviour of a system is usually the most well understood behaviour, so we would like to keep it in check. Of course as mentioned previously the L^2 measure is also better at producing fitted functions which will minimize a chi-square, which is what physicists are in the business of doing.

3.1.2 Example of L^2 minimization vs averaging minimization

In this section we will see that a watchful eye can prevent us from having to deal with the mess of minimizing messy L^2 integrals, and we will be able to continue fitting as usual. Modifying our example g above from Eq. (3.4b), and setting our generic model to $(ax+b)^2+1$ we can simulate data sets taken from the specific function $(0.9x-0.4)^2+1$, and perform two t_0 fitting procedures: in the first the iterated guess is the average of the parameters of all the best fits as usual, and in the second the iterated guess is the L^2 minimized parameters from solving Eq. (3.14). What we find at first is rather alarming.

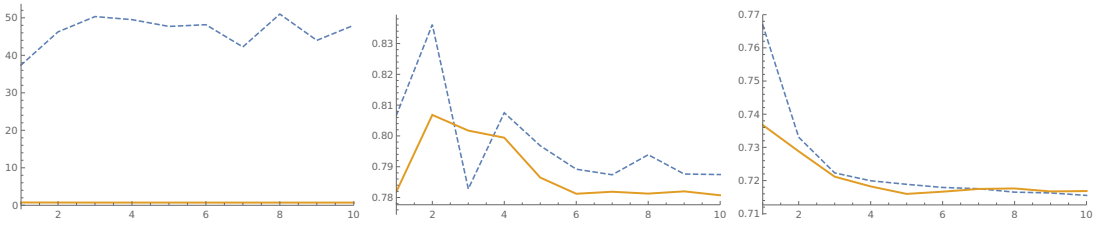

FIGURE 3.2: Three plots of the χ^2 *vs iteration* for each of the two t_0 methods: L^2 minimized iteration (solid orange) and average parameter iteration (dashed blue). The first figure is the generic fitting process. The second figure is the fitting process with an enforced sign convention. The third is an average of many plots like the second sub-figure. Without taking into account ambiguities present in the model – and the multiple solutions which come with them – naively averaging parameters can lead to poor estimates. Accounting for this however leads to near-ideal performance as seen in sub-figures (b) and (c).

In Fig. (3.2a) we can see the effect on the chi-square of performing the L^2 iteration against the average parameter iteration. For this simple non-linear model the average parameter iteration gives a guess that is completely wrong, never converging on the correct result, while the L^2 iteration hones in on parameter values which minimize the chi-square almost immediately. Where does the parameter averaging go so wrong? The answer to this is in the model's ambiguity: notice that inside the square, only the relative sign between a and b matters, not the absolute signs. Because of this, a fitting program will often bifurcate the fitted parameters of the replica data around $\boldsymbol{\beta} \approx \{0.9, -0.4\}$ and around $\boldsymbol{\beta} \approx \{-0.9, 0.4\}$ both of which are good fits. When we average these parameters, we will always find mean-parameters very close to 0. This is the case of Fig. (3.2a). It is also clear why no amount of iterating will ever allow the fit to improve, because the issue appears every time we average to build the next iteration.

Recognizing this we may choose a convention before hand, for example: if a fit produces two parameters with the same sign, force both to be positive, and if they have a relative sign difference, force a to be positive. Implementing this sign convention ensures the fit parameters do not undergo a bifurcation, and as we can see in Fig. (3.2(b-c)) completely restores the fitting capabilities of the average parameter method, which makes fitting far less computationally expensive for complicated models and many replicas.

We have established that the t_0 method wherein one plugs in the model evaluated on the average parameters can still work even for non-linear models, and that in cases of slow convergence or ill-behaved averaging we may resort to L^2 minimization to build our iterated best fit. With all this out of the way there is one last piece of this ordeal which is left uncertain: what does one do when L^2 fitting simultaneous data sets which constrain the same parameters but which are modelled differently? For example, when fitting nucleon form factors with cross section data and polarization data simultaneously, we may wish to perform an L^2 minimization to extract the best fit parameters, but we have two different models on hand – which one should we

minimize to build our model which is closest to the best fit? Do we simply minimize the sum of the two L^2 measures, perhaps with some weighting factors? This question remains unanswered for the time being. Luckily, we'll find that the average parameter approach works for the remainder of this thesis, even when incorporating two kinds of data, so we never find ourselves in need of an answer to this question, but surely an answer can and should be found eventually. With all this out of the way we may finally focus on the most important aspect of data fitting: choosing a good model.

3.2 The z-expansion model

A flexible model for the form factors is the so-called z-expansion model, of which there is a good dissection in Lee *et al.* [18]. The model is as follows:

$$G_E\left(Q^2\right) = \sum_{k=0}^{k_{\max}} a_k z^k, \tag{3.17a}$$

$$G_M\left(Q^2\right) = \sum_{k=0}^{k_{\max}} b_k z^k, \tag{3.17b}$$

$$\text{with} \quad z\left(t, t_{\text{cut}}, t_0\right) = \frac{\sqrt{t_{\text{cut}} - t} - \sqrt{t_{\text{cut}} - t_0}}{\sqrt{t_{\text{cut}} - t} + \sqrt{t_{\text{cut}} - t_0}}. \tag{3.17c}$$

Where a_k and b_k are the free parameters of the model. Figure (3.3) is from Ref. [17], the article wherein the model originated, and shows how the change of variables maps

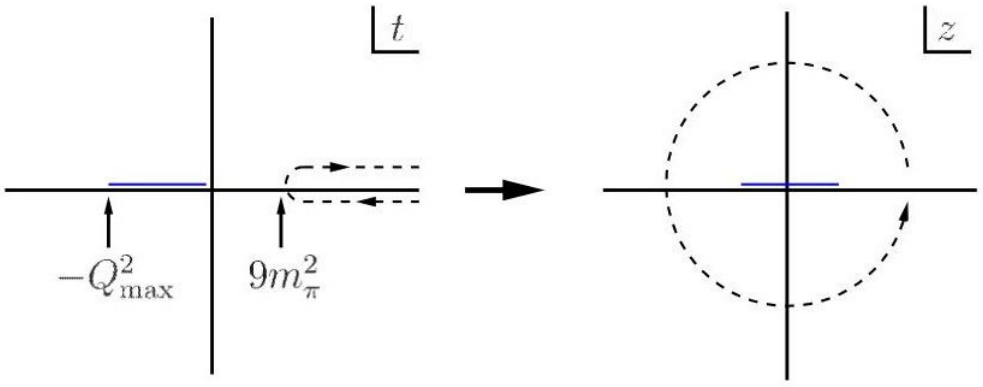

FIGURE 3.3: Conformal mapping of the cut-plane to the unit circle, taken from Ref. [17].

from the Mandelstam variable $t = -Q^2$, to the new variable z. This model ensures the form factor is always analytic when Q^2 is real.

In the example given, t_{cut} corresponds to $9m_\pi^2$ (chosen so that the form factor would be analytic up to the 3 pion production threshold), and t_0 corresponds to which value on the t axis is mapped to $z = 0$. In all fits invoking the z-expansion model, we use the following values for the parameters t_{cut} and t_0 (that is to say they are never involved in a fitting procedure):[3]

$$t_{\text{cut}} = 9m_\pi^2 \approx 9\,(0.14\ \text{GeV})^2, \tag{3.18a}$$

$$t_0 = t_{\text{cut}}\left(1 - \sqrt{1 + \frac{1\text{GeV}}{t_{\text{cut}}}}\right) \approx -0.279\ \text{GeV}^2. \tag{3.18b}$$

Another appealing feature of the z-expansion model, is the ability to encode correct QCD scaling laws for the form factors in the large momentum limit. The Sachs form factors have been shown, according to chromodynamical arguments (see Ref. [6]), to fall off as $1/Q^4$ (up to terms involving logs of Q^2). As shown in Ref. [18] this condition is equivalent to the coefficients being subject to the following sum rules

$$\sum_{k=n}^{k_{\max}} \frac{k!}{(k-n)!} a_k = 0, \quad n = 0, 1, 2, 3, \tag{3.19}$$

and the same for b_i of G_M. Choosing $k_{\max} = 8$ gives us nine parameters total for each form factor, four of which in either case are constrained by the sum rules. Additionally $a_0[b_0]$ is constrained by the fact $G_{p[n]}(0) = 1[\mu_p]$. This leaves 4 free parameters for each form factor, 8 in total. With all this machinery in place we are ready to fit the 'uncorrected' and TPE-corrected data in order to compare with the linear models of chapter (2), and see if non-linear models generally improve our fits.

[3] See Ref. [17] for where these meta parameters come from. We did not find much variability in the fitting ability while fiddling with these meta parameters of the model, as such these choices merely stuck around as the fitting carried on, there is nothing particularly special about them.

3.3 Nuances of non-linear fitting

Since we are committed to non-linear fitting, we can compare the extended t_0 method against the improved penalty trick from Eq. (1.32). In fact, this typically leads to more reasonable fits, and fitting with the first penalty trick gives a great example of the effects of ambiguity in non-linear fitting. If one fits with the z-expansion model as prescribed above, and builds the first penalty trick with 9 normalization parameters, the fits for G_M become rather surprising, as seen in Fig. (3.4).

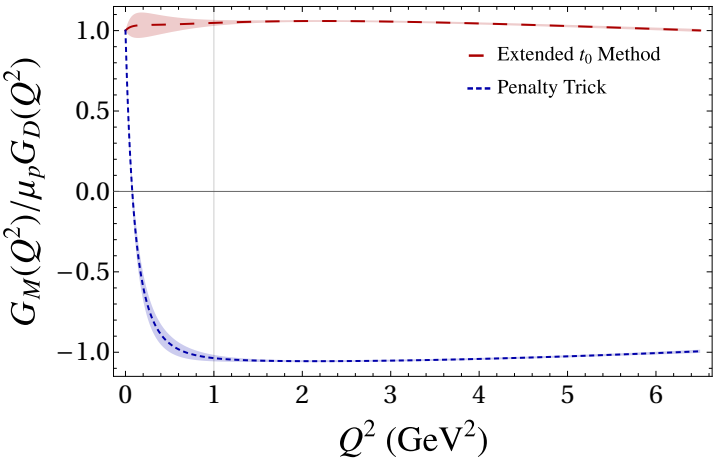

FIGURE 3.4: Fits of G_M to 'uncorrected' data. The non-linearity of the model allows the fits to bifurcate into mirrored sections, while still constraining both form factors to be 1 at $Q^2 = 0$.

This behaviour is possible for a few reasons. Firstly and most importantly, the cross section depends only on the square of the form factors. This means the fits can bifurcate, having identical behaviours differing only by a sign. One may imagine forcing the form factor to be appropriately normalized at $Q^2 = 0$ would avoid this, but as we can see if the model is flexible enough it can get around this. The final reason this is possible is that the data we are using stops at $Q^2 = 1$, so there is no punishment for the steep behaviour at lower Q^2. If we include polarization ratio data in the fit, this issue subsides, as the fit will need to pass through the polarization data as well, putting everything back in place. These kinds of fits are possible for all the fitting procedures we have seen so far, so it is good to be wary of them.

Additionally, as this our first non-linear model fit, we ought to verify the t_0 method actually has converged on a minimum and that we have not merely landed on a convenient iteration of the fitting procedure.

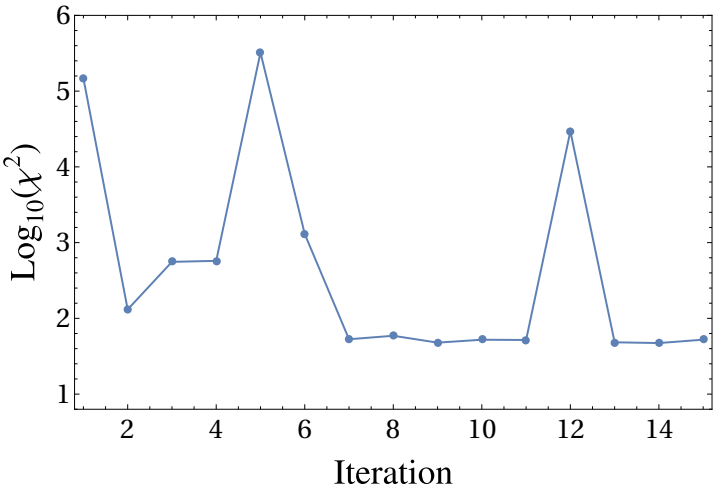

FIGURE 3.5: Convergence of the t_0 chi-square for the above z-expansion model fit to 'uncorrected' data. We can see that unlike in the linear case, we cannot necessarily expect convergence in as quickly as three iterations as in Ref. [9], though the convergence can still be relatively quick and reliable. At the twelfth iteration the fit is 'perturbed' by choosing a sub-optimal local minimum of the chi-square to demonstrate the perils of non-linear fitting.

We can see that while the chi-square is by no means guaranteed to be monotonically decreasing, and may take a few more iterations than the linear case, the fit certainly does converge upon a best fit. One thing to watch out for with non-linear models is the existence of multiple local minima for the 'minimum' chi-square to fall into, especially because most global solvers (such as Mathematica's `NMinimize`) resort to local solvers when the problem is non-linear. In Fig. (3.5) at the 12^{th} iteration, a larger local minimum was intentionally chosen to display how the convergence of a fit can be thrown off by the sub-optimal minima being found. If one iteration in the chi-square finds a much larger local minimum, the whole fitting process is essentially reset. The best way to avoid this is to use multiple different minimization techniques, and pick the minimum solution found each time. The penalty trick is not immune to this, as the greater number of parameters results in most minimization schemes finding a sub-optimal local minimum, so one has to be careful not to blindly trust their

algorithms. One last important note to make is that for the non-linear penalty trick fits, the inverse of the Hessian is only approximately the correct covariance matrix of the fit, since it depends on all the parameters. As such the covariance matrix of the fit is taken to be this inverse Hessian, evaluated at the best fit parameters. One could acquire a more correct covariance matrix by performing the penalty trick on many Monte Carlo replicated data sets, and finding the covariance of those fits. However at that point, one is only a few steps removed from performing the extended t_0 method anyway, so the comparison seems moot. With these possibilities carefully accounted for, and convinced of the convergence of the extended t_0 method on non-linear models, we are confident discussions about this fit are meaningful.

3.4 z-expansion fit to 'uncorrected' data

Fitting now via the extended t_0 method, and the upgraded penalty trick, we find the following non-linear fits to the 'uncorrected' data.

	$i=1$	$i=2$	$i=3$	$i=4$
a_i	-1.73 ± 0.49	1.64 ± 0.63	-0.552 ± 6.6	$4.64 \pm 27.$
b_i	-1.82 ± 0.16	1.45 ± 0.075	1.37 ± 2.2	-0.474 ± 8.0

TABLE 3.1: The best fit parameters of the z-expansion model, fit to the 'uncorrected' data via the t_0 method. The fit has a $\chi^2_{t_0} = 52.5$ with 77 degrees of freedom. The covariance matrix for the fit is Eq. (B.5).

	$i=1$	$i=2$	$i=3$	$i=4$
a_i	-1.810 ± 1.2	1.388 ± 1.5	$1.081 \pm 15.$	$2.284 \pm 65.$
b_i	-1.771 ± 0.24	1.451 ± 0.12	0.6292 ± 3.4	$1.997 \pm 12.$

TABLE 3.2: The best fit parameters of the z-expansion model, fit to the 'uncorrected' data via the penalty trick. The fit has a $\chi^2 = 53.1$ with 68 degrees of freedom. The covariance matrix for the fit is Eq. (B.6).

	$i=1$	$i=2$	$i=3$	$i=4$	$i=5$
n_i	1.007 ± 0.008	1.005 ± 0.008	0.9611 ± 0.01	0.9819 ± 0.009	1.001 ± 0.01
	$i=6$	$i=7$	$i=8$	$i=9$	
n_i	1.019 ± 0.01	1.066 ± 0.009	1.007 ± 0.02	0.9967 ± 0.008	

TABLE 3.3: Fitted normalizations for the OPE data fit to the z-expansion model (via the penalty trick)

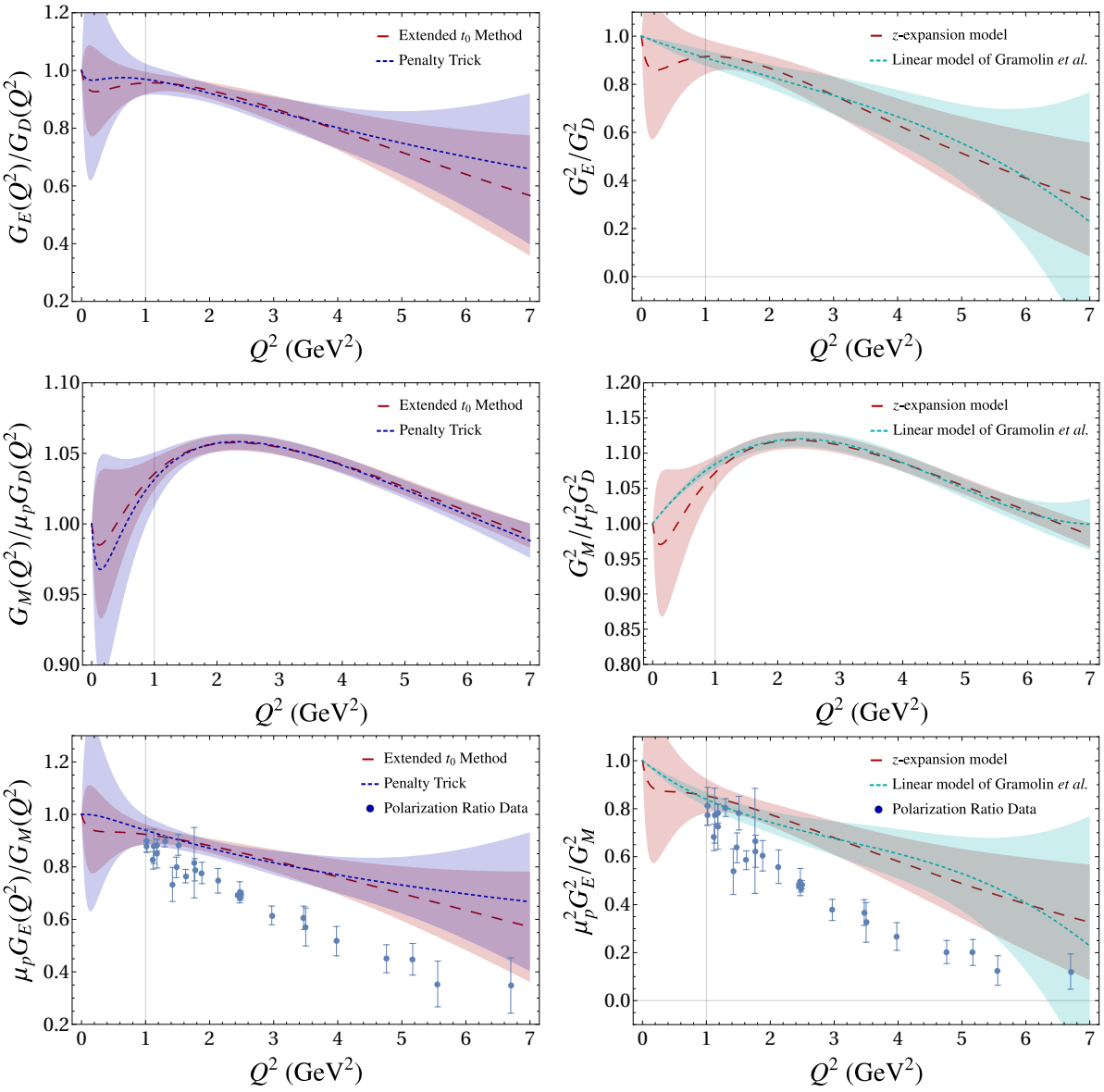

FIGURE 3.6: On the left are fitted form factors with the z-expansion model via the two methods, both for 'uncorrected' cross section data. On the right are the t_0 fit 'uncorrected' fitted form factors plotted squared, alongside the square form factors from the previous section (Tab. (2.3)).

Firstly we can observe that the switch to non-linear fitting has not lost us anything, as the square form factors on the right hand side of Fig. (3.6) in all cases essentially overlap through the relevant Q^2 range. The uncertainties are larger where there is no data (such as left of the vertical line at $Q^2 = 1$), and this is a general feature of non-linear models: they are much less reliable outside the data range than linear models. Also noteworthy is how, even without the low Q^2 data, the more flexible fits

are already developing the characteristic negative slope at 0. We can also notice that the non-linear square form factor ratio, on the bottom right of Fig. (3.6), behaves more reasonably and does not begin to dip towards negative values, due to it's being positive definite in construction.

3.5 z-expansion fit to TPE-corrected data

Fitting just as above, but to TPE-corrected data, we find the results plotted in Fig. (3.7).

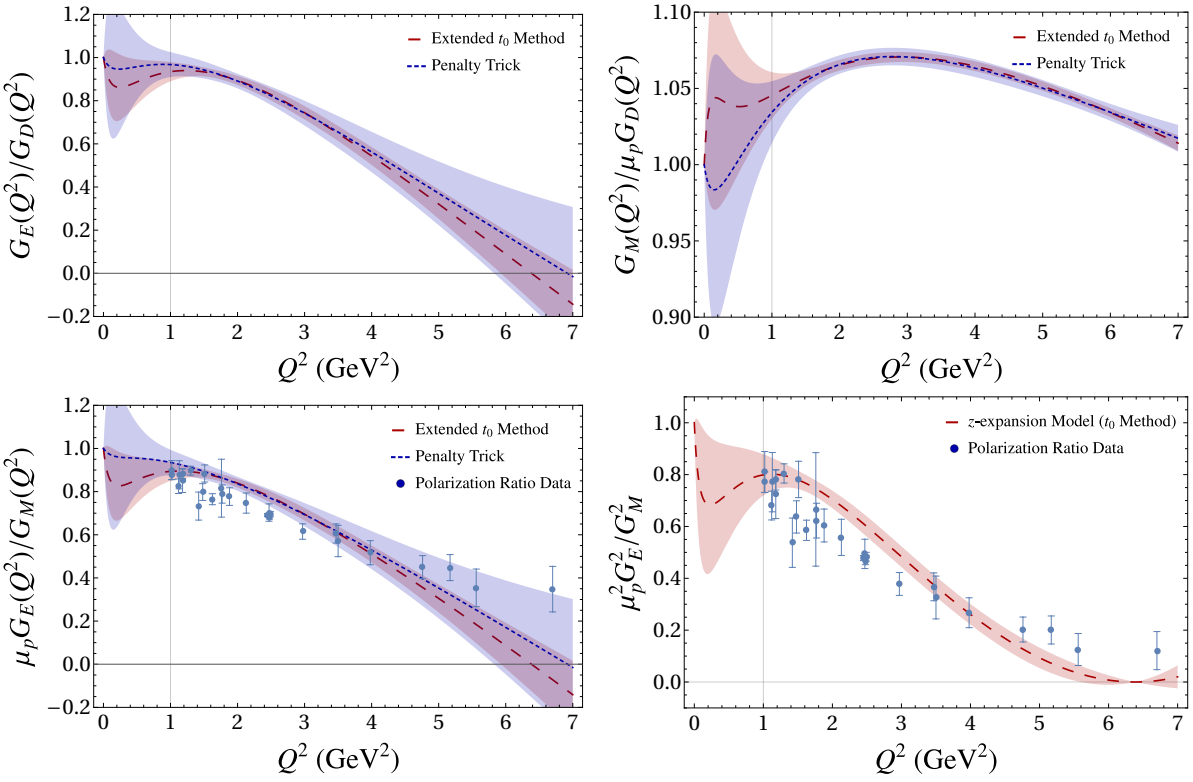

FIGURE 3.7: Fitted form factors using the z-expansion model, to TPE-corrected cross section data, via the extended t_0 method (red large dashing), and via the Penalty Trick (blue small dashing).

Just as in the linear case, we discover the extended t_0 fits to TPE-corrected data have far less variation than the 'uncorrected' data. However unlike before, this tightening of the error bands does not carry over to the penalty trick fit. We also see a larger divergence between the fitting procedures, though this is technically accounted

	$i=1$	$i=2$	$i=3$	$i=4$
a_i	-1.772 ± 1.1	1.696 ± 1.5	$-0.1988 \pm 14.$	$1.247 \pm 61.$
b_i	-1.824 ± 0.26	1.523 ± 0.12	1.294 ± 3.7	$-1.124 \pm 13.$

TABLE 3.4: The best fit parameters of the z-expansion model, fit to the TPE data via the penalty trick. The fit has a $\chi^2 = 55.3$ with 68 degrees of freedom. The covariance matrix for the fit is Eq. (B.7).

	$i=1$	$i=2$	$i=3$	$i=4$
a_i	-1.59 ± 0.47	2.08 ± 0.65	-3.50 ± 6.7	$7.91 \pm 24.$
b_i	-2.00 ± 0.22	1.57 ± 0.073	3.82 ± 3.1	$-10.4 \pm 11.$

TABLE 3.5: The best fit parameters of the z-expansion model, fit to the TPE data via the extended t_0 method. The fit has a $\chi^2_{t_0} = 53.6$ with 77 degrees of freedom. The covariance matrix for the fit is Eq. (B.8).

for by the penalty trick fits larger error band. One last observation is how much better a fit the non-linear model is to the (unfitted) polarization ratio data, due to its non-negative nature. Clearly the TPE corrections do a good job at stripping higher order effects out of the data, showing the data to appear more like the polarization ratio data.

3.6 Global cross section fit of the z-expansion model

For the following fits, we will be using the global cross section data set, from the GMp12 collaboration [8] (see Tab. (C.1)). This total data set was built specifically from those experiments for which past radiative corrections could be undone and then re-calculated with updated corrections, to ensure the analysis was consistent across all the data. The GMp12 collaboration use the following model, s, to fit the cross-section data via the penalty trick:

$$s = \left(\frac{1}{\mu_p^2}\,\mathrm{RS}\,\varepsilon + \tau\right) G_M^2, \tag{3.20a}$$

$$\mathrm{RS} = 1 + c_1\tau + c_2\tau^2, \tag{3.20b}$$

$$G_M = \mu_p \frac{1 + a_1\tau}{1 + b_1\tau + b_2\tau^2 + b_3\tau^3}. \tag{3.20c}$$

Here RS stands for 'Rosenbluth Slope' and in theory is equal to $\mu_p^2 G_E^2/G_M^2$. Just as with the z-expansion, we can see G_M is designed to fall off as $1/Q^4$, unfortunately the simple parametrization of RS means G_E falls off as $1/Q^2$. The GMp12 collaboration use the penalty trick (Eq. (1.32)) to account for the normalization uncertainty in their fits, implementing the t_0 method here and comparing against polarization ratio data gives us a another clean comparison between the fitting procedures.

With the usual 100 replica's per iteration, and 10 iterations, we find the following fitted form factors using the z-expansion model to fit the global data set:

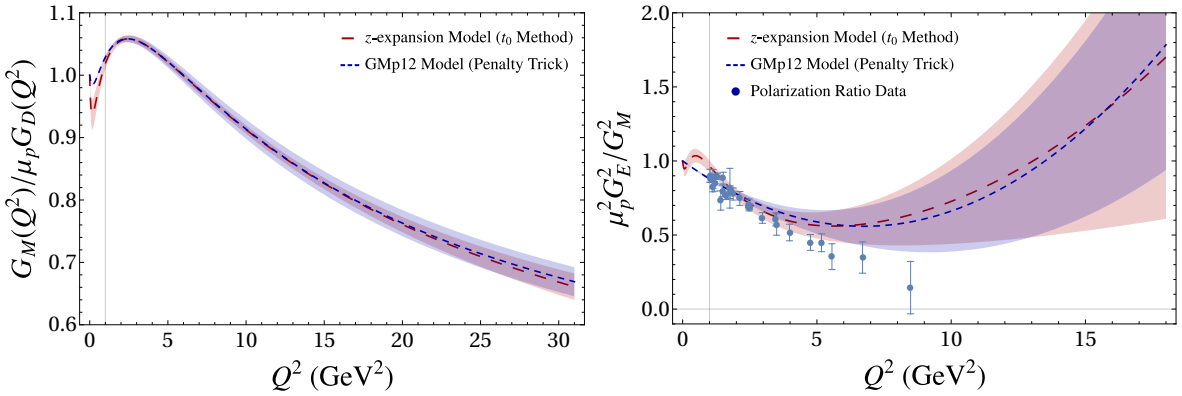

FIGURE 3.8: The z-expansion model fit to the global 'uncorrected' data set, using the extended t_0 method (red large dashing), plotted with the GMp12 collaboration's results using their model via the penalty trick[4] (blue small dashing), and in the case of the square form factor ratio (right) plotted alongside polarization ratio data (Tab. (C.2)) (the polarization data is not included in the fit).

	$i=1$	$i=2$	$i=3$	$i=4$
a_i	-1.59 ± 0.11	0.740 ± 0.38	-0.993 ± 1.2	16.7 ± 7.3
b_i	-1.70 ± 0.063	1.54 ± 0.045	-0.594 ± 0.96	5.22 ± 3.0

TABLE 3.6: The best fit parameters of the z-expansion model, fit to the global data set via the t_0 method. The fit has a $\chi^2_{t_0} = 80.0$ with 113 degrees of freedom. The covariance matrix for the fit is Eq. (B.9).

We can note the linear nature of the GMp12 group's RS parametrization by the way the error bands come to a point at low Q^2, while the z-expansion has the characteristic negative slope. Other than this however, the fits are approximately the same. These

[4]The GMp12 collaboration does not provide the covariance matrix of their fitted parameters (despite saying otherwise), so the error bands reported for the GMp12 fit via the penalty trick (blue small dashing) were constructed by eye to resemble the plots in Ref. [8] as it was not possible to reproduce them exactly.

fits also show us that unless further polarization ratio data reveals an upturn, the TPE-corrections become increasingly important at large Q^2.

3.7 Combining cross section data and polarization ratio data

We would like to see how good the TPE-corrections presented thus far are. One way to do this would be to see how much including polarization ratio data in the fitting procedure changes the fits to the cross section data. If there is little change, the TPE corrections are compatible. If the inclusion of polarization ratio data strains the fit a great deal, the corrections are incompatible. In order to simultaneously fit the two types of data, cross section and polarization ratio, the first option which comes to mind is to simply build a chi-square for the polarization fit, a chi-square for the cross section fit, and minimize their sum. For example, if we have a model for G_E and G_M, then we also have models for the observables of the cross section and polarization ratio respectively:

$$s = \varepsilon G_E^2 + \tau G_M^2, \tag{3.21a}$$

$$p = \sqrt{\mathrm{RS}} = \mu_p \frac{G_E}{G_M}. \tag{3.21b}$$

The total chi-square for $\mathcal{N}_{\mathrm{cs}}$ cross-section data sets and $\mathcal{N}_{\mathrm{pol}}$ polarization ratio data sets then looks like:

$$\chi^2 = \sum_{i=1}^{\mathcal{N}_{\mathrm{cs}}} \left[\sum_{j=1}^{N_i} \frac{\left(n_i^{\mathrm{R}} \sigma_{ij}^{\mathrm{R}} - s_{ij}\right)^2}{\left(\Delta\sigma_{ij}\right)^2 + \left(s_{ij}^{(k)} \Delta n_i\right)^2} \right] + \sum_{i=1}^{\mathcal{N}_{\mathrm{pol}}} \left[\sum_{j=1}^{N_i} \frac{\left(\varrho_{ij}^{\mathrm{R}} - p_{ij}\right)^2}{\left(\Delta\varrho_{ij}\right)^2} \right]. \tag{3.22}$$

This is merely a t_0 chi square just as in Eq. (2.3) for the cross section data σ (of course for multiple data points, replace the presence of the denominator with an inner product of inverse covariance matrices), plus a traditional chi-square for the polarization data ϱ. It should be clear now why we care so much about non-linear fitting: if we plan to have models for G_E and G_M, there is no way to fit the

simultaneous data sets without having a nonlinear model for at least one of the relevant observables. A common way around this is to model the polarization ratio itself, such as in Ref. [8], but this is rarely of greater utility than modelling the form factors, and is only done for ease of fitting. Important to note is that we are still Monte Carlo replicating all the data, including the polarization ratio data – while it is not needed to account for any normalization uncertainty, it is still enormously useful for extracting uncertainties of non-linear fits.

There is one contentious fact about this combined chi-square when dealing with multiple experiments with single data points: as previously discussed the normalization uncertainty changes the 'expected' value of a good fit. When all the data are single points from different experiments, all the cross section data will be suppressed by the factor in the denominator, and when there are multiple data points, the covariance matrix makes things too complicated to come up with a reasonable expected value of a good fit. What this means is polarization ratio data and cross section data will generally contribute uneven amounts, per data point, to the total chi-square. Perhaps this is fair; after all, the traditional chi-square is the special case of the t_0 chi-square where $\Delta n = 0$. If we are taking all the data at face value, then this should be a perfectly acceptable thing to minimize (as well, from the likelihood standpoint this is the chi-square we arrive at by directly multiplying the Gaussian distributions). One may believe a better fit may be had by scaling of one kind of data by some factor in order to weigh it more or less in the overall chi-square. For the data at hand, a few modifications we attempted throughout the flitting procedure, which had only very minor effects on the fits. As such, for the sake of statistical rigor, the simple sum of the chi-squares in Eq. (3.22) is used through the rest of the thesis.

3.8 Simultaneous fit to TPE-corrected LT data and polarization ratio data

Performing this simultaneous fit now to TPE-corrected cross section data, and polarization ratio data, we find the fit presented in Fig. (3.9), along with the previous t_0 method fit from Fig. (3.7), in order to see how including the polarization ratio data in the fitting procedure strains the corrected fits. In theory, if the TPE corrections perfectly close the gap between LT and PT data, there should be no significant change to the chi-square value specific to the LT data.

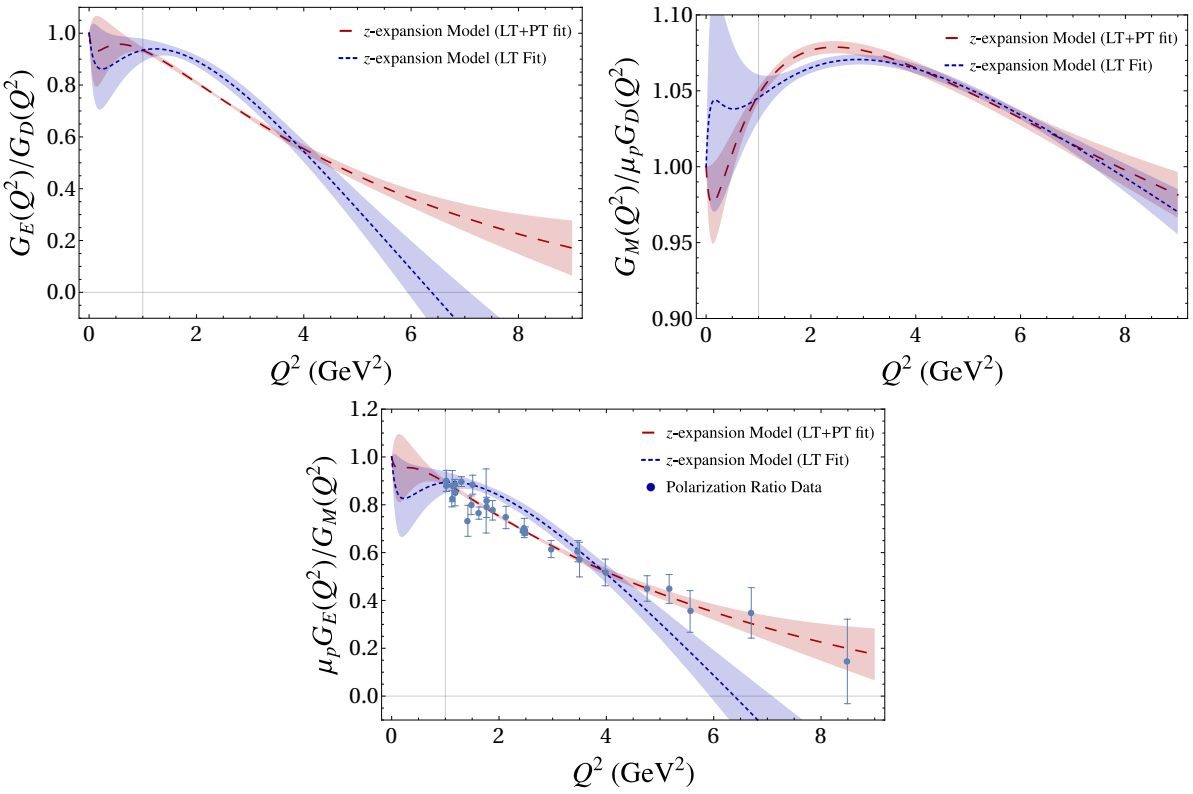

FIGURE 3.9: Simultaneous fit to the TPE-Corrected LT data and polarization ratio data (red large dashing), contrasted with the same model and method fit to only the LT data (blue small dashing). Both fits are of the z-expansion model via the extended t_0 method.

Table (3.7) tells us that fitting to the polarization ratio data cost us a 14.5% increase in the cross section chi-square, and so likely there are still improvements to be had in theoretical corrections, specifically model dependent TPE-corrections.

fit	χ^2_{LT}
LT	53.56
LT+PT	61.33

TABLE 3.7: The chi-square value of the resulting model fit via the extended t_0 method for the different data sets, specifically looking at quality of fit to the cross section data. There are 85 cross section data points for which TPE-corrections can be applied.

For completeness we also perform the global fit of the z-expansion via the penalty trick (unplotted), and report those fitted parameters in Tab. (3.9).

	$i=1$	$i=2$	$i=3$	$i=4$
a_i	-1.69 ± 0.45	1.04 ± 0.44	-0.269 ± 5.9	$11.3 \pm 25.$
b_i	-1.78 ± 0.084	1.40 ± 0.067	0.858 ± 1.1	1.53 ± 4.5

TABLE 3.8: The best fit parameters of the z-expansion model, fit to the TPE cross section data and polarization ratio data simultaneously via the extended t_0 method. The fit has $\chi^2_{t_0} = 61.3 + 19.4 = 80.8$ with 105 degrees of freedom. The covariance matrix for the fit is Eq. (B.11).

	$i=1$	$i=2$	$i=3$	$i=4$
a_i	-0.9689 ± 0.52	0.3854 ± 0.48	-9.696 ± 6.9	$51.03 \pm 29.$
b_i	-1.838 ± 0.099	1.444 ± 0.072	1.633 ± 1.3	-1.620 ± 5.3

TABLE 3.9: The best fit parameters of the z-expansion model, fit to the TPE cross section data and polarization ratio data simultaneously via the penalty trick. The fit has $\chi^2 = 58.8 + 20.4 = 79.1$ with 96 degrees of freedom. The covariance matrix for the fit and its fitted normalizations are found at Eq. (B.10).

	$i=1$	$i=2$	$i=3$	$i=4$	$i=5$
n_i	1.005 ± 0.008	1.005 ± 0.008	0.9622 ± 0.009	0.9824 ± 0.009	1.002 ± 0.01
	$i=6$	$i=7$	$i=8$	$i=9$	
n_i	1.017 ± 0.01	1.065 ± 0.008	1.007 ± 0.02	0.9966 ± 0.008	

TABLE 3.10: Fitted normalizations for the TPE-Corrected-LT data+PT data fit to the z-expansion model (via the penalty trick)

3.9 A curious case of improperly treated uncertainties

If at one point during the analysis, one decides to improperly treat the correlated nature of the multiplicative uncertainties, and fits each data point as if it is from its

own experiment, one finds the remarkable coincidence that the LT data does not disagree significantly with the PT data, as shown in Fig. (3.10)

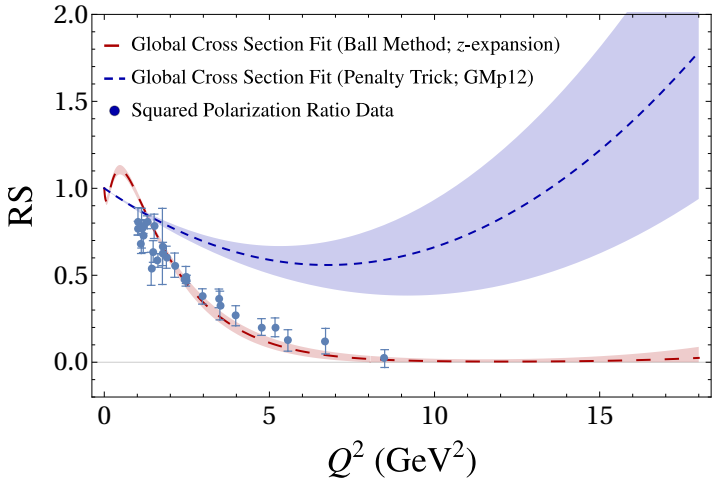

FIGURE 3.10: Global cross section fits of the GMp12 group (blue small dashing) compared to a global fit of the z-expansion where the correlated normalization uncertainties are ignored, and fitted as if each data point comes from its own experiment.

If one ignores the correlated nature of the normalization uncertainty, a global cross section fit goes right through the polarization transfer data. However, it is unlikely this is indicative of any mishaps regarding the classification of uncertainties, because individual experiments alone (and hence are without the worries regarding methods for combining normalization uncertainties) report that LT data disagrees with PT data. Though it is noteworthy how well it fits the PT data given that it could, being an improper fit, go anywhere, it should not be taken seriously as a fit because it does not correctly take into account the correlated nature of the normalization uncertainties. The only way this fit could be taken seriously, is if it were the case that point-to-point statistical and systematic uncertainties were characterized wrongly as normalization uncertainties, or more generally if the normalization uncertainties were significantly over-estimated.

Chapter 4

Recalculation of $F_{1|3}^{\gamma Z}$ via Quark Model Helicity Amplitudes

4.1 Preliminary math and definitions

4.1.1 Helicity amplitudes and structure functions

The form factors of the previous sections are related to what are known as structure functions, in the elastic limit. Structure functions are functions not only of Q^2, but also of the invariant mass squared W^2 of the target during inelastic scattering. As such, when the scattering is elastic, the form factors and the structure functions should have something to do with each other. Indeed they do in the elastic limit, where the invariant mass $W^2 = M_p^2$. For example, the structure function $F_3^{\gamma z}$ is related to the nucleon form factors as follows:

$$F_3^{\gamma Z}\left(Q^2, W^2 = M_p^2\right) = -Q^2 G_M\left(Q^2\right) G_A^Z\left(Q^2\right) \delta\left(W^2 - M_p^2\right) \tag{4.1}$$

where G_A^Z is the protons axial form factor, not relevant for understanding the protons electromagnetic properties. The other form factors can be related similarly.

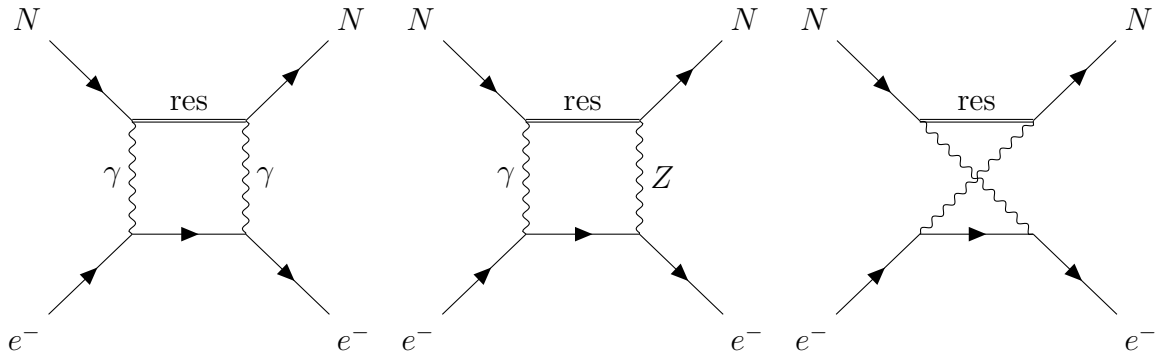

FIGURE 4.1: The 1-loop diagrams, so called (neutral) box diagrams $\Box_{\gamma\gamma}$ and $\Box_{\gamma Z}$. An incoming nucleon (N) enters a resonant state 'res' through an inelastic scattering of the incoming electron. The nucleon decays and returns to its ground state by emitting a second boson. For $\Box_{\gamma Z}$ there is also a second diagram where the Z boson is emitted first: $\Box_{Z\gamma}$. For each box diagram there is also the 'cross box' diagram (right).

The structure function of an arbitrary resonance of the nucleon is derived from the contraction of the boson polarization vectors ϵ^{μ} with the hadronic tensor $W_{\mu\nu}$, definitions for both of which are readily found in most treatments of inelastic scattering, such as Rislow's thesis [19]. For $\Box_{\gamma\gamma}$ this expression looks like:

$$\begin{aligned} F_1^{\gamma\gamma}|_{N\to res} &= \epsilon_+^{\mu *}\epsilon_+^{\nu} W_{\mu\nu}^{\gamma\gamma} \\ &= \sum_{\lambda} \int \mathrm{d}^4\mathrm{z}\, e^{iqz} \left\langle N, s \left| \epsilon_+^* \cdot J^{\gamma}(z) \right| res, \lambda \right\rangle \left\langle res, \lambda \left| \epsilon_+ \cdot J^{\gamma}(0) \right| N, s \right\rangle \\ &= \sum_{\lambda} A_{\lambda}^{\gamma} A_{\lambda}^{\gamma}. \end{aligned} \tag{4.2}$$

This serves as a definition for the helicity amplitude A_{λ}^{γ}. The helicity amplitude may be seen as the amplitude of transitioning via a neutral weak Z boson or photon, from a nucleon resonance state back to the nucleon ground state. For $\Box_{\gamma Z}$ the situation is nearly identical, except we gain a factor of 2 due to greater number of ways the diagram can uniquely happen:

$$\begin{aligned} F_1^{\gamma Z}\Big|_{res} &= \epsilon_+^{\mu *}\epsilon_+^{\nu} W_{\mu\nu}^{\gamma Z} \\ &= 2\sum_{\lambda} \int \mathrm{d}^4\mathrm{z}\, e^{iqz} \left\langle N, s \left| \epsilon_+^* \cdot J^{Z}(z) \right| res, \lambda \right\rangle \left\langle res, \lambda \left| \epsilon_+ \cdot J^{\gamma}(0) \right| N, s \right\rangle \\ &= 2\sum_{\lambda} A_{\lambda}^{Z} A_{\lambda}^{\gamma}. \end{aligned} \tag{4.3}$$

The resonance region contribution to the total structure functions is then the sum of the structure function for each resonance:

$$F_1^{\gamma\gamma} = \sum_{res} F_1^{\gamma\gamma}|_{res}, \tag{4.4a}$$

$$F_1^{\gamma Z} = \sum_{res} F_1^{\gamma Z}|_{res}. \tag{4.4b}$$

For phenomenological reasons, it is extremely convenient to build connections between the structure functions, so that measurements and calculations of one structure function lend themselves to constraining of another structure function. Rislow and Carlson go on to relate these aforementioned quantities in the following way [19]:

$$F_1^{\gamma Z} = \sum_{res} C_{res} \times F_1^{\gamma\gamma}|_{res}\,, \tag{4.5a}$$

$$C_{res} = \left.\frac{F_1^{\gamma Z}}{F_1^{\gamma\gamma}}\right|_{res} = 2\frac{\sum_\lambda A_\lambda^\gamma A_\lambda^Z}{\sum_\lambda \left(A_\lambda^\gamma\right)^2}. \tag{4.5b}$$

This means we are modeling the form factor of each γZ resonance as a modification to the analogous $\gamma\gamma$ resonance. With access to helicity amplitudes via quark model wavefuntions we can find these corrective pre-factors, which will directly constrain $F_1^{\gamma Z}$ from $F_1^{\gamma\gamma}$. Simplifying expressions for the helicity amplitudes

$$\langle res, \lambda \left|\epsilon_+ \cdot J^\gamma\right| N, s\rangle = 3\left\langle \psi_{res}\phi_{res}\chi_\lambda \left|\epsilon_+^\mu \bar{u}\left(k', \lambda'\right) e_q \gamma_\mu u\left(k, s'\right)\right| \psi_N \phi_N \chi_s\right\rangle, \tag{4.6}$$

where $k(k')$ and $s'(\lambda')$ are the initial (final) momentum and spin projection for the struck quark. The operator e_q arises from the vertex factor, and by symmetry it is clear that we may simply compute the current for the third quark and then multiply our result by three. With unit normalized spinors

$$u = \sqrt{\frac{E + m_q}{2m_q}} \begin{pmatrix} \xi_s \\ \frac{\vec{k}\cdot\sigma}{2m_q}\xi_s \end{pmatrix}, \tag{4.7}$$

we may simplify the interior of Eq. (4.6):

$$3e_q^{(3)} \left\langle \psi_{res}\phi_{res}\chi_\lambda \left| \frac{1}{m_q\sqrt{2}} \xi^\dagger_{\lambda'} \left(k_+ + q_z S_+\right) \xi_{s'} \right| \psi_N \phi_N \chi_s \right\rangle, \tag{4.8}$$

where $k_+ = k_1 + ik_2$. Using the Wigner-Eckhart theorem we know that we may write any spherical tensor operator as a scaling of the angular momentum operators. As such the matrix element above may be massaged into the form:[1]

$$A^\gamma_{\lambda=1/2} = 3\, e_q^{(3)} \left\langle \psi_N \phi_N \chi_s \left| \left(AL_+ + B\sigma_z S_+\right)^\dagger \right| \psi_{res}\phi_{res}\chi_\lambda \right\rangle, \tag{4.9}$$

where A and B are coefficients that contain information about the momentum and mass of the quark, generally depend on Q^2, and will be different for different spacial wave functions. To write it a bit more generally

$$A_\lambda = \langle N_s | \hat{\mathcal{O}} | Res_\lambda \rangle, \tag{4.10}$$

where N is the nucleon ground state, s is the spin projection of the nucleon, λ is the total angular momentum projection (J_z) of the resonance, and

$$\hat{\mathcal{O}} = 3e_q^{(3)}(AL_- + B\sigma_z^{(3)} S_-). \tag{4.11}$$

After we build the wavefunctions we will see how to apply this operator to find the helicity amplitudes.

4.1.2 Representation theory of multi-quark states

A quark-model wavefunction for a generally excited nucleon $|N\rangle$, has four factors: space $|\psi\rangle$, spin $|\chi\rangle$, flavour $|\phi\rangle$, and colour $|c\rangle$. This is to say the general wave-function is a linear superposition of the following form:

[1] Note that the aforementioned authors implement a mysterious sign convention for their lowering operator S_-. This convention exactly corresponds to appending a σ_z on the left of the lowering operator. Thus if one tries to reproduce their work one will be missing minus signs on every spin $-\frac{1}{2}$ state acted upon for the second term of the operator.

$$|N\rangle = \sum_i k_i \, |\psi_i\rangle \otimes |\chi_i\rangle \otimes |\phi_i\rangle \otimes |c_i\rangle \, , \tag{4.12}$$

with sufficiently normalized complex coefficients k_i. Under the valance quark model, each nucleon is built out of 3 quarks. What this means is that while the total proton wave function lives in the aforementioned tensor product space, each component of that space, itself comes from the tensor product of the individual quark spaces.

4.1.3 Spin

The spin state of a single quark lives in the **2** dimensional representation of $SU(2)$. In the non-relativistic case, a general particle of spin s lives in the irreducible representation of $SU(2)$ of dimension $\mathbf{d} = 2s + 1$. The state space of the spin of a system of two quarks is the tensor product of the individual state spaces

$$\mathbf{2} \otimes \mathbf{2} = \mathbf{3} \oplus \mathbf{1}, \tag{4.13}$$

which of course decomposes into the usual spin state space of two fermions: the triplet and the singlet. Adding a third quark we get to our important group decomposition for the final 3-quark spin state space:

$$\mathbf{2} \otimes \mathbf{2} \otimes \mathbf{2} = \mathbf{4} \oplus \mathbf{2} \oplus \mathbf{2}. \tag{4.14}$$

The way to read this is that the total spin state-space of a nucleon with 3 quarks decomposes into three subspaces, one 4-dimensional subspace of total spin $\frac{3}{2}$ and two 2-dimensional subspaces of total spin $\frac{1}{2}$. It is easy to explicitly build the unique state with total spin $\frac{3}{2}$ and spin projection $\frac{3}{2}$:

$$|\uparrow\rangle \otimes |\uparrow\rangle \otimes |\uparrow\rangle = |\uparrow\uparrow\uparrow\rangle \, . \tag{4.15}$$

From this state, we can use lowering operators and orthogonality to build the states with spin projection $\frac{1}{2}$ to build the remaining wavefunctions. Arranging these into a

convenient orthonormal basis we may write them as:

$$|\chi_S\rangle = \frac{1}{\sqrt{3}}(|\uparrow\uparrow\downarrow\rangle + |\uparrow\downarrow\uparrow\rangle + |\downarrow\uparrow\uparrow\rangle), \tag{4.16a}$$

$$|\chi_{MS}^{23}\rangle = \frac{1}{\sqrt{6}}(2\,|\downarrow\uparrow\uparrow\rangle - |\uparrow\uparrow\downarrow\rangle - |\uparrow\downarrow\uparrow\rangle), \tag{4.16b}$$

$$|\chi_{MA}^{23}\rangle = \frac{1}{\sqrt{2}}(|\uparrow\uparrow\downarrow\rangle - |\uparrow\downarrow\uparrow\rangle). \tag{4.16c}$$

This basis is extra convenient because of its well defined symmetry properties. The subscripts denote the symmetry of the state (**M**ixed, **S**ymmetric, **A**nti-Symmetric), and the superscripts denote which quarks are (anti-)symmetric in the mixed states. For convenience later we will also be using states defined analogously for mixed symmetry in quarks 1 & 2, and 1 & 3, which can be found via cyclic permutations of the quarks.

4.1.4 Isospin

Because isospin transforms via another $SU(2)$, just as spin did, all of our results are the same, but we replace the notion of 'spin up' and 'spin down' with 'isospin up' and 'isospin down' (quark flavours up and down respectively). This gives the flavour space with iso-spin projection $\frac{1}{2}$ the following analogous basis:

$$|\phi_S\rangle = \frac{1}{\sqrt{3}}(|uud\rangle + |udu\rangle + |duu\rangle), \tag{4.17a}$$

$$|\phi_{MS}^{23}\rangle = \frac{1}{\sqrt{6}}(2|duu\rangle - |uud\rangle - |udu\rangle), \tag{4.17b}$$

$$|\phi_{MA}^{23}\rangle = \frac{1}{\sqrt{2}}(|uud\rangle - |udu\rangle), \tag{4.17c}$$

where again other spin projection states may be found via raising and lowering operators.

4.1.5 Colour

Quarks' colour charge is their least familiar aspect. The colour charge transforms under the fundamental group **3** of $SU(3)$, and thus the colour state space of the proton lives in $\mathbf{3} \otimes \mathbf{3} \otimes \mathbf{3} = \mathbf{10} \oplus \mathbf{8} \oplus \mathbf{8} \oplus \mathbf{1}$. This is a rather large state space to explore

but we are lucky enough that nature saves us the effort. In all of the work following we will assume the colour factor of any 3-quark wavefunction is the totally anti-symmetric singlet state:

$$|c\rangle = \frac{1}{\sqrt{6}}(|rgb\rangle - |rbg\rangle + |gbr\rangle - |grb\rangle + |brg\rangle - |bgr\rangle). \tag{4.18}$$

This state is essentially forced upon us by the observation that no nucleons are ever seen with a net colour charge (there is no long range chromodynamics). It may be possible for some extremely short lived excited states to violate this, but for now this restriction proves fruitful.

4.1.6 Space

Typically when using the quark model one uses a central potential like the harmonic oscillator as a simple model of the quark behaviour. This factors the spacial components into radial and angular components. This is arguably the most complicated part of the wavefunction: while all the other group representations the quarks inhabit are fundamental to the quark, a quark can belong to any representation of $SO(3)$, as the angular part of the wave-function corresponds to the orbital component of the total angular momentum. A non-zero orbital angular momentum implies that at least one of the valence quarks is in an excited state – the angular components of these excited states are well catalogued: they are the spherical harmonics. The radial components of these wavefunctions are less well understood because the forces between the quarks are not well understood. For our purposes here, we will leave the spacial wavefunctions rather general: the i^{th} quark with coordinates $\mathbf{r_i}$ and orbital angular momentum quantum numbers l, m has the spacial wavefuntion: $\Psi_{lm}(\mathbf{r}_i)$. Often we will invoke the shorthand of a coordinate superscript to mean the same thing: Ψ^i_{lm}.

An example with $n = 1$ is illuminating as to the complexity of the spacial wavefunctions. We can have one, two, or three quarks with quantum number $l = 1$

which give way to the following possible group decomposition's:

$$\mathbf{1} \otimes \mathbf{1} \otimes \mathbf{3} = \mathbf{3}, \tag{4.19a}$$

$$\mathbf{1} \otimes \mathbf{3} \otimes \mathbf{3} = \mathbf{5} \oplus \mathbf{3} \oplus \mathbf{1}, \tag{4.19b}$$

$$\mathbf{3} \otimes \mathbf{3} \otimes \mathbf{3} = \mathbf{7} \oplus \mathbf{5} \oplus \mathbf{5} \oplus \mathbf{3} \oplus \mathbf{3} \oplus \mathbf{3} \oplus \mathbf{1}. \tag{4.19c}$$

For the *total* spacial wavefunction to have, for example, $L = 1, M = 0$, there are 5 possibilities here (one from each $\mathbf{3}$). For larger N this state-space is even more difficult to wade through. What follows are some examples of how one might go about actually building some of these many possibilities. Continuing the example of caring about $L = 1, M = 0$, for the case in Eq. (4.19a) we may write the total wavefunction ψ_{LM} in terms of the single quark wavefunctions Ψ_{lm}:

$$\psi_{10}^{MS}(\mathbf{r}_1, \mathbf{r}_2, \mathbf{r}_3) = \frac{1}{\sqrt{3}} \left[\Psi_{00}(\mathbf{r}_1)\Psi_{00}(\mathbf{r}_2)\Psi_{10}(\mathbf{r}_3)\right]. \tag{4.20}$$

This wave function is mixed symmetric under the exchange of quark coordinates 1 and 2. Given a mixed-symmetric object, a usual technique to build a more symmetric object is to sum over cyclic permutations of the quark labels (coordinates) [20]. Employing the shorthand $\Psi_{lm}(\mathbf{r}_i) = \Psi_{lm}^i$ we find a totally symmetric $L = 1, M = 0$ three-quark wavefunction:

$$\begin{aligned} \psi_{10}^{S} &= \sum_{\sigma} \Psi_{00}^1 \Psi_{00}^2 \Psi_{10}^3 \\ &= \frac{1}{\sqrt{3}} \left(\Psi_{00}^1 \Psi_{00}^2 \Psi_{10}^3 + \Psi_{00}^1 \Psi_{10}^2 \Psi_{00}^3 + \Psi_{10}^1 \Psi_{00}^2 \Psi_{00}^3\right). \end{aligned} \tag{4.21}$$

Here the sum over σ (standing in the set of cyclic permutations on 3 elements) implies we are summing over all possible cyclic permutations of the quark labels (coordinates). This sum will result in an object that is totally symmetric.[2] Note that the correspondence between spacial parity and exchange parity of a wavefunction only exists for for two particle states. This state is totally symmetric under fermion

[2]Sometimes this sum results in 0, such as when one tries to symmetrize the mixed symmetric spin wavefunction of Eq. (4.16b).

swapping and still retains its negative parity. Continuing our example for the case in Eq. (4.19b):

$$\begin{aligned}\psi_{10}^{A} = \Psi_{11}^{1}\Psi_{1-1}^{2}\Psi_{00}^{3} - \Psi_{1-1}^{1}\Psi_{11}^{2}\Psi_{00}^{3} + \Psi_{1-1}^{1}\Psi_{00}^{2}\Psi_{11}^{3} \\ - \Psi_{11}^{1}\Psi_{00}^{2}\Psi_{1-1}^{3} + \Psi_{00}^{1}\Psi_{11}^{2}\Psi_{1-1}^{3} - \Psi_{00}^{1}\Psi_{1-1}^{2}\Psi_{11}^{3},\end{aligned} \tag{4.22}$$

we find a totally anti-symmetric wavefunction. Another great example of how swapping and parity decouple for odd numbers of particle, since it can be seen this state has total $L = 1$ and a positive parity. Finally for the case of Eq. (4.19c) we find three distinct possibilities:

$$\begin{aligned}\psi_{10}^{S} = \frac{1}{\sqrt{15}}\big(&\Psi_{11}^{1}\Psi_{1-1}^{2}\Psi_{10}^{3} + \Psi_{11}^{1}\Psi_{10}^{2}\Psi_{1-1}^{3} + \Psi_{1-1}^{1}\Psi_{11}^{2}\Psi_{10}^{3} + \Psi_{10}^{1}\Psi_{11}^{2}\Psi_{1-1}^{3} \\ &+ \Psi_{1-1}^{1}\Psi_{10}^{2}\Psi_{11}^{3} + \Psi_{10}^{1}\Psi_{1-1}^{2}\Psi_{11}^{3} - 3\Psi_{10}^{1}\Psi_{10}^{2}\Psi_{10}^{3}\big)\end{aligned}, \tag{4.23}$$

totally symmetric, and

$$\begin{aligned}\psi_{10}^{MS} = \frac{1}{2\sqrt{3}}\big(&2\Psi_{1-1}^{1}\Psi_{11}^{2}\Psi_{10}^{3} - \Psi_{1-1}^{1}\Psi_{10}^{2}\Psi_{11}^{3} - \Psi_{11}^{1}\Psi_{10}^{2}\Psi_{1-1}^{3} \\ &+ 2\Psi_{11}^{1}\Psi_{1-1}^{2}\Psi_{10}^{3} - \Psi_{10}^{1}\Psi_{1-1}^{2}\Psi_{11}^{3} - \Psi_{10}^{1}\Psi_{11}^{2}\Psi_{1-1}^{3}\big)\end{aligned}, \tag{4.24}$$

mixed symmetric in quarks 1 and 2, and

$$\psi_{10}^{MA} = \frac{1}{2}\left(\Psi_{11}^{1}\Psi_{10}^{2}\Psi_{1-1}^{3} - \Psi_{10}^{1}\Psi_{11}^{2}\Psi_{1-1}^{3} - \Psi_{10}^{1}\Psi_{1-1}^{2}\Psi_{11}^{3} + \Psi_{1-1}^{1}\Psi_{10}^{2}\Psi_{11}^{3}\right), \tag{4.25}$$

mixed anti-symmetric in quarks 1 and 2. Unlike before, the mixed symmetric wavefunctions here go to 0 when they are symmetrized by addition of cyclic permutations of the quark coordinates. However this does not make them unphysical. If one has mixed symmetric spin-flavour wavefunctions, then a totally symmetric wavefunction may still be built:

$$|N\rangle \propto \sum_{\sigma} \psi_{lm}^{M} \left|\phi\chi\right\rangle^{M}, \tag{4.26}$$

with the sum over matching mixed symmetries. This wave function will be manifestly

symmetric, and we'll see examples of these kinds of wavefunctions while building the quark model wavefunctions for the nucleon resonances.

4.2 Building nucleon wavefunctions

Name	N	L^π	$2S$	Sym
$P_{33}(1232)$	0	0^+	3	S
$S_{11}(1535)$	1	1^-	1	MS
$D_{13}(1520)$	1	1^-	1	MS
$F_{15}(1680)$	2	2^+	1	S
$S_{11}(1650)$	1	1^-	3	MS
$P_{11}(1440)$	2	0^+	1	S
$F_{37}(1950)$	2	2^+	3	S

TABLE 4.1: The properties of the seven Christy-Bosted [21] resonances. Subscripts are twice the isospin, twice the total angular momentum, bracketed values are the masses in MeV, N is the principle quantum number in the harmonic oscillator model, L is the orbital quantum number, π is the parity of the wave-function, $2S$ is twice the total spin angular momentum quantum number, and Sym is the symmetry of the spacial wave-function. Do not confuse the name of the resonance with its orbital quantum number, for historical reasons those letters corresponds to the orbital quantum numbers of the resonances' most common decay products.

Because all nucleon excitations are fermions, the total wavefunction must be anti-symmetric. As the colour component is taken to be totally anti-symmetric, the rest of the wavefunction must be totally symmetric. Focusing first on the spin-isospin combinations, it is simple to build composite wavefunctions $|I, S, Sym\rangle$ which remain simultaneous eigenstates of spin and iso-spin while having well defined symmetry properties (labels for I_3 and S_3 are suppressed since they are each $+\frac{1}{2}$ in all the

following):[3]

$$\left|\frac{3}{2},\frac{3}{2},\ \mathrm{S}\right\rangle = \left|\phi^S\right\rangle\left|\chi^S\right\rangle, \tag{4.27a}$$

$$\left|\frac{1}{2},\frac{3}{2},\mathrm{MS}\right\rangle = \left|\phi^{MS}\right\rangle\left|\chi^S\right\rangle, \tag{4.27b}$$

$$\left|\frac{1}{2},\frac{3}{2},\mathrm{MA}\right\rangle = \left|\phi^{MA}\right\rangle\left|\chi^S\right\rangle, \tag{4.27c}$$

$$\left|\frac{3}{2},\frac{1}{2},\mathrm{MS}\right\rangle = \left|\phi^S\right\rangle\left|\chi^{MS}\right\rangle, \tag{4.27d}$$

$$\left|\frac{3}{2},\frac{1}{2},\mathrm{MA}\right\rangle = \left|\phi^S\right\rangle\left|\chi^{MA}\right\rangle, \tag{4.27e}$$

$$\left|\frac{1}{2},\frac{1}{2},\ \mathrm{S}\right\rangle = \frac{1}{\sqrt{2}}\left[|\phi^{MS}\rangle|\chi^{MS}\rangle + |\phi^{MA}\rangle|\chi^{MA}\rangle\right], \tag{4.27f}$$

$$\left|\frac{1}{2},\frac{1}{2},\ \mathrm{A}\right\rangle = \frac{1}{\sqrt{2}}\left[|\phi^{MS}\rangle|\chi^{MA}\rangle - |\phi^{MA}\rangle|\chi^{MS}\rangle\right], \tag{4.27g}$$

$$\left|\frac{1}{2},\frac{1}{2},\mathrm{MS}\right\rangle = \frac{1}{\sqrt{2}}\left[|\phi^{MS}\rangle|\chi^{MS}\rangle - |\phi^{MA}\rangle|\chi^{MA}\rangle\right], \tag{4.27h}$$

$$\left|\frac{1}{2},\frac{1}{2},\mathrm{MA}\right\rangle = \frac{1}{\sqrt{2}}\left[|\phi^{MS}\rangle|\chi^{MA}\rangle + |\phi^{MA}\rangle|\chi^{MS}\rangle\right]. \tag{4.27i}$$

Given the spin and isospin spaces are each 3 dimensional, we can be sure this set of 9 orthonormal kets is in fact a basis for the space of $S_z = \frac{1}{2}$, $I_3 = \frac{1}{2}$ wavefunctions.

4.2.1 The Proton

The first nucleon we care about is of course the proton. We know the proton has quantum numbers $l = 0, I = \frac{1}{2}, S = \frac{1}{2}$ which with Fermi-Dirac statistics forces upon us

[3] It is not obvious by inspection why this way of writing down the wave functions in Eq. (4.27f) and Eq. (4.27g) should give the total symmetries reported, but building this family of wavefunctions via sums of cyclic permutations and ensuring orthogonality will help one see why this form gives the totally (anti-)symmetric wavefunctions in this case. For further discussion and classification of quark wavefunctions see *An Introduction to Quarks and Partons* by F. E. Close [22].

the wavefunction of Eq. (4.27f):[4]

$$\begin{aligned}|N^+\uparrow\rangle &= |\phi^{23}_{MS}\rangle|\chi^{23}_{MS}\rangle + |\phi^{13}_{MS}\rangle|\chi^{13}_{MS}\rangle + |\phi^{12}_{MS}\rangle|\chi^{12}_{MS}\rangle \\ &= \frac{1}{\sqrt{18}}\begin{pmatrix} 2|u\uparrow u\uparrow d\downarrow\rangle - |u\uparrow u\downarrow d\uparrow\rangle - |u\downarrow u\uparrow d\uparrow\rangle \\ -|u\uparrow d\uparrow u\downarrow\rangle + 2|u\uparrow d\downarrow u\uparrow\rangle - |u\downarrow d\uparrow u\uparrow\rangle \\ -|d\uparrow u\uparrow u\downarrow\rangle - |d\uparrow u\downarrow u\uparrow\rangle - 2|d\downarrow u\uparrow u\uparrow\rangle \end{pmatrix},\end{aligned} \tag{4.28}$$

introducing the usual condensed notation

$$|u\uparrow u\downarrow d\uparrow\rangle = |uud\rangle\,|\uparrow\downarrow\uparrow\rangle = (|u\rangle\otimes|u\rangle\otimes|d\rangle)\otimes(|\uparrow\rangle\otimes|\downarrow\rangle\otimes|\uparrow\rangle). \tag{4.29}$$

With an abuse of notation we can write this more compactly as:

$$|N^+,\uparrow\rangle = \frac{1}{\sqrt{18}}\begin{bmatrix}|uud\rangle\\|udu\rangle\\|duu\rangle\end{bmatrix}^T\begin{bmatrix}2&-1&-1\\-1&2&-1\\-1&-1&2\end{bmatrix}\begin{bmatrix}|\uparrow\uparrow\downarrow\rangle\\|\uparrow\downarrow\uparrow\rangle\\|\downarrow\uparrow\uparrow\rangle\end{bmatrix}. \tag{4.30}$$

Finally the proton is certainly in a ground state, and so its spacial wavefunction will be one of the trivial combination of 0 orbital angular momentum $\psi_{00} = \Psi^1_{00}\Psi^2_{00}\Psi^3_{00}$. With the colour component assumed, the proton's wavefunction has been exactly defined.

4.2.2 The Delta baryon

The Delta baryon's structure can be quickly deduced, since it must have total spin and isospin each $\frac{3}{2}$:

$$|P_{33}\uparrow\rangle = |\phi^S\rangle|\chi^S\rangle = \frac{1}{3}\begin{bmatrix}|uud\rangle\\|udu\rangle\\|duu\rangle\end{bmatrix}^T\begin{bmatrix}1&1&1\\1&1&1\\1&1&1\end{bmatrix}\begin{bmatrix}|\uparrow\uparrow\downarrow\rangle\\|\uparrow\downarrow\uparrow\rangle\\|\downarrow\uparrow\uparrow\rangle\end{bmatrix}. \tag{4.31}$$

Similar to the proton, there is no orbital angular momentum to worry about here, and so assuming a ground-state ψ_{00} leaves the wavefunction completely described.

[4] all of these results of course hold for the analogous neutron situation with d↔u

4.2.3 The $D_{13}(1520)$ resonance

For $D_{13}(1520)$ it can be shown (see Ref. [22]) that the appropriate spin-flavour combination is that of Eq. (4.27h):

$$|D_{13}(1520)\uparrow\rangle \propto \frac{1}{3}\begin{bmatrix} |uud\rangle \\ |udu\rangle \\ |duu\rangle \end{bmatrix}^T \begin{bmatrix} -1 & -1 & 2 \\ -1 & 2 & -1 \\ 2 & -1 & -1 \end{bmatrix} \begin{bmatrix} |\uparrow\uparrow\downarrow\rangle \\ |\uparrow\downarrow\uparrow\rangle \\ |\downarrow\uparrow\uparrow\rangle \end{bmatrix}. \tag{4.32}$$

Here we have a proportionality[5] instead of equality, since the totally symmetric version of the wavefunction will be this wavefunction, appended via the tensor product to a matching mixed symmetric spacial wavefunction, summed cyclically over the possible mixed symmetries. That is to say, the spacial wavefunction for D_{13} will have to be mixed symmetric in order to ensure the overall wavefunction remains anti-symmetric.

4.2.4 The $S_{11}(1650)$ resonance

The last resonance wavefunction we will need written out explicitly is the spin-isospin piece for $S_{11}(1650)$, which given all of its quantum numbers from Tab. (4.1), can be shown to be Eq. (4.27b):

$$|S_{11}(1650)\rangle \propto \left|\phi^{MS}\right\rangle \left|\chi^{S}\right\rangle \propto \frac{1}{3}\begin{bmatrix} |uud\rangle \\ |udu\rangle \\ |duu\rangle \end{bmatrix}^T \begin{bmatrix} -2 & -2 & -2 \\ 1 & 1 & 1 \\ 1 & 1 & 1 \end{bmatrix} \begin{bmatrix} |\uparrow\uparrow\downarrow\rangle \\ |\uparrow\downarrow\uparrow\rangle \\ |\downarrow\uparrow\uparrow\rangle \end{bmatrix}. \tag{4.33}$$

[5]The normalization factor of $\frac{1}{3}$ is left in along with the proportionality in the explicit cases of $S_{11}(1650)$ and $D_{13}(1520)$, because it is needed for future calculations even though the total wave function is not. The factor is the the overall normalization factor of the symmetrized wavefunction, when the spacial components are left compressed as ψ_{lm}^{MS} but the spin-isospin piece is fully expanded out, which is how we use the wavefunctions later on.

4.2.5 The remaining resonances

The remaining resonances all have a directly analogous spin-flavour structure to one of the above.

$$|F_{15}(1680)\rangle \propto |P_{11}(1440)\rangle \propto \left|N^{+}(938)\right\rangle, \tag{4.34a}$$

$$|F_{37}(1950)\rangle \propto |P_{33}(1232)\rangle, \tag{4.34b}$$

$$|S_{11}(1535)\rangle \propto |D_{13}(1520)\rangle. \tag{4.34c}$$

With all these properties and wavefunctions established, we can now see how having the quark model wavefunctions allows us to construct helicity amplitudes, and furthermore, build structure functions of the Nucleon.

4.3 Example: explicit calculation for D_{13}

Let's analyze the D_{13} resonance: For $\lambda = \frac{3}{2}$ there is only 1 possible combination of angular momentum, and so we do not need to worry about pulling out our Clebsh-Gordan tables. The helicity amplitude is thus:

$$\begin{aligned}
A_{3/2}^{\gamma} &= 3\left\langle \psi_{00}N^{+}, \frac{1}{2}\right| e_q\left(AL_{-} + B\sigma_z S_{-}\right)\left|D_{13}, \frac{3}{2}\right\rangle \\
&= 3\left\langle \psi_{00}N_{\uparrow}^{+}\right| e_q\left(AL_{-} + B\sigma_z S_{-}\right)\left|\psi_{11}\phi_{D13}\chi_{\frac{1}{2}}\right\rangle \\
&= 3\left\langle \psi_{00}N_{\uparrow}^{+}\left|e_q\, AL_{-}\right|\psi_{11}\phi_{D13}\chi_{\frac{1}{2}}\right\rangle + 3\left\langle \psi_{00}N_{\uparrow}^{+}\left|e_q\, B\sigma_z S_{-}\right|\psi_{11}\phi_{D13}\chi_{\frac{1}{2}}\right\rangle \\
&= 3\left\langle \psi_{00}N_{\uparrow}^{+}\left|e_q\, A\sqrt{2}\right|\psi_{10}\phi_{D13}\chi_{\frac{1}{2}}\right\rangle - 3\left\langle \psi_{00}N_{\uparrow}^{+}\left|e_q\, B\right|\psi_{11}\phi_{D13}\chi_{-\frac{1}{2}}\right\rangle \\
&= 3\left\langle \psi_{00}N_{\uparrow}^{+}\left|e_q\, A\sqrt{2}\right|\psi_{10}\phi_{D13}\chi_{\frac{1}{2}}\right\rangle - 0 \\
&= 3\left\langle \psi_{00}\left|\, A\sqrt{2}\right|\psi_{10}\right\rangle\left\langle N_{\uparrow}^{+}\left|e_q\right|\phi_{D13}\chi_{\frac{1}{2}}\right\rangle.
\end{aligned} \tag{4.35}$$

Here the superscript has been dropped with the understanding we're acting on the third quark, and a short hand notation is used to keep track of the spacial, flavour, and spin of the states involved. We lose the second term because the inner product of the spin states will give 0 no matter the remaining properties of the wave-function.

The factor of $\sqrt{2}$ is left over from the lowering operator L_-. Focusing on the second factor, the spin-isospin inner product:

$$\begin{aligned}
&\frac{1}{\sqrt{18}}\begin{pmatrix} 2\langle u\uparrow u\uparrow d\downarrow| - \langle u\uparrow u\downarrow d\uparrow| - \langle u\downarrow u\uparrow d\uparrow| \\ +2\langle u\uparrow d\downarrow u\uparrow| - \langle u\downarrow d\uparrow u\uparrow| - \langle u\uparrow d\uparrow u\downarrow| \\ +2\langle d\downarrow u\uparrow u\uparrow| - \langle d\uparrow u\downarrow u\uparrow| - \langle d\uparrow u\uparrow u\downarrow| \end{pmatrix} \\
&\cdot\frac{1}{3}\begin{pmatrix} -e_d|u\uparrow u\uparrow d\downarrow\rangle + 2e_d|u\uparrow u\downarrow d\uparrow\rangle - e_d|u\downarrow u\uparrow d\uparrow\rangle \\ -e_u|u\uparrow d\downarrow u\uparrow\rangle - e_u|u\downarrow d\uparrow u\uparrow\rangle + 2e_u|u\uparrow d\uparrow u\downarrow\rangle \\ +2e_u|d\downarrow u\uparrow u\uparrow\rangle - e_u|d\uparrow u\downarrow u\uparrow\rangle - e_u|d\uparrow u\uparrow u\downarrow\rangle \end{pmatrix}
\end{aligned} \tag{4.36}$$

$$\begin{aligned}
&= \frac{1}{3\sqrt{18}}\left(-2e_d - 2e_d + e_d - 2e_u + e_u - 2e_u + 4e_u + e_u + e_u\right) \\
&= \frac{1}{3\sqrt{18}}\left(3e_u - 3e_d\right) = \frac{1}{\sqrt{18}}\left(e_u - e_d\right).
\end{aligned} \tag{4.37}$$

What's left to figure out is the spacial inner product $\left\langle \psi_{00}\right|A\sqrt{2}\left|\psi_{10}\right\rangle$, which we simply label A_{10} (note we include the lowering coefficient in the compact notation). Thus the final helicity amplitude is:

$$A_{3/2}^{\gamma} = \frac{A_{10}}{\sqrt{2}}(e_u - e_d). \tag{4.38}$$

Moving on to the $\lambda = \frac{1}{2}$ state of the D_{13} resonance, there are two possible combinations of spin and orbital angular momentum which result in this total angular momentum. The relevant piece of our favourite table is:

	J	$3/2$	$1/2$
L	S	$+1/2$	$+1/2$
1	$-1/2$	$\sqrt{1/3}$	$\sqrt{2/3}$
0	$+1/2$	$\sqrt{2/3}$	$-\sqrt{1/3}$

(4.39)

We know D_{13} has total angular momentum $3/2$, so from the first column we can see:

$$\left|D_{13},\frac{1}{2}\right\rangle = \sqrt{\frac{1}{3}}\left|\psi_{11}\phi_{D13}\chi_{-\frac{1}{2}}\right\rangle + \sqrt{\frac{2}{3}}\left|\psi_{10}\phi_{D13}\chi_{\frac{1}{2}}\right\rangle. \tag{4.40}$$

inputting this for the D_{13} ket in the helicity amplitude:

$$\begin{aligned}
A_{1/2}^{\gamma} &= 3\left\langle \psi_{00}N_{\downarrow}^{+}\left|e_q(AL_- + B\sigma_z S_-)\right|D_{13},\frac{1}{2}\right\rangle \\
&= 3\left\langle \psi_{00}N_{\downarrow}^{+}|e_q(AL_- + B\sigma_z S_-)\left(\sqrt{\frac{1}{3}}\left|\psi_{11}\phi_{D13}\chi_{-\frac{1}{2}}\right\rangle + \sqrt{\frac{2}{3}}\left|\psi_{10}\phi_{D13}\chi_{\frac{1}{2}}\right\rangle\right)\right. \\
&= \frac{3}{\sqrt{3}}\left\langle \psi_{00}N_{\downarrow}^{+}|e_q AL_-\left|\psi_{11}\phi_{D13}\chi_{-\frac{1}{2}}\right\rangle + 3\sqrt{\frac{2}{3}}\left\langle \psi_{00}N_{\downarrow}^{+}|e_q B\sigma_z S_-\left|\psi_{10}\phi_{D13}\chi_{\frac{1}{2}}\right\rangle\right. \\
&= \frac{A_{10}}{\sqrt{6}}(e_u - e_d) + 3\sqrt{\frac{2}{3}}\left\langle \psi_{00}N_{\downarrow}^{+}|e_q B\sigma_z S_-\left|\psi_{10}\phi_{D13}\chi_{\frac{1}{2}}\right\rangle\right. \\
&= \frac{A_{10}}{\sqrt{6}}(e_u - e_d) + 3\sqrt{\frac{2}{3}}\left\langle \psi_{00}|B\left|\psi_{10}\right\rangle\right.\left\langle N_{\downarrow}^{+}|e_q\sigma_z S_-\left|\phi_{D13}\chi_{\frac{1}{2}}\right\rangle\right..
\end{aligned} \tag{4.41}$$

If we choose to act to the left with both operators, the inner product here will be nearly identical to that of Eq. (4.37), with a few terms having their signs changed, which changes the sum of charges into:

$$(2e_d - 2e_d + e_d - 2e_u + e_u + 2e_u + 4e_u + e_u - e_u) = 5e_u + e_d, \tag{4.42}$$

giving us a final $\lambda = 1/2$ helicity amplitude

$$\begin{aligned}
A_{1/2}^{\gamma} &= \frac{A_{10}}{\sqrt{6}}(e_u - e_d) + 3\sqrt{\frac{2}{3}}\left\langle \psi_{00}|B\left|\psi_{10}\right\rangle\right.\sqrt{\frac{1}{18}}\frac{1}{3}(5e_u + e_d) \\
&= \frac{1}{\sqrt{6}}\left(A_{10}(e_u - e_d) + \sqrt{2}\,B_{10}\left(\frac{5}{3}e_u + \frac{1}{3}e_d\right)\right).
\end{aligned} \tag{4.43}$$

For the Z helicity amplitudes, both calculations resulting in Eq. (4.43) and Eq. (4.38) would be functionally identical, except the charge operator would be replaced with the weak vector coupling

$$g_q^V = T_q^3 + 2e_q \sin^2(\theta_W). \tag{4.44}$$

This results in:

$$A_{3/2}^{Z} = \frac{A_{10}}{\sqrt{2}}(g_u^V - g_d^V), \tag{4.45a}$$

$$A_{1/2}^{Z} = \frac{1}{\sqrt{6}}\left(A_{10}(g_u^V - g_d^V) + \sqrt{2}\,B_{10}\left(\frac{5}{3}g_u^V + \frac{1}{3}g_d^V\right)\right). \tag{4.45b}$$

4.3.1 Finding C_{D13}

Now that we have the helicity amplitudes of D_{13} we can move on to finding C_{D13}, and then use these coefficients to connect the structure functions. First we must deal with the strange A_{j0} and B_{j0} coefficients, which we will do as Carlson and Rislow [19] do with polarization ratios, defined as:

$$P = \frac{|A_{1/2}^{\gamma}|^2 - |A_{3/2}^{\gamma}|^2}{|A_{1/2}^{\gamma}|^2 + |A_{3/2}^{\gamma}|^2}. \tag{4.46}$$

Which in the specific case of D_{13} simplifies to:

$$\begin{aligned} P &= \frac{|\frac{1}{\sqrt{6}}\left(A_{10}(e_u - e_d) + \sqrt{2}\, B_{10}\ \left(\frac{5}{3}e_u + \frac{1}{3}e_d\right)\right)|^2 - |\frac{A_{10}}{\sqrt{2}}(e_u - e_d)|^2}{|\frac{1}{\sqrt{6}}\left(A_{10}(e_u - e_d) + \sqrt{2}\, B_{10}\ \left(\frac{5}{3}e_u + \frac{1}{3}e_d\right)\right)|^2 + |\frac{A_{10}}{\sqrt{2}}(e_u - e_d)|^2} \\ &= \frac{|\left(A_{10} + \sqrt{2}\, B_{10}\right)|^2 - 3A_{10}^2}{|\left(A_{10} + \sqrt{2}\, B_{10}\right)|^2 + 3A_{10}^2} \\ &= \frac{-2A_{10}^2 + 2B_{10}^2 + 2\sqrt{2}A_{10}B_{10}}{4A_{10}^2 + 2B_{10}^2 + 2\sqrt{2}A_{10}B_{10}}. \end{aligned} \tag{4.47}$$

Data from Ref. [23] and Ref. [24], indicate that as $Q^2 \to 0$, $P\left(Q^2\right) \to -1$. From this fact we can find a relationship between A_{10} and B_{10} at 0 momentum transfer:

$$\begin{aligned} -1 &= \frac{-2A_{10}^2 + 2B_{10}^2 + 2\sqrt{2}A_{10}B_{10}}{4A_{10}^2 + 2B_{10}^2 + 2\sqrt{2}A_{10}B_{10}}, \\ 0 &= 2A_{10}^2 + 4B_{10}^2 + 4\sqrt{2}A_{10}B_{10} \\ &= \frac{A_{10}^2}{B_{10}^2} + 2 + 2\sqrt{2}\frac{A_{10}}{B_{10}} = \left(\frac{A_{10}}{B_{10}} + \sqrt{2}\right)^2 \\ &\Rightarrow A_{10}\left(Q^2 = 0\right) = -\sqrt{2}B_{10}\left(Q^2 = 0\right). \end{aligned} \tag{4.48}$$

The other useful limit is that as $Q^2 \to \infty, P\left(Q^2\right) \to 1$. To satisfy this limit the quotient of A and B can be parameterized by any function f_1 which goes to 0 at infinity. Here is an example of a monopole function of Q^2 which fits both limits

$$\frac{A_{10}\left(Q^2\right)}{B_{10}\left(Q^2\right)} = -\sqrt{2}\, f_1\left(Q^2\right) = -\sqrt{2}\, \frac{1}{1 + Q^2/\Lambda_1^2}. \tag{4.49}$$

Heading back to our definition of C_{res} and remembering that $A^\gamma \to A^Z$ when $e_q \to g_q^V$.

$$C_{D13} = 2\frac{\sum_\lambda A_\lambda^\gamma A_\lambda^Z}{\sum_\lambda \left(A_\lambda^\gamma\right)^2} = 2\frac{A_{1/2}^\gamma A_{1/2}^Z + A_{3/2}^\gamma A_{3/2}^Z}{\left(A_{1/2}^\gamma\right)^2 + \left(A_{3/2}^\gamma\right)^2}, \tag{4.50}$$

substituting the quark charges into the A^γ values, and plugging everything in

$$\begin{aligned} &= \frac{\frac{1}{3}\left(A_{10} + \sqrt{2}\, B_{10}\right)\left(A_{10}(g_u^V - g_d^V) + \frac{\sqrt{2}}{3}B_{10}\left(5g_u^V + g_d^V\right)\right) + A_{10}^2(g_u^V - g_d^V)}{\left(\frac{1}{\sqrt{6}}\left(A_{10} + \sqrt{2}B_{10}\right)\right)^2 + \left(\frac{A_{10}}{\sqrt{2}}\right)^2} \\ &= \frac{\left(4A_{10}^2 + \sqrt{2}A_{10}B_{10}\right)(g_u^V - g_d^V) + \left(\frac{\sqrt{2}}{3}\, A_{10}B_{10} + \frac{2}{3}\, B_{10}^2\right)\left(5g_u^V + g_d^V\right)}{2A_{10}^2 + B_{10}^2 + \sqrt{2}A_{10}B_{10}}. \end{aligned} \tag{4.51}$$

Substituting in for the functional ratio of the coefficients f_1, and inputting the vector couplings of the quarks with the substitution $S^2 = \sin^2\theta_W$:

$$\begin{aligned} &= 2\frac{(4f_1^2 - f_1)(1 - 2S^2) + \left(-\frac{1}{3}\, f_1 + \frac{1}{3}\right)(2 - 6S^2)}{4f_1^2 + 1 - 2f_1} \\ &= \frac{8f_1^2 - 16f_1^2S^2 + 8f_1S^2 - \frac{10}{3}f_1 + \frac{4}{3} - 4S^2}{4f_1^2 + 1 - 2f_1} \\ &= \frac{4f_1^2 - 16f_1^2S^2 + 1 - 4S^2 - 2f_1 + 8f_1S^2 - \frac{4}{3}f_1 + \frac{1}{3} + 4f_1^2}{4f_1^2 + 1 - 2f_1} \\ &= \frac{(4f_1^2 + 1 - 2f_1)(1 - 4S^2) - \frac{4}{3}f_1 + \frac{1}{3} + 4f_1^2}{4f_1^2 + 1 - 2f_1} \\ &= \frac{(4f_1^2 + 1 - 2f_1)(1 - 4S^2) - \frac{4}{3}f_1 + \frac{1}{3} + 4f_1^2}{4f_1^2 + 1 - 2f_1} \\ &= \frac{4f_1^2 - \frac{4}{3}f_1 + \frac{1}{3}}{4f_1^2 - 2f_1 + 1} + (1 - 4S^2) = \frac{3f_1^2 + (f_1 - 1/3)(f_1 - 1)}{3f_1^2 + (f_1 - 1)^2} + Q_W^{p,LO} = C_{D13}^p, \end{aligned} \tag{4.52}$$

where $Q_W^{p,LO}$ is the weak charge of the proton when computed using leading order diagrams. It is equal to $1 - 4\sin^2\theta_W$. The procedure to get C_{D13}^n, the equivalent coefficient from the helicity amplitudes of the neutron, is identical, one simply swaps $e_u \leftrightarrow e_d$ and $g_u^V \leftrightarrow g_d^V$. Doing so and simplifying we find:

$$C_{D13}^n = \frac{3f_1^2 + (f_1 - 1/3)(f_1 - 1)}{3f_1^2 + (f_1 - 1/3)^2} + Q_W^{p,LO}. \tag{4.53}$$

4.4 Summary of resonance helicity amplitudes:

Resonance	Helicty Amplitude (A_λ^γ)
$P_{33}(1232)$	$A_{1/2} = 2\sqrt{2}B_{00}(\frac{1}{3}e_u - \frac{1}{3}e_d)$
$S_{11}(1535)$	$A_{1/2} = \sqrt{\frac{1}{3}}A_{10}(e_u - e_d) - \sqrt{\frac{1}{6}}B_{10}\left(\frac{5}{3}e_u + \frac{1}{3}e_d\right)$
$D_{13}(1520)$	$A_{1/2} = \sqrt{\frac{1}{6}}A_{10}(e_u - e_d) + \sqrt{\frac{1}{3}}B_{10}\left(\frac{5}{3}e_u + \frac{1}{3}e_d\right)$
	$A_{3/2} = \sqrt{\frac{1}{2}}A_{10}(e_u - e_d)$
$F_{15}(1680)$	$A_{1/2} = \sqrt{\frac{2}{5}}\,A_{20}\,(2e_u + e_d) + \sqrt{\frac{3}{5}}\,B_{20}\left(\frac{4}{3}e_u - \frac{1}{3}e_d\right)$
	$A_{3/2} = \sqrt{\frac{4}{5}}\,A_{20}\,(2e_u + e_d)$
$S_{11}(1650)$	$A_{1/2} = -\sqrt{\frac{2}{3}}B_{10}\left(\frac{1}{3}e_u + \frac{2}{3}e_d\right)$
$P_{11}(1440)$	$A_{1/2} = B_{00}\left(\frac{4}{3}e_u - \frac{1}{3}e_d\right)$
$F_{37}(1950)$	$A_{1/2} \propto (e_u - e_d)$

TABLE 4.2: Summary of the Quark Model Helicity Amplitudes. To find the neutron or vector (Z) helicity amplitudes, simply swap $e_u \leftrightarrow e_d$ or replace $e_q \to g_q^V$ respectively.

Performing the calculations in the preceding section for each of the seven Christy-Bosted resonances (explicitly shown in Appendix (A)), we find the helicity amplitudes collected in Tab. (4.2), and the corrective prefactors C_{res} in Tab. (4.3).

Resonance	$C_{res}^p - Q_W^{p,LO}$	$C_{res}^n - Q_W^{p,LO}$
$P_{33}(1232)$	2	1
$S_{11}(1535)$	$\frac{2f_1+1/3}{2f_1+1}$	$\frac{2f_1+1}{2f_1+1/3}$
$D_{13}(1520)$	$\frac{3f_1^2+(f_1-1/3)(f_1-1)}{3f_1^2+(1-f_1)^2}$	$\frac{3f_1^2+(f_1-1/3)(f_1-1)}{3f_1^2+(f_1-1/3)^2}$
$F_{15}(1680)$	$\frac{2/3(1-f_2)}{(1-f_2)^2+2f_2^2}$	$\frac{3}{2}(1-f_2)$
$S_{11}(1650)$	∞[6]	$-Q_W^{p,LO}/2$
$P_{11}(1440)$	2/3	3/2
$F_{37}(1950)$	1	1

TABLE 4.3: Corrective pre-factors for connecting $F_1^{\gamma Z}$ to $F_1^{\gamma\gamma}$.

[6]Notice the photon helicity amplitude for $S_{11}(1650)$ resonance is 0 for the usual electric quark charges, and as such this coefficient is not defined.

4.4.1 Axial helicity amplitudes:

The axial amplitudes look exactly as the electromagnetic amplitudes as defined in Eq. (4.6), except that the coupling is g_q^A, and there is a factor of γ^5 in the spinor product:

$$A_\lambda^{ZA} = 3g_q^A \left\langle \psi_{res}\phi_{res}\chi_\lambda \left| \epsilon_+^\mu \bar{u}\left(k',\lambda'\right)\gamma^5\gamma_\mu u\left(k,s'\right)\right| \psi_N\phi_N\chi_s \right\rangle . \tag{4.54}$$

For reasons not completely obvious, Rislow and Carlson jump immediately to the non-relativistic limit, where the mass of the quark is much greater than the quark momentum. For completeness we make the same leap, which results in the following simplified axial helicity amplitude:

$$A_\lambda^{ZA} = 3g_q^A \left\langle \psi_N\phi_N\chi_s \left| B\sigma_z S_- \right| \psi_{res}\phi_{res}\chi_\lambda \right\rangle \frac{4m_q\nu}{q_z^2}. \tag{4.55}$$

Here the new factors of quark mass m_q, boson momentum q_z, and boson energy ν, are pulled out to ensure in both cases we are talking about the same $B_{\ell 0}$ factors as before. This simplification immediately omits the option of a non-zero $A_{3/2}^{ZA}$, and effectively gives us all the same helicity amplitudes as before, with $A_{00} = A_{10} = A_{20} = 0$. This makes the axial table of helicity amplitudes simple to compute, and shown in Tab. (4.4).

Resonance	A^{ZA}	$C_{res}^{pA}/(\frac{4m_q\nu}{q_z^2})$	$C_{res}^{nA}/(\frac{4m_q\nu}{q_z^2})$
$P_{33}(1232)$	$A_{1/2} = \frac{2\sqrt{2}}{3}B_{00}(g_u^A - g_d^A)$	$1\cdot 2$	2
$S_{11}(1535)$	$A_{1/2} = -\frac{1}{\sqrt{6}}B_{10}\left(\frac{5}{3}g_u^A + \frac{1}{3}g_d^A\right)$	$3\cdot\frac{4}{3(2f_1+1)}$	$\frac{4/3}{2f_1+1/3}$
$D_{13}(1520)$	$A_{1/2} = \sqrt{\frac{1}{3}}\,B_{10}\left(\frac{5}{3}g_u^A + \frac{1}{3}g_d^A\right)$	$1\cdot\frac{4/3(1-f_1)}{(1-f_1)^2+3f_1^2}$	$\frac{4/3(1/3-f_1)}{(1/3-f_1)^2+3f_1^2}$
$F_{15}(1680)$	$A_{1/2} = \sqrt{\frac{3}{5}}\,B_{20}\left(\frac{4}{3}g_u^A - \frac{1}{3}g_d^A\right)$	$1\cdot\frac{5/3(1-f_2)}{(1-f_2)^2+2f_2^2}$	5/2
$S_{11}(1650)$	$A_{1/2} = -\sqrt{\frac{2}{27}}\,B_{10}\left(g_u^A + 2g_d^A\right)$	∞[7]	1
$P_{11}(1440)$	$A_{1/2} = B_{00}\left(\frac{4}{3}g_u^A - \frac{1}{3}g_d^A\right)$	$1\cdot 5/3$	5/2
$F_{37}(1950)$	$A_{1/2} \propto (g_u^A - g_d^A)$	$1\cdot 2$	2

TABLE 4.4: Summary of the non-relativistic axial quark model helicity amplitudes. Factors preceding a $\cdot$ highlight the minor differences between this work and the published results in Ref. [19]. Not listed for the neutron which is not reported in the aforementioned work.

[7] See footnote 6 from the analogous entry in Tab. (4.3).

4.5 A concern regarding mixed symmetric wavefunctions

After all this, there is a minor concern about the technique for those resonances with mixed-symmetric wavefunctions ($D_{13}(1520)$, $S_{11}(1535)$, and $S_{11}(1650)$). With these resonances we computed the helicity amplitudes for only one of the cyclic permutations, specifically with symmetry under swapping of quarks 2 and 3. One might suspect the result of the calculations for the wavefunctions of mixed symmetry under quarks 3 and 1 and mixed symmetry under quarks 1 and 2 should give the same helicity amplitudes, but this turns out to be wrong. For the second mixed symmetry under quarks 3 and 1, the helicity amplitude derived remains the same and so the wrong hypothesis appears to gain credibility, however for mixed symmetry under quarks 1 and 2, the derived helicity amplitude is twice the negative of the original. That is to say for the relevant resonances:

$$A_\lambda^{12} = -2A_\lambda^{23} = -2A_\lambda^{31}, \tag{4.56}$$

where A_λ^{ab} is the the helicity amplitude derived using the spin-isospin wavefunction which is symmetric under swapping quarks a and b. It is plain to see by inspection (see for e.g. the top of Eq. (4.37)) why this tease of symmetry happens: only one permutation will match the ket with coefficient $2e_d$ with a bra of coefficient 2 in the proton wavefunction, while for the other two permutations that pairing will happen to a factor of $2e_u$. If we do not closely inspect the spacial factors in the matrix element, it is clear this implies that all the helicity amplitudes of these three resonances should be 0. One way out of this uncomfortable position would be to assume generally that the mixed symmetric wavefunctions will have different spacial factors A and B. Thus for the spacial wave function with mixed symmetry under quarks a and b one has:

$$A_{\ell 0}^{ab} = \langle \psi_{00} | \, A \, c \, \left| \psi_{\ell 0}^{ab} \right\rangle , \tag{4.57a}$$

$$B_{\ell 0}^{ab} = \langle \psi_{00} | \, B \, \left| \psi_{\ell 0}^{ab} \right\rangle , \tag{4.57b}$$

where c is the constant that falls out of the operator L_+. One could go on to define

$$A_{\ell 0}^{M} = A_{\ell 0}^{23} + A_{\ell 0}^{31} - 2A_{\ell 0}^{12} \tag{4.58a}$$

$$B_{\ell 0}^{M} = B_{\ell 0}^{23} + B_{\ell 0}^{31} - 2B_{\ell 0}^{12} \tag{4.58b}$$

(where M stands for 'mixed'), and then the analysis would carry on as usual with these newly defined $A_{\ell 0}^{M}$ and $B_{\ell 0}^{M}$. There is no reason a priori to anticipate in either case that $A_{\ell 0}^{M} = A_{\ell 0}$ or $A_{\ell 0}^{M} = A_{\ell 0}$, so in general one would need new functions f_{ℓ}^{M} to ensure they are not confused with f_ℓ, which would be reserved for those C_{res} computed for wavefunctions with symmetric spacial components.

Chapter 5

Conclusions

In this thesis a new unbiased global analysis of the proton elastic form factors was presented. In order to perform these fits, we constructed an extension of the unbiased fitting method used by Ball *et al.* [9], which allows for fitting whole functions which are linear in their parameters, and not only single parameters. In addition to this, we found ways for extending the new method to work for models of observables which are non-linear in their parameters. In the resulting analysis, we found that unbiased fitting leads to minor improvements to fits of form factor models to the world cross section data. The analysis shows that the common fitted normalizations resulting from the penalty trick are only useful as a crutch to approximate the unbiased fitting, and as such are not physically meaningful. We find that TPE-corrections are needed in order to make LT data consistent with PT data. We also find that fitting TPE-corrected LT data alongside PT data, still places a minor strain on the TPE-corrected LT fit, implying there are still improvements to be had in the calculation of TPE-corrections. In addition to this, a review of the constituent quark model was performed in order to independently verify the results of Ref. [19], which resulted in only minor corrections.

5.1 Future work

Both the low Q^2 global analysis by Bernauer *et al.* [7], and recent work closing the gap on the proton radius discrepancy (such as Ref. [25]), use the penalty trick in order to fit their global data sets. In order to ensure correctness and soundness of the results presented, it would be worthwhile to perform reanalysis of these works in order to check if the unbiased fitting leads to any improvements in the extracted values and fits. Additionally, for utilitarian and phenomenological purposes, the author intends to perform a truly global analysis of all readily available cross section and polarization ratio data, to construct the worlds foremost models of the protons elastic form factors.

Appendix A

Helicty Amplitudes of the Nucleon Resonances

A.1 $S_{11}(1535)$

Before any explicit calculations we may quickly see that

$$A_{3/2} = 3 \left\langle \psi_{00} N^+, \frac{1}{2} \left| e_q (AL_- + B\sigma_z S_-) \right| S_{11}(1535), \frac{3}{2} \right\rangle = 0, \tag{A.1}$$

since $S_{11}(1535)$ has no $J_z = 3/2$ state. It does have a $J_z = 1/2$ state which is easily constructed via the usual combination of angular momentum with Clebsh-Gordon coefficients:

$$\left| S_{11}(1535), \frac{1}{2} \right\rangle = \sqrt{\frac{2}{3}} \left| \psi_{11} \phi_{D13} \chi_{-\frac{1}{2}} \right\rangle - \sqrt{\frac{1}{3}} \left| \psi_{10} \phi_{D13} \chi_{\frac{1}{2}} \right\rangle . \tag{A.2}$$

Because D_{13} and $S_{11}(1535)$ share the same spin-flavour wave-function, we've written the above wave function in said form. As well, from this similarity it is not difficult to repeat our calculations for D_{13} and find our helicity amplitude for this state is nearly

the same as for D_{13}, with only Clebsh-Gordan coefficients modified:

$$A_{1/2} = \frac{1}{\sqrt{6}}\left(\sqrt{2}A_{10}(e_u - e_d) - B_{10}\left(\frac{5}{3}e_u + \frac{1}{3}e_d\right)\right). \tag{A.3}$$

From this we can find C_{S11}:

$$C^p_{S11} = 2\frac{A^Z_{1/2}}{A^\gamma_{1/2}} = 2\frac{\sqrt{2}A_{10}(g^V_u - g^V_d) - B_{10}\left(\frac{5}{3}g^V_u + \frac{1}{3}g^V_d\right)}{\sqrt{2}A_{10}(e_u - e_d) - B_{10}\left(\frac{5}{3}e_u + \frac{1}{3}e_d\right)} = \frac{2f_1 + 1/3}{2f_1 + 1} + Q^{p,LO}_W, \tag{A.4a}$$

$$C^n_{S11} = 2\frac{A^Z_{1/2}}{A^\gamma_{1/2}} = 2\frac{\sqrt{2}A_{10}(g^V_d - g^V_u) - B_{10}\left(\frac{5}{3}g^V_d + \frac{1}{3}g^V_u\right)}{\sqrt{2}A_{10}(e_d - e_u) - B_{10}\left(\frac{5}{3}e_d + \frac{1}{3}e_u\right)} = \frac{2f_1 + 1}{2f_1 + 1/3} + Q^{p,LO}_W. \tag{A.4b}$$

A.2 $P_{33}(1232)$ and $F_{37}(1950)$

Similarly to above,

$$A_{3/2} = 3\left\langle \psi_{00}N^+, \frac{1}{2}\right| e_q(AL_- + B\sigma_z S_-)\left|P_{33}, \frac{3}{2}\right\rangle = 0, \tag{A.5}$$

since P_{33} has no $J_z = 3/2$ state.[1] It does have a $J_z = 1/2$ state:

$$\begin{aligned} A_{1/2} &= 3\left\langle \psi_{00}N^+, -\frac{1}{2}\left|e_q(AL_- + B\sigma_z S_-)\right| P_{33}, \frac{1}{2}\right\rangle \\ &= 3\left\langle \psi_{00}N^+, -\frac{1}{2}\left|e_q(AL_- + B\sigma_z S_-)\right| \psi_{00}\phi_{P33}\chi_{\frac{1}{2}}\right\rangle \\ &= 3\left\langle \psi_{00}N^+, -\frac{1}{2}\left|e_q(B\sigma_z S_-)\right| \psi_{00}\phi_{P33}\chi_{\frac{1}{2}}\right\rangle \\ &= 3\left\langle \psi_{00}\right|B\left|\psi_{00}\right\rangle \left\langle N^+, -\frac{1}{2}\left|e_q(\sigma_z S_-)\right| \phi_{P33}\chi_{\frac{1}{2}}\right\rangle \end{aligned} \tag{A.6}$$

[1] Of course in general P_{33}, the Delta, has this state. But in the context of helicity amplitudes we are restricted to both spin and isospin states with projection 1/2 respectively. With no orbital angular momentum, the total angular momentum can only be 1/2.

$$
\begin{aligned}
&= \frac{3B_{00}}{\sqrt{18}} \begin{pmatrix} -2\langle u\uparrow u\uparrow d\downarrow| - \langle u\uparrow u\downarrow d\uparrow| - \langle u\downarrow u\uparrow d\uparrow| \\ +2\langle u\uparrow d\downarrow u\uparrow| - \langle u\downarrow d\uparrow u\uparrow| + \langle u\uparrow d\uparrow u\downarrow| \\ +2\langle d\downarrow u\uparrow u\uparrow| - \langle d\uparrow u\downarrow u\uparrow| + \langle d\uparrow u\uparrow u\downarrow| \end{pmatrix} \\
&\quad \cdot\frac{1}{3} \begin{pmatrix} e_d|u\uparrow u\uparrow d\downarrow\rangle + e_d|u\uparrow u\downarrow d\uparrow\rangle + e_d|u\downarrow u\uparrow d\uparrow\rangle \\ +e_u|u\uparrow d\downarrow u\uparrow\rangle + e_u|u\downarrow d\uparrow u\uparrow\rangle + e_u|u\uparrow d\uparrow u\downarrow\rangle \\ +e_u|d\downarrow u\uparrow u\uparrow\rangle + e_u|d\uparrow u\downarrow u\uparrow\rangle + e_u|d\uparrow u\uparrow u\downarrow\rangle \end{pmatrix}.
\end{aligned} \tag{A.7}
$$

Evaluating and simplifying this inner product delivers us the following helicity amplitude,

$$A_{1/2} = \frac{2\sqrt{2}B_{00}}{3}(e_u - e_d). \tag{A.8}$$

This leads to a simple C_{P33} in both cases:

$$
\begin{aligned}
C^p_{P33} = C^n_{P33} &= 2\frac{\sum_\lambda A^\gamma_\lambda A^Z_\lambda}{\sum_\lambda \left(A^\gamma_\lambda\right)^2} = 2\frac{A^\gamma_{1/2}A^Z_{1/2} + A^\gamma_{3/2}A^Z_{3/2}}{\left(A^\gamma_{1/2}\right)^2 + \left(A^\gamma_{3/2}\right)^2} = 2\frac{A^Z_{1/2}}{A^\gamma_{1/2}} \\
&= 2 - 4S^2 = 1 + Q^{p,LO}_W.
\end{aligned} \tag{A.9}
$$

A.3 $F_{15}(1680)$

There are two possible combinations of spin and orbital angular momenta to generate this excitation with $J = 5/2, J_z = 3/2$, and they combine in the following way:

$$\left|F_{15}, \frac{3}{2}\right\rangle = \sqrt{\frac{1}{5}}\left|\psi_{22}\phi_{F15}\chi_{-\frac{1}{2}}\right\rangle + \sqrt{\frac{4}{5}}\left|\psi_{21}\phi_{F15}\chi_{\frac{1}{2}}\right\rangle. \tag{A.10}$$

Substituting this resonance into the helicity amplitude, we find:

$$
\begin{aligned}
A_{3/2} &= 3\left\langle \psi_{00}N^+, \frac{1}{2}\left|e_q(AL_- + B\sigma_z S_-)\right| F_{15}, \frac{3}{2}\right\rangle \\
A_{3/2} &= 0 + 3\sqrt{\frac{4}{5}}\left\langle \psi_{00}N^+, \frac{1}{2}|e_q(AL_- + B\sigma_z S_-)|\psi_{21}\phi_{F15}\chi_{\frac{1}{2}}\right\rangle \\
&= \frac{6}{\sqrt{5}}\left\langle\psi_{00}|AL_-|\psi_{21}\right\rangle\left\langle N^+_\uparrow|e_q|\phi_{F15}\chi_{\frac{1}{2}}\right\rangle \\
&= \frac{6}{\sqrt{5}}A_{20}\frac{12e_u + 6e_d}{18} = \frac{2}{\sqrt{5}}A_{20}\left(2e_u + e_d\right).
\end{aligned} \tag{A.11}
$$

Similarly the state with $J = 5/2, J_z = 1/2$ is built from:

$$\left| F_{15}, \frac{1}{2} \right\rangle = \sqrt{\frac{2}{5}} \left| \psi_{21} \phi_{F15} \chi_{-\frac{1}{2}} \right\rangle + \sqrt{\frac{3}{5}} \left| \psi_{20} \phi_{F15} \chi_{\frac{1}{2}} \right\rangle . \tag{A.12}$$

Plugging this in as usual,

$$\begin{aligned} A_{1/2} &= 3 \left\langle \psi_{00} N^+_\downarrow \left| e_q (AL_- + B\sigma_z S_-) \right| F_{15}, \frac{1}{2} \right\rangle \\ &= 3\sqrt{\frac{2}{5}} \left\langle \psi_{00} N^+_\downarrow | e_q (AL_-) | \psi_{21} \phi_{F15} \chi_{-\frac{1}{2}} \right\rangle \\ &\qquad + 3\sqrt{\frac{3}{5}} \left\langle \psi_{00} N^+_\downarrow, | e_q (B\sigma_z S_-) | \psi_{20} \phi_{F15} \chi_{\frac{1}{2}} \right\rangle , \end{aligned} \tag{A.13}$$

and focusing first on the 'A' term:

$$\begin{aligned} & 3\sqrt{\frac{2}{5}} \left\langle \psi_{00} N^+_\downarrow | e_q (AL_-) | \psi_{21} \phi_{F15} \chi_{-\frac{1}{2}} \right\rangle \\ &= 3\sqrt{\frac{2}{5}} \left\langle \psi_{00} | AL_- | \psi_{21} \right\rangle \left\langle N^+, -\frac{1}{2} | e_q | \phi_{F15} \chi_{-\frac{1}{2}} \right\rangle \\ &= \sqrt{\frac{2}{5}} A_{20} \left(2e_u + e_d \right) , \end{aligned} \tag{A.14}$$

then focusing on the 'B' term:

$$\begin{aligned} & 3\sqrt{\frac{3}{5}} \left\langle \psi_{00} N^+_\downarrow, | e_q (B\sigma_z S_-) | \psi_{20} \phi_{F15} \chi_{\frac{1}{2}} \right\rangle \\ &= 3\sqrt{\frac{3}{5}} \left\langle \psi_{00} | B | \psi_{20} \right\rangle \left\langle N^+, -\frac{1}{2} | e_q (\sigma_z S_-) | \phi_{F15} \chi_{\frac{1}{2}} \right\rangle \\ &= \sqrt{\frac{3}{5}} B_{20} \frac{(4e_u - e_d)}{3}, \end{aligned} \tag{A.15}$$

and summing them we get the total helicity amplitude:

$$A_{1/2} = \sqrt{\frac{2}{5}} A_{20} \left(2e_u + e_d \right) + \sqrt{\frac{3}{5}} B_{20} \frac{(4e_u - e_d)}{3}. \tag{A.16}$$

With these new coefficients A_{20} and B_{20} we need to find a new function $f_2(Q^2)$ which fits similar polarization limits, just as we did for f_1 before. Starting again from the

polarization ratio Eq. (4.46)

$$-1 = \frac{(-2A_{20}^2 + 2\sqrt{6}A_{20}B_{20} + 3B_{20}^2)}{(6A_{20}^2 + 2\sqrt{6}A_{20}B_{20} + 3B_{20}^2)}, \tag{A.17a}$$

$$0 = \frac{A_{20}^2}{B_{20}^2} + \sqrt{6}\frac{A_{20}}{B_{20}} + 3/2 = \left(\frac{A_{20}}{B_{20}} + \sqrt{\frac{3}{2}}\right)^2. \tag{A.17b}$$

Thus any function which goes to 0 at infinity and is $-\sqrt{3/2}$ at 0 may be used to model $A_{20}/B_{20} = f_2$. Once again we may use this function to simplify our expressions for C_{F15}:

$$\begin{aligned} C_{F15}^p &= 2\frac{\sum_\lambda A_\lambda^\gamma A_\lambda^Z}{\sum_\lambda \left(A_\lambda^\gamma\right)^2} = 2\frac{A_{1/2}^\gamma A_{1/2}^Z + A_{3/2}^\gamma A_{3/2}^Z}{\left(A_{1/2}^\gamma\right)^2 + \left(A_{3/2}^\gamma\right)^2} \\ &= 2\frac{\left(\sqrt{2}\sqrt{3}\, A_{20}B_{20} + 6\, A_{20}^2\right)\left(2g_u^V + g_d^V\right) + \left(\sqrt{3}\sqrt{2}\, A_{10}B_{20} + 3\, B_{20}^2\right)\frac{\left(4g_u^V - g_d^V\right)}{3}}{(6A_{20}^2 + 2\sqrt{2}A_{20}\sqrt{3}B_{20} + 3B_{20}^2)} \\ &= \frac{(-3f_2 + 9\, f_2^2)\,(1 - 4S^2) + (-f_2 + 1)\,(5 - 12S^2)}{(9f_2^2 - 6f_2 + 3)} \\ &= \frac{9f_2^2 - 6f_2 + 3 - 36f_2^2S^2 + 24f_2S^2 - 12S^2 - 2f_2 + 2}{(9f_2^2 - 6f_2 + 3)} \\ &= \frac{2/3(1 - f_2)}{(f_1 - 1)^2 + 2f_2^2} + Q_W^{p,LO}. \end{aligned} \tag{A.18}$$

The analgous calculation for the resonance of the neutron gives:

$$\begin{aligned} C_{F15}^n &= \frac{-\sqrt{3}\sqrt{2}\, A_{20}\,(-1/2) - B_{20}\,(-5/2 + 4S^2)}{B_{20}} \\ &= \frac{3}{2}(1 - f_2) + Q_W^{p,LO}. \end{aligned} \tag{A.19}$$

A.4 $S_{11}(1650)$

We know

$$A_{3/2} = 3\left\langle \psi_{00}N^+, \frac{1}{2}\left|e_q(AL_- + B\sigma_z S_-)\right| S_{11}(1650), \frac{3}{2}\right\rangle = 0, \tag{A.20}$$

since $S_{11}(1650)$ has no $J_z = 3/2$ state. It does have a $J_z = 1/2$ state:

$$\left|S_{11}(1535), \frac{1}{2}\right\rangle = \sqrt{\frac{1}{6}}\left|\psi_{11}\phi_{S11}\chi_{-\frac{1}{2}}\right\rangle - \sqrt{\frac{1}{3}}\left|\psi_{10}\phi_{S11}\chi_{\frac{1}{2}}\right\rangle, \tag{A.21}$$

which allows us to find the helicity amplitude

$$\begin{aligned}
A_{1/2} &= 3\sqrt{\frac{1}{6}}\left\langle \psi_{00}N^+, -\frac{1}{2}|e_q(AL_- + B\sigma_z S_-)|\psi_{11}\phi_{S11}\chi_{-\frac{1}{2}}\right\rangle \\
&\qquad - 3\sqrt{\frac{1}{3}}\left\langle \psi_{00}N^+, -\frac{1}{2}|e_q(AL_- + B\sigma_z S_-)|\psi_{10}\phi_{S11}\chi_{\frac{1}{2}}\right\rangle \\
&= 0 - 3\sqrt{\frac{1}{3}}\left\langle \psi_{00}N^+, -\frac{1}{2}|e_q(B\sigma_z S_-)|\psi_{10}\phi_{S11}\chi_{\frac{1}{2}}\right\rangle \\
&= -3\sqrt{\frac{1}{3}}\,\langle\psi_{00}|B|\psi_{10}\rangle\left\langle N^+, -\frac{1}{2}|e_q(\sigma_z S_-)|\phi_{S11}\chi_{\frac{1}{2}}\right\rangle \\
&= -3\sqrt{\frac{1}{3}}\,B_{10}\frac{2e_u + 4e_d}{3\sqrt{18}} \\
&= -\sqrt{\frac{2}{27}}\,B_{10}\,(e_u + 2e_d)\,.
\end{aligned} \tag{A.22}$$

This is an interesting resonance because the first 0 is a consequence of the structure of the wave-function, and the charge operator, not a result of orthogonality; additionally values of the quark charges mean the helicity amplitude should always be 0 for the proton, and thus unobservable. However this state can and does mix the other S_{11} resonance and thus we have observed it. As such all other properties (such as C_{S11}) will be taken from the $S_{11}(1535)$ resonance and not this one, as to avoid divisions by 0. For what it's worth:

$$C^n_{S11} = \frac{Q^{p,LO}_W}{2}. \tag{A.23}$$

A.5 $P_{11}(1440)$

This resonance, also known as the Roper resonance, is particularly simple to work with as it is a radial excitation of the nucleon. With this we know the orbital angular momentum operator will annihilate any ket it acts on. Thus we are only left with the

'B' part of the operator:

$$\begin{aligned} A_{1/2} &= 3\left\langle \psi_{00}N^{+}, -\frac{1}{2}|e_q B\sigma_z S_-|\psi_{00}N^{+}, \frac{1}{2}\right\rangle = \frac{3B_{00}}{18}\left(8e_u - 2e_d\right) \\ &= B_{00}\left(\frac{4}{3}e_u - \frac{1}{3}e_d\right). \end{aligned} \tag{A.24}$$

From this we acquire the corrective pre-factors quite simply:

$$\begin{aligned} C^{p}_{P11} &= (5/3 - 4S^2) = 2/3 + Q_W^{p,LO} textrm, \\ C^{n}_{P11} &= \left(5/2 - 4S^2\right) = 3/2 + Q_W^{p,LO}. \end{aligned} \tag{A.25}$$

Appendix B

Covariance Matrices for Fits

B.1 Convention for element ordering

All covariance matrices are ordered such that the parameters are ordered first alphabetically then numerically.

For Gramolin model fits, the ordering of the parameters is: $\{a_1, a_2, a_3, b_1, b_2, b_3\}$.

For all z-expansion model fits, the ordering of the parameters is: $\{a_1, a_2, a_3, a_4, b_1, b_2, b_3, b_4\}$.

B.2 Chapter 2 fits

Covariance sub-matrix for the penalty trick fit of the Gramolin and Nikolenko model to the uncorrected data, resulting in Tab. (2.1). It is the inverse Hessian of the penalty chi-square for the fit. It is constant and exact, however the 15×15 matrix does not reasonably fit on any page, so the relevant model parameter correlations are listed, without the normalization parameters. Please contact the author if you seek the full covariance matrix.

$$\begin{pmatrix} 0.0393 & -0.0784 & 0.0359 & -0.00221 & 0.00647 & -0.00314 \\ -0.0784 & 0.205 & -0.105 & 0.000850 & -0.0108 & 0.00654 \\ 0.0359 & -0.105 & 0.0584 & 0.000258 & 0.00444 & -0.00315 \\ -0.00221 & 0.000850 & 0.000258 & 0.00156 & -0.00202 & 0.000693 \\ 0.00647 & -0.0108 & 0.00444 & -0.00202 & 0.00326 & -0.00129 \\ -0.00314 & 0.00654 & -0.00315 & 0.000693 & -0.00129 & 0.000558 \end{pmatrix} \tag{B.1}$$

Covariance matrix for the extended t_0 fit result in Tab. (2.3):

$$\begin{pmatrix} 0.0395 & -0.0765 & 0.0329 & -0.00245 & 0.00695 & -0.00329 \\ -0.0765 & 0.198 & -0.0965 & 0.00163 & -0.0120 & 0.00688 \\ 0.0329 & -0.0965 & 0.0520 & -0.000157 & 0.00484 & -0.00319 \\ -0.00245 & 0.00163 & -0.000157 & 0.00136 & -0.00176 & 0.000593 \\ 0.00695 & -0.0120 & 0.00484 & -0.00176 & 0.00295 & -0.00118 \\ -0.00329 & 0.00688 & -0.00319 & 0.000593 & -0.00118 & 0.000518 \end{pmatrix} \tag{B.2}$$

Covariance sub-matrix for the penalty trick fit of the Gramolin and Nikolenko model to the TPE-corrected data, resulting in Tab. (2.5). It is the inverse Hessian of the penalty chi-square for the fit. It is constant and exact, however the 15×15 matrix does not reasonably fit on any page, so the relevant model parameter correlations are listed, without the normalization parameters. Please contact the author if you seek the

full covariance matrix.

$$\begin{pmatrix} 0.0402 & -0.0810 & 0.0372 & -0.00228 & 0.00674 & -0.00328 \\ -0.0810 & 0.214 & -0.109 & 0.000888 & -0.0114 & 0.00690 \\ 0.0372 & -0.109 & 0.0615 & 0.000236 & 0.00473 & -0.00337 \\ -0.00228 & 0.000888 & 0.000236 & 0.00160 & -0.00207 & 0.000713 \\ 0.00674 & -0.0114 & 0.00473 & -0.00207 & 0.00337 & -0.00134 \\ -0.00328 & 0.00690 & -0.00337 & 0.000713 & -0.00134 & 0.000584 \end{pmatrix} \tag{B.3}$$

Covariance matrix for the extended t_0 fit result in Tab. (2.7):

$$\begin{pmatrix} 0.0362 & -0.0755 & 0.0364 & -0.00145 & 0.00559 & -0.00296 \\ -0.0755 & 0.194 & -0.102 & 0.000674 & -0.0104 & 0.00653 \\ 0.0364 & -0.102 & 0.0579 & 0.000171 & 0.00455 & -0.00328 \\ -0.00145 & 0.000674 & 0.000171 & 0.00138 & -0.00180 & 0.000617 \\ 0.00559 & -0.0104 & 0.00455 & -0.00180 & 0.00300 & -0.00121 \\ -0.00296 & 0.00653 & -0.00328 & 0.000617 & -0.00121 & 0.000543 \end{pmatrix} \tag{B.4}$$

B.3 Chapter 3 fits

Covariance matrix for the fit result in Tab. (3.1):

$$\begin{pmatrix}
0.238 & -0.160 & -3.20 & 12.8 & -0.0444 & 0.0152 & 0.620 & -2.31 \\
-0.160 & 0.396 & 1.67 & -10.4 & -0.0291 & -0.00575 & 0.431 & -1.41 \\
-3.20 & 1.67 & 43.8 & -169. & 0.696 & -0.211 & -9.76 & 36.0 \\
12.8 & -10.4 & -169. & 703. & -2.03 & 0.767 & 28.2 & -106. \\
-0.0444 & -0.0291 & 0.696 & -2.03 & 0.0244 & -0.00648 & -0.344 & 1.26 \\
0.0152 & -0.00575 & -0.211 & 0.767 & -0.00648 & 0.00565 & 0.0847 & -0.352 \\
0.620 & 0.431 & -9.76 & 28.2 & -0.344 & 0.0847 & 4.85 & -17.6 \\
-2.31 & -1.41 & 36.0 & -106. & 1.26 & -0.352 & -17.6 & 64.7
\end{pmatrix} \tag{B.5}$$

Covariance matrix for the fit result in Tab. (3.2):

$$\begin{pmatrix}
1.34 & -1.43 & -17.0 & 74.8 & -0.119 & 0.112 & 1.54 & -6.54 \\
-1.43 & 2.15 & 17.2 & -83.5 & -0.0293 & -0.124 & 0.629 & -0.803 \\
-17.0 & 17.2 & 219. & -948. & 1.77 & -1.42 & -23.4 & 96.4 \\
74.8 & -83.5 & -948. & 4210. & -5.76 & 6.27 & 73.3 & -322. \\
-0.119 & -0.0293 & 1.77 & -5.76 & 0.0565 & -0.0114 & -0.801 & 2.89 \\
0.112 & -0.124 & -1.42 & 6.27 & -0.0114 & 0.0155 & 0.140 & -0.650 \\
1.54 & 0.629 & -23.4 & 73.3 & -0.801 & 0.140 & 11.4 & -40.9 \\
-6.54 & -0.803 & 96.4 & -322. & 2.89 & -0.650 & -40.9 & 149.
\end{pmatrix} \tag{B.6}$$

Covariance matrix for the fit result in Tab. (3.4):

$$\begin{pmatrix}
1.18 & -1.29 & -15.1 & 66.5 & -0.0750 & 0.0770 & 0.962 & -4.17 \\
-1.29 & 2.21 & 15.1 & -77.4 & -0.129 & -0.0594 & 1.97 & -6.15 \\
-15.1 & 15.1 & 194. & -837. & 1.30 & -1.02 & -17.3 & 70.8 \\
66.5 & -77.4 & -837. & 3760. & -2.97 & 4.11 & 36.3 & -171. \\
-0.0750 & -0.129 & 1.30 & -2.97 & 0.0678 & -0.0136 & -0.961 & 3.47 \\
0.0770 & -0.0594 & -1.02 & 4.11 & -0.0136 & 0.0149 & 0.173 & -0.755 \\
0.962 & 1.97 & -17.3 & 36.3 & -0.961 & 0.173 & 13.7 & -49.1 \\
-4.17 & -6.15 & 70.8 & -171. & 3.47 & -0.755 & -49.1 & 178.
\end{pmatrix} \tag{B.7}$$

Covariance matrix for the fit result in Tab. (3.5):

$$\begin{pmatrix}
0.222 & -0.0630 & -3.12 & 11.4 & -0.0589 & 0.0177 & 0.826 & -3.05 \\
-0.0630 & 0.417 & 0.224 & -5.67 & -0.0914 & 0.0107 & 1.31 & -4.63 \\
-3.12 & 0.224 & 45.0 & -156. & 1.01 & -0.277 & -14.2 & 52.0 \\
11.4 & -5.67 & -156. & 600. & -2.37 & 0.793 & 33.0 & -123. \\
-0.0589 & -0.0914 & 1.01 & -2.37 & 0.0470 & -0.0103 & -0.666 & 2.41 \\
0.0177 & 0.0107 & -0.277 & 0.793 & -0.0103 & 0.00534 & 0.141 & -0.545 \\
0.826 & 1.31 & -14.2 & 33.0 & -0.666 & 0.141 & 9.44 & -34.1 \\
-3.05 & -4.63 & 52.0 & -123. & 2.41 & -0.545 & -34.1 & 124.
\end{pmatrix} \tag{B.8}$$

Covariance matrix for the fit result in Tab. (3.6):

$$\begin{pmatrix}
0.0123 & -0.0322 & -0.127 & 0.792 & 0.00211 & 0.00247 & -0.0347 & 0.0946 \\
-0.0322 & 0.141 & 0.242 & -2.40 & -0.0179 & -0.00970 & 0.276 & -0.846 \\
-0.127 & 0.242 & 1.46 & -7.65 & -0.00222 & -0.0201 & 0.0656 & -0.0312 \\
0.792 & -2.40 & -7.65 & 53.2 & 0.199 & 0.161 & -3.16 & 9.20 \\
0.00211 & -0.0179 & -0.00222 & 0.199 & 0.00394 & 0.00167 & -0.0599 & 0.189 \\
0.00247 & -0.00970 & -0.0201 & 0.161 & 0.00167 & 0.00205 & -0.0276 & 0.0759 \\
-0.0347 & 0.276 & 0.0656 & -3.16 & -0.0599 & -0.0276 & 0.915 & -2.87 \\
0.0946 & -0.846 & -0.0312 & 9.20 & 0.189 & 0.0759 & -2.87 & 9.10
\end{pmatrix} \tag{B.9}$$

Covariance matrix for the fit result in Tab. (3.9):

$$\begin{pmatrix}
0.274 & -0.239 & -3.58 & 15.0 & -0.0287 & 0.0176 & 0.387 & -1.53 \\
-0.239 & 0.231 & 3.09 & -13.2 & 0.0206 & -0.0146 & -0.275 & 1.11 \\
-3.58 & 3.09 & 46.9 & -196. & 0.383 & -0.232 & -5.17 & 20.4 \\
15.0 & -13.2 & -196. & 822. & -1.54 & 0.958 & 20.8 & -82.4 \\
-0.0287 & 0.0206 & 0.383 & -1.54 & 0.00976 & -0.00583 & -0.132 & 0.520 \\
0.0176 & -0.0146 & -0.232 & 0.958 & -0.00583 & 0.00520 & 0.0761 & -0.319 \\
0.387 & -0.275 & -5.17 & 20.8 & -0.132 & 0.0761 & 1.79 & -7.03 \\
-1.53 & 1.11 & 20.4 & -82.4 & 0.520 & -0.319 & -7.03 & 27.8
\end{pmatrix} \tag{B.10}$$

Covariance matrix for the fit result in Tab. (3.8):

$$\begin{pmatrix} 0.203 & -0.189 & -2.64 & 11.2 & -0.0136 & 0.00819 & 0.185 & -0.729 \\ -0.189 & 0.196 & 2.43 & -10.5 & 0.00954 & -0.00665 & -0.128 & 0.517 \\ -2.64 & 2.43 & 34.3 & -145. & 0.183 & -0.108 & -2.48 & 9.73 \\ 11.2 & -10.5 & -145. & 616. & -0.734 & 0.445 & 9.93 & -39.2 \\ -0.0136 & 0.00954 & 0.183 & -0.734 & 0.00713 & -0.00488 & -0.0955 & 0.383 \\ 0.00819 & -0.00665 & -0.108 & 0.445 & -0.00488 & 0.00448 & 0.0635 & -0.267 \\ 0.185 & -0.128 & -2.48 & 9.93 & -0.0955 & 0.0635 & 1.28 & -5.12 \\ -0.729 & 0.517 & 9.73 & -39.2 & 0.383 & -0.267 & -5.12 & 20.6 \end{pmatrix} \quad \text{(B.11)}$$

Appendix C

Data

C.1 Cross section data

Below are the cross section data used in the fits of the thesis:

Experiment	Q^2	ε	E_{beam}	θ_e	$\sigma \times 100$	$\Delta\sigma \times 100$	Δn	δ-TPE
Walker	1	0.6918	1.594	45.221	527.44	4.98	0.019	-0.0054
Walker	0.9996	0.8687	2.403	27.277	1780.5	18.5	0.019	-0.0039
Walker	1.0001	0.9298	3.2381	19.453	3951.1	39.3	0.019	-0.003
Walker	2.003	0.6345	2.408	46.389	44.476	0.466	0.019	-0.0083
Walker	2.0023	0.7348	2.8	37.47	78.101	0.704	0.019	-0.0071
Walker	2.0025	0.8076	3.25	30.81	128.94	1.02	0.019	-0.006
Walker	2.0025	0.8775	4.003	23.822	242.23	2.62	0.019	-0.0049
Walker	2.0022	0.938	5.4892	16.512	574.63	14.	0.019	-0.0036
Walker	2.4968	0.6195	2.796	45.947	18.998	0.197	0.019	-0.0107
Walker	2.4968	0.723	3.241	37.024	33.76	0.333	0.019	-0.009
Walker	2.4969	0.8002	3.766	30.245	56.358	0.453	0.019	-0.0076
Walker	2.4975	0.846	4.242	25.989	83.003	0.876	0.019	-0.0067
Walker	3.0061	0.6233	3.251	43.976	9.6956	0.106	0.019	-0.0138
Walker	3.0063	0.7614	4.008	32.422	21.979	0.217	0.019	-0.0108
Walker	3.0065	0.9102	6.2462	18.526	90.873	2.36	0.019	-0.0069
Walker	3.0064	0.9316	7.0741	16.02	131.51	1.53	0.019	-0.0062
Andivahis$_1$	1.75	0.25	1.511	90.066	14.497	0.176	0.0177	-0.0136
Andivahis$_1$	1.75	0.7037	2.407	41.11	103.06	1.09	0.0177	-0.0068
Andivahis$_1$	1.7499	0.9497	5.507	15.145	1154.9	13.4	0.0177	-0.003
Andivahis$_1$	2.5	0.2266	1.968	89.948	3.4185	0.0487	0.0177	-0.0188
Andivahis$_1$	2.5	0.4786	2.407	58.882	9.8993	0.132	0.0177	-0.013
Andivahis$_1$	2.5	0.6303	2.837	44.993	19.95	0.265	0.0177	-0.0105

$Andivahis_1$	2.5	0.7498	3.4	34.694	39.566	0.427	0.0177	-0.0085
$Andivahis_1$	2.4937	0.8204	3.95	28.409	66.215	0.764	0.0177	-0.0072
$Andivahis_1$	2.5001	0.9128	5.5069	18.981	177.93	2.12	0.0177	-0.0052
$Andivahis_1$	3.25	0.4264	2.837	61.205	2.8638	0.0447	0.0177	-0.0202
$Andivahis_1$	3.2501	0.6086	3.4	44.482	6.8047	0.0891	0.0177	-0.0158
$Andivahis_1$	3.25	0.7188	3.956	35.382	12.583	0.164	0.0177	-0.0132
$Andivahis_1$	3.25	0.8647	5.507	22.804	39.	0.434	0.0177	-0.0093
$Andivahis_1$	4	0.4368	3.4	57.572	1.3045	0.0226	0.0177	-0.0269
$Andivahis_1$	4.0001	0.5927	3.956	43.707	2.7796	0.0442	0.0177	-0.0219
$Andivahis_1$	4.0001	0.6944	4.507	35.592	4.9401	0.0787	0.0177	-0.0187
$Andivahis_1$	4	0.8046	5.5069	26.823	10.241	0.137	0.0177	-0.0151
$Andivahis_1$	3.9999	0.9455	9.8	13.248	61.798	0.807	0.0177	-0.0087
$Andivahis_1$	5.0001	0.3895	3.956	59.291	0.42354	0.00963	0.0177	-0.0374
$Andivahis_1$	5.0001	0.5383	4.507	45.658	0.84997	0.015	0.0177	-0.0311
$Andivahis_1$	5	0.7042	5.507	32.829	2.1325	0.0309	0.0177	-0.0245
$Andivahis_1$	5.0001	0.919	9.8	15.367	15.761	0.234	0.0177	-0.0136
$Andivahis_1$	5.9998	0.8863	9.8001	17.515	4.7503	0.0771	0.0177	-0.0202
$Andivahis_1$	7.0001	0.8466	9.8	19.753	1.708	0.0425	0.0177	-
$Andivahis_2$	1.75	0.25	1.511	90.066	15.242	0.17	0.027	-0.0136
$Andivahis_2$	2.5	0.2266	1.968	89.948	3.5758	0.0408	0.027	-0.0188
$Andivahis_2$	3.25	0.2063	2.407	90.004	1.1063	0.0143	0.027	-0.0274
$Andivahis_2$	4	0.1899	2.837	89.966	0.414	0.0057	0.027	-0.0373
$Andivahis_2$	5.0001	0.1713	3.4	89.985	0.13579	0.00197	0.027	-0.0504
$Andivahis_2$	6.0001	0.1562	3.956	89.981	0.052471	0.000889	0.027	-0.0671
$Andivahis_2$	7.0001	0.1434	4.507	89.992	0.022891	0.000578	0.027	-
$Andivahis_2$	8.8301	0.1247	5.507	90.017	0.00615	0.000249	0.027	-
GMp12L	1.5771	0.7009	2.222	42.001	145.24	1.37	0.016	-0.0064
GMp12L	4.5434	0.8255	6.4269	24.25	7.7469	0.116	0.016	-0.0169
GMp12L	5.9471	0.7087	6.4271	30.909	1.1103	0.0155	0.016	-0.0313
GMp12L	6.9929	0.5992	6.427	37.008	0.29083	0.00407	0.016	-
GMp12L	7.9918	0.4775	6.427	44.5	0.082383	0.00124	0.016	-
GMp12L	9.0021	0.6478	8.518	30.909	0.12885	0.00193	0.016	-
GMp12L	9.8073	0.5796	8.518	34.4	0.0589	0.000884	0.016	-
GMp12L	11.187	0.4482	8.518	42.001	0.0155	0.000248	0.016	-
GMp12R	1.8585	0.6155	2.222	48.666	53.178	1.01	0.02	-0.0081
GMp12R	9.0526	0.3322	6.427	55.9	0.020732	0.000456	0.02	-
GMp12R	12.069	0.3558	8.5179	48.666	0.00619	0.000136	0.02	-
GMp12R	12.568	0.301	8.5181	53.501	0.00359	0.000115	0.02	-
GMp12R	15.755	0.3088	10.5871	48.665	0.00137	0.0000371	0.02	-
Kirk	0.999	0.9549	3.9962	15.439	6473.2	118.	0.04	-0.0024
Kirk	1.4987	0.9687	6.1974	12.149	3242.2	57.9	0.04	-0.0022
Kirk	1.9983	0.9524	6.1968	14.4	811.2	16.6	0.04	-0.0032
Kirk	2.5012	0.96	7.9091	12.59	464.81	7.43	0.04	-0.0037

Kirk	3.7592	0.9531	9.998	12.45	92.422	1.85	0.04	-0.0074
Kirk	5.0752	0.9315	10.6999	13.99	18.052	0.389	0.04	-0.0129
Kirk	6.275	0.911	11.3499	15.1	5.3018	0.243	0.04	-0.0195
Kirk	7.5038	0.8891	11.9999	16.07	1.8909	0.0582	0.04	-
Kirk	8.7479	0.8674	12.6899	16.85	0.69092	0.0407	0.04	-
Kirk	9.9841	0.8449	13.33	17.59	0.35	0.0135	0.04	-
Kirk	12.507	0.8003	14.6604	18.8	0.082	0.0059	0.04	-
Kirk	15.098	0.7579	16.0605	19.72	0.0263	0.0027	0.04	-
Kirk	19.991	0.6229	17.3104	24.04	0.00302	0.000588	0.04	-
Kirk	25.021	0.3816	17.3101	35.09	0.000463	0.000203	0.04	-
Rock	2.4946	0.9745	9.7494	10.001	769.87	5.	0.03	-0.003
Rock	3.9896	0.9684	12.571	10	111.68	1.1	0.03	-0.0067
Rock	5.9961	0.9603	15.7362	10	17.947	0.24	0.03	-0.0125
Rock	7.9883	0.9524	18.4822	10	4.4793	0.1	0.03	-
Rock	10.004	0.9445	21.006	10	1.4498	0.05	0.03	-
Sill	2.8617	0.8892	5.4639	21.01	80.206	3.04	0.036	-0.007
Sill	3.6214	0.8337	5.4641	25.01	19.309	0.807	0.036	-0.0121
Sill	5.0266	0.8569	7.632	21.01	6.9322	0.252	0.036	-0.0175
Sill	4.9906	0.8079	6.657	25.01	4.5531	0.179	0.036	-0.0199
Sill	5.0166	0.7014	5.499	33.01	2.0433	0.0763	0.036	-0.0247
Sill	7.3004	0.8255	9.6061	21.01	1.0906	0.0447	0.036	-
Sill	9.624	0.7957	11.45	21.01	0.25119	0.0108	0.036	-
Sill	11.985	0.7676	13.2102	21.01	0.080878	0.00358	0.036	-
Sill	15.719	0.7269	15.8399	21.01	0.017923	0.00108	0.036	-
Sill	19.48	0.6901	18.3604	21.01	0.00468	0.000363	0.036	-
Sill	23.238	0.6568	20.7898	21.01	0.00182	0.000166	0.036	-
Sill	26.993	0.5398	21.1804	25.01	0.000453	0.0000527	0.036	-
Sill	31.205	0.3661	21.1903	33.01	0.0000866	0.0000154	0.036	-
Christy	0.4243	0.9739	3.1141	12.47	89649.	992.	0.017	-
Christy	0.6185	0.9186	2.235	21.97	10977.	117.	0.017	-
Christy	0.6203	0.6823	1.148	47.97	1735.	16.4	0.017	-
Christy	0.6635	0.9553	3.114	15.97	18913.	215.	0.017	-
Christy	0.8175	0.5491	1.148	59.99	482.02	4.64	0.017	-
Christy	0.8999	0.8104	1.882	33.95	1464.2	14.3	0.017	-
Christy	0.9313	0.9308	3.114	19.46	4800.7	50.4	0.017	-
Christy	1.1121	0.8226	2.2349	31.95	893.95	8.96	0.017	-0.0046
Christy	1.3435	0.9654	5.4942	12.989	4050.	51.2	0.017	-0.0022
Christy	1.6353	0.6879	2.235	42.97	118.54	1.23	0.017	-0.0067
Christy	2.0354	0.7835	3.114	32.97	101.76	1.02	0.017	-0.0065
Christy	2.2471	0.4884	2.235	58.969	15.269	0.165	0.017	-0.0114
Christy	2.2886	0.9239	5.494	17.96	287.	3.55	0.017	-0.0044
Christy	2.6203	0.6726	3.114	40.97	21.284	0.214	0.017	-0.0105
Christy	2.7806	0.2843	2.235	79.97	2.8865	0.0344	0.017	-0.0196

Christy	2.7829	0.8955	5.4939	20.47	98.244	1.17	0.017	-0.0065
Christy	3.1682	0.5479	3.114	49.97	5.5845	0.0601	0.017	-0.0166
Christy	3.2689	0.8627	5.494	22.97	37.709	0.446	0.017	-0.0095
Christy	3.7392	0.826	5.494	25.47	16.088	0.228	0.017	-0.013
Christy	3.7257	0.4025	3.114	61.97	1.4945	0.0173	0.017	-0.0255
Christy	3.7986	0.6577	4.104	38.97	4.9285	0.0564	0.017	-0.0185
Christy	4.1874	0.7864	5.494	27.97	7.7554	0.0983	0.017	-0.0167
Christy	4.2325	0.2574	3.114	77.97	0.42943	0.00638	0.017	-0.0363
Christy	4.4008	0.5527	4.104	45.96	1.587	0.0327	0.017	-0.0261
Christy	4.7964	0.5526	4.413	44.98	1.1015	0.0229	0.017	-0.029
Christy	5.0036	0.7022	5.494	32.97	2.1524	0.0312	0.017	-0.0246
Christy	5.2619	0.4685	4.413	50.99	0.492	0.00872	0.017	-0.0363
Christy	5.3703	0.6593	5.494	35.48	1.2696	0.0234	0.017	-0.0289

TABLE C.1: In this table are 9 data sets from several experiments, namely Refs. [26] [1] [8] [27] [28] [29] [30]. The data in totality, is referred to as 'the global cross section data set' throughout the thesis and consists of $16+24+8+8+5+14+5+13+28=121$ data points. When looking at TPE corrections, we restrict ourselves to the data where $Q^2 \in [1.0, 6.275]\,\mathrm{GeV}^2$. This is referred to as the 'Uncorrected Data' or 'OPE Data' when not yet corrected, and 'Corrected Data' or 'TPE-Corrected Data' after the correction has been applied. The latter two data subsets consist of $16+23+6+3+1+7+3+5+21=85$ data points. The subsets of the (un)corrected data which are strictly from Walker and Andivahis, are used in chapter (2) to compare with similar work done by Gramolin *et al.* [13]. This smaller subset consists of 45 data points.

The headers of the table are:

Q^2: the negative of the momentum transfer, reported in GeV^2

ε: the virtual photon polarization, dimensionless

E_{beam}: the energy of the incoming electron, in GeV^2

θ_e: is the angle in the lab frame of the incoming electron, in degrees

$\sigma \times 100$: the cross section scaled by a factor of 100, in nb/sr

$\Delta\sigma \times 100$: the uncertainty in the cross section scaled by a factor of 100, in nb/sr

Δn: the overall normalization uncertainty of the experiment, dimensionless

$\delta -$ TPE: the TPE correction, dimensionless

The cross section reported in this table is *not* the reduced cross section. The reduced cross section is:

$$\frac{\varepsilon(1+\tau)}{\sigma_{\mathrm{Mott}}}\sigma \tag{C.1}$$

where the sigma with no subscript is the one reported in the table. As for the correction, it is applied to the data as follows:

$$\sigma_c = \sigma \exp(-\delta) \tag{C.2}$$

i.e. the TPE effects are cancelled out of the data to get at the more accurate representation of the 'uncorrected' cross section.

C.2 Polarization ratio data

Experiment	Q^2	R	ΔR
Punjabi	1.18	0.883	0.0222036
Punjabi	1.48	0.798	0.0389487
Punjabi	1.77	0.789	0.0424382
Punjabi	1.88	0.777	0.0408044
Punjabi	2.13	0.747	0.0466905
Punjabi	2.47	0.703	0.0402244
Punjabi	2.97	0.615	0.035805
Punjabi	3.47	0.606	0.0442719
Gayou	1.02	0.9	0.043909
Gayou	1.12	0.825	0.0336006
Gayou	1.18	0.851	0.0550364
Gayou	1.42	0.733	0.064846
Gayou	1.76	0.816	0.134112
Puckett	3.5	0.571	0.0723395
Puckett	3.98	0.517	0.0557315
Puckett	4.76	0.45	0.0533667
Puckett	5.56	0.354	0.0870976
Strauch	1.02	0.878	0.0224722
Strauch	1.625	0.765	0.0254951
Jones	1.51	0.884	0.0396232
MacLachlan	1.13	0.878	0.0651153
Paolone	1.3	0.897	0.0206155
Puckett	5.17	0.448	0.0602993
Puckett	6.7	0.348	0.105475
Puckett	8.49	0.145	0.176638
Puckett	2.491	0.6953	0.0120507
Puckett	2.477	0.6809	0.00806226
Puckett	2.449	0.6915	0.00707248

TABLE C.2: In this table are 9 data sets from experiments and analyses in Refs. [31] [32] [33] [34] [35] [36] [37]. Each of these sources contain further polarization data, but in this thesis only those points with $Q^2 > 1$ GeV^2 are used for the global analysis.

The headers of the table are:

Q^2: the negative of the momentum transfer, reported in GeV^2

R: the polarization ratio $= \mu_p G_E^p / G_M^p$, dimensionless

ΔR: the uncertainty in the polarization ratio, dimensionless

Bibliography

[1] L. Andivahis *et al.*, Phys. Rev. D **50**, 5491 (1994).

[2] NIST, Web, Accessed 2022-12-08, https://physics.nist.gov/cuu/Constants/ (2018).

[3] F. Halzen and A. D. Martin, *Quarks & Leptons: An Introductory Course In Modern Particle Physics* (John Wiley & Sons, 2008).

[4] R. Jaffe, Phys. Rev. D **103**, 016017 (2021).

[5] J. Arrington, P.G.Blunden, and W.Melnitchouk, Elsevier **66**, 782 (2011).

[6] G. P. Lepage and S. J. Brodsky, Phys. Rev. D **22**, 2157 (1980).

[7] J. Bernauer *et al.*, Phys. Rev. C **90**, 015206 (2014).

[8] M. E. Christy *et al.*, Phys. Rev. Lett. **128**, 102002 (2022).

[9] R. Ball *et al.*, J. High Energ. Phys. **75** (2010).

[10] J. Ahmed, P. G. Blunden, and W. Melnitchouk, Phys. Rev. C **102**, 045205 (2020).

[11] R. Andrae, T. Schulze-Hartung, and P. Melchior, ArXiv e-prints 1012.3754 (2010).

[12] Y. Pawitan, *In All Likelihood: Statistical Modelling and Inference Using Likelihood* (Oxford Clarendon Press, 2001).

[13] A. Gramolin and D. Nikolenko, Phys. Rev. C **93**, 055201 (2016).

[14] G. D'Agostini, Web, Accessed 2022-10-07, https://www.roma1.infn.it/∼dagos/cern/node98.html (2003).

[15] H. J. Behrend *et al.*, Phys. Lett. B **3**, 400 (1987).

[16] J.-M. Muller *et al.*, *Handbook of Floating-Point Arithmetic* (Birkhäuser, 2010).

[17] B. Bhattacharya, R. J. Hill, and G. Paz, Phys. Rev. D **84**, 073006 (2011).

[18] G. Lee, J. R. Arrington, and R. J. Hill, Phys. Rev. D **92**, 013013 (2015).

[19] B. C. Rislow and C. E. Carlson, Phys. Rev. D **88**, 013018 (2013).

[20] G. Baym, *Lectures on Quantum Mechanics* (W. A. Benajmin, INC., 1969).

[21] M. E. Christy and P. E. Bosted, Phys. Rev. C **81**, 055213 (2010).

[22] F. E. Close, *An Introduction to Quarks and Partons* (Academic Press, 1979).

[23] C. E. Carlson, Phys. Rev. D **34**, 2704 (1986).

[24] S. J. Brodsky and G. P. Lepage, Phys. Rev. D **24**, 2848 (1981).

[25] Y.-H. Lin, H.-W. Hammer, and U.-G. Meißner, Phys. Rev. Lett. **128**, 052002 (2022).

[26] R. Walker *et al.*, Phys. Rev. D **49**, 5671 (1994).

[27] P. N. Kirk *et al.*, Phys. Rev. D **8**, 63 (1973).

[28] S. Rock *et al.*, Phys. Rev. D **46**, 24 (1992).

[29] A. Sill *et al.*, Phys. Rev. D **48**, 29 (1993).

[30] M. Christy *et al.*, Phys. Rev. C **70**, 015206 (2004).

[31] V. Punjabi *et al.*, Phys. Rev. C **71**, 055202 (2005).

[32] O. Gayou *et al.*, Phys. Rev. C **64**, 038202 (2001).

[33] A. J. R. Puckett *et al.*, Phys. Rev. C **85**, 045203 (2012).

[34] S. Strauch *et al.*, Phys. Rev. Lett. **91**, 052301 (2003).

[35] M. Jones *et al.*, Phys. Rev. C **74**, 035201 (2006).

[36] G. MacLachlan *et al.*, Nuclear Phys. A **764**, 261 (2005).

[37] M. Paolone *et al.*, Phys. Rev. Lett. **105**, 072001 (2010).